12-2011

Characterizing Mechanical Heterogeneity in Cardiovascular Cells

Sandra Deitch
Clemson University, sdeitch@gmail.com

CHARACTERIZING MECHANICAL HETEROGENEITY IN CARDIOVASCULAR CELLS

A Dissertation
Presented to
the Graduate School of
Clemson University

In Partial Fulfillment
of the Requirements for the Degree
Doctor of Philosophy
Bioengineering

---

by
Sandra Beth Deitch
December 2011

Accepted by:
Dr. Delphine Dean, Committee Chair
Dr. Martine LaBerge
Dr. Jiro Nagatomi
Dr. Edie Goldsmith

ABSTRACT

Most tissue-level mechanical models assume homogeneous mechanical properties within a single cell type. However, measurements of cellular mechanical properties show large variability in whole-cell mechanical properties between cells from a single population. This heterogeneity has been observed in many cell populations and with several measurement techniques but the sources are not yet fully understood. Cell mechanical properties are directly related to the composition and organization of the cytoskeleton, which is physically coupled to neighboring cells through adherens junctions and to underlying matrix scaffolds through focal adhesion complexes. As such, we believe that this high level of heterogeneity can be attributed to varying local microenvironment conditions throughout the sample.

To test this hypothesis, cardiomyocytes and vascular smooth muscle cells were cultured under several conditions that limited the variability in their microenvironment. First, cells were cultured on aligned collagen and fibronectin matrices (more uniform extracellular matrix). Next, cell-cell and cell-matrix interactions were limited by using antibodies to N-cadherin and integrin β1. Finally, these experiments were replicated on gels and under tension conditions to more closely mimic the native cellular microenvironment. Under each of these conditions, cellular viscoelastic mechanical properties were characterized through AFM testing and cellular structure was analyzed through immunofluorescence imaging.

The results of these studies provide insights from a basic science prospective about the impact of the cellular microenvironment on cell behavior. Additionally,

researchers may use these results to consider heterogeneity in the cellular microenvironment *in vivo*, especially in disease conditions where there is often elevated disorganization, and incorporate realistic levels of cellular heterogeneity in tissue-level mechanical models. Such models may help to better understand tissue behavior in both health and disease.

DEDICATION

This work is dedicated to my family and friends who have supported me throughout my graduate education. I would especially like to thank my parents, Amy and Robert, for teaching me the value of an education and providing me with endless encouragement. I would also like to thank Kevin Geraghty for his unwavering support at each step in my progress towards obtaining a doctoral degree.

ACKNOWLEDGMENTS

I would like to thank my advisor, Dr. Delphine Dean, for her positive guidance and support throughout my project. She has been a great role model and I'm fortunate to have learned so much from her that will serve me well throughout my career. I would also like to acknowledge my committee members, Dr. Martine LaBerge, Dr. Jiro Nagatomi, and Dr. Edie Goldsmith, whose instruction and feedback helped guide my research. I especially appreciate their various points of view that helped me to understand all aspects of my work and to consider additional applications. Additionally, I would like to thank the laboratory of Dr. Thomas Boland for use of their modified inkjet printer and the laboratories of Dr. Bruce Z. Gao and Dr. Martine LaBerge for harvesting the cells that were used in this work. I would like to thank the members of my lab and other students, especially Scott Wood, Laura Datko, Elliott Mappus, Brad Winn, Catherine Kunkle, Ian Moore, and Dr. Jason Hemmer, for assistance with various aspects of my research. Finally, I would like to acknowledge the following funding sources: NIH HL K25 092228, NIH HL R21 097214, NIH P20 RR-016461, and NSF EPS-0903795.

TABLE OF CONTENTS

Page

Table of Contents (Continued)

Page

Table of Contents (Continued)

Page

LIST OF TABLES

LIST OF FIGURES

List of Figures (Continued)

List of Figures (Continued)

Figure Page

List of Figures (Continued)

CHAPTER ONE

INTRODUCTION

1.1 Motivation

There is a close association between cellular mechanics and various diseases. Modeling cell and tissue mechanics is a cost-effective method to predict behavior in both health and disease. Most tissue-level models assume homogeneous mechanical properties within a single cell type. However, measurements of cellular mechanical properties show a large variability in whole-cell mechanical properties between cells from a single population. This heterogeneity has been observed in many cell populations and with several measurement techniques. The sources of this mechanical heterogeneity are not yet fully understood. The cytoskeleton within the cell provides structural integrity and is physically coupled to components in its microenvironment. We hypothesized that differences in microenvironment conditions from one cell to another result in varied cytoskeletal structure within these cells, explaining the high level of heterogeneity that is observed in mechanical properties between cells from a single population.

The purpose of this research was to fully quantify and account for cellular mechanical heterogeneity, using cardiomyocytes and vascular smooth muscle cells (VSMCs) as model cells. Specifically, we investigated the effects of limiting microenvironment conditions (cell-cell and cell-matrix interactions) on cellular structure and mechanical properties. We compared the structure and mechanical properties of cells in 2D culture, looking for factors that lead to decreased heterogeneity in these cellular

properties within each population. Our specific research aims are described here with an overview of samples for each aim outlined in Figure 1.1.

1.2 Research Aims

1.2.1 Aim 1: Quantify Effects of Matrix Composition and Orientation on Cardiomyocyte and VSMC Mechanical Properties in 2D Culture

Most of the studies where cellular mechanical heterogeneity has been noted have used a single matrix component (eg. collagen, fibronectin, or laminin) as a substrate. Therefore, diversified adhesion to different matrix proteins cannot be held accountable for this heterogeneity. Within a single sample, however, varied matrix protein orientations may have had an impact. For example, the matrix proteins may be highly aligned at one location and amorphous at another. In this aim, we quantified the effects of matrix alignment on cardiomyocyte and VSMC mechanical properties for both collagen and fibronectin samples. The two cell types and matrix compositions were used to provide alignment measures in multiple populations. In addition, a comparison of the results from the two matrix materials yielded valuable information as cells interact with several ECM proteins in the body. Cells were cultured on the different matrices for up to fifteen days, with AFM cytoindentation testing at several time points. Force-indentation and stress relaxation measurements were obtained and analyzed using elastic and viscoelastic models. The elastic moduli and percentage relaxation data was compared and variability within each sample assessed. Immunofluorescence imaging was used to compare the cytoskeletal architecture within the cells on each sample.

1.2.2 Aim 2: Quantify Effects of Cell-Cell and Cell Matrix Interactions on VSMC Mechanical Properties in 2D Culture

The heterogeneity observed in cells from a single population may be due to differences in cell-cell and cell-matrix interactions throughout the sample. Local microenvironment conditions, including the number of neighboring cells and amount of matrix components, vary from location to location. For example, one cell may have an abundance of matrix proteins to adhere to while another may have more neighboring cells to interact with. We hypothesized that these varying interactions account for at least some of the documented cell-to-cell variability. To test this hypothesis, antibodies were added to the VSMC media to block N-cadherin mediated cell-cell interactions and integrin β1 mediated cell-matrix interactions on both unaligned collagen and unaligned fibronectin matrices. Through AFM cytoindentation studies on day five VSMCs, the elastic moduli and percentage relaxation were calculated for cells on each sample. The cellular mechanical properties on the different samples were compared and variability within each sample assessed. Immunofluorescence imaging was utilized to compare cytoskeletal architecture and to confirm antibody blocking.

1.2.3 Aim 3: Quantify Effects of Substrate Stiffness and Mechanical Tension on VSMC Mechanical Properties in 2D Culture

Aims 1 and 2 attempted to quantify and account for the mechanical heterogeneity that is observed in 2D cell culture experiments. This aim represents a move towards incorporating realistic levels of heterogeneity in an *in vivo* model by investigating

heterogeneity under more realistic culture conditions. Specifically, we replicated some of the previous experiments while varying the substrate stiffness and applying mechanical tension to the cells. In the body, all cells are surrounded by various substances, most of which are much less stiff than the glass coverslips that were used in Aims 1 and 2. For example, VSMCs are embedded in a network of collagen (types I, III, & V), elastin, and proteoglycans within the tunica media of blood vessels. In addition, tissue mechanics often change with disease. Three different concentrations of polyacrylamide gels, with elastic moduli ranging from 10 kPa (similar to cell stiffness) to 75 kPa (similar to elastin-rich region within tunica media), were coated with unaligned collagen and used as the substrates for these studies.

VSMCs also experience significant loading with vessel dilation and retraction as blood flows through the vessel. Simulating these mechanical forces experienced by native VSMCs took us a step closer to anticipating heterogeneity *in vivo*. For this, physiologically relevant levels of cyclic strain were applied to VSMCs on collagen on days 3 through 5 in culture.

For both the gel and tension conditions, integrin β1 antibodies were added to the media to examine cell-matrix effects. The same AFM mechanical testing, elastic and viscoelastic mechanical modeling, and immunofluorescence imaging procedures as used in the previous aims were performed to fully characterize and compare the different samples.

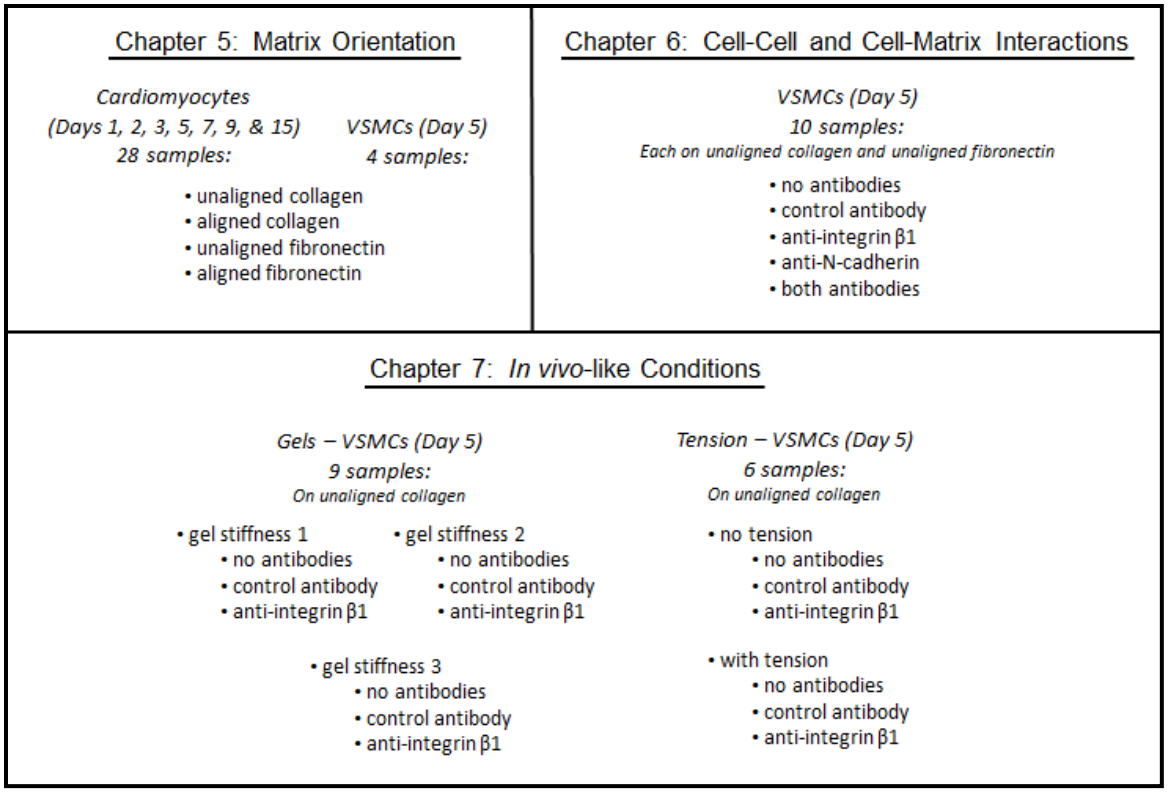

Figure 1.1. Outline of experimental conditions for each study. Aims 1, 2, and 3 are the subjects of Chapters 5, 6, and 7, respectively.

1.3 Significance

This research represents the first attempt to specifically account for the heterogeneity that is observed in measures of cellular mechanical properties. A review of previous research reveals suggestions for specific factors that may promote heterogeneity but previous studies do not fully explain the levels of heterogeneity that are observed. In this work, we investigated several of the conditions that are suspected of causing this heterogeneity at the 2D level. The results of these studies provide insights from a basic science prospective about the impact of the cellular microenvironment on cell behavior, specifically helping us to understand the causes of mechanical heterogeneity within cell

populations. The results of the studies that replicated *in vivo* conditions provided data that may be used as a first step in estimating realistic levels of heterogeneity for *in vivo* conditions, with the ultimate potential for better tissue-level mechanical models. Such models may help to better understand tissue behavior and disease progression.

CHAPTER TWO

LITERATURE REVIEW: CELL TYPES

2.1 Cardiomyocytes

2.1.1 Location

Cardiomyocytes (aka cardiac myocytes) are the fundamental contractile muscle cells of the heart. The wall of the heart is composed of three layers (Figure 2.1) [1]. The outer epicardium (visceral pericardium) forms a protective covering and reduces friction by secreting a serous fluid. This layer is composed of connective tissue covered by epithelium and it includes capillaries, lymphatic vessels, nerve fibers, and fat (particularly near blood vessels). The myocardium is the thick middle layer of the heart wall that is responsible for contraction, pumping blood from the chambers of the heart. This layer consists of cardiac muscle fibers arranged in planes, separated by connective tissues and an abundance of capillaries, lymphatic vessels, and nerve fibers. Cardiomyocytes account for over 90% of the myocardium volume [2]. The endocardium forms a protective inner lining for the cambers and valves of the heart and is composed of epithelium and underlying connective tissue, blood vessels, and Purkinje fibers (specialized muscle fibers that conduct electrical impulses for contraction).

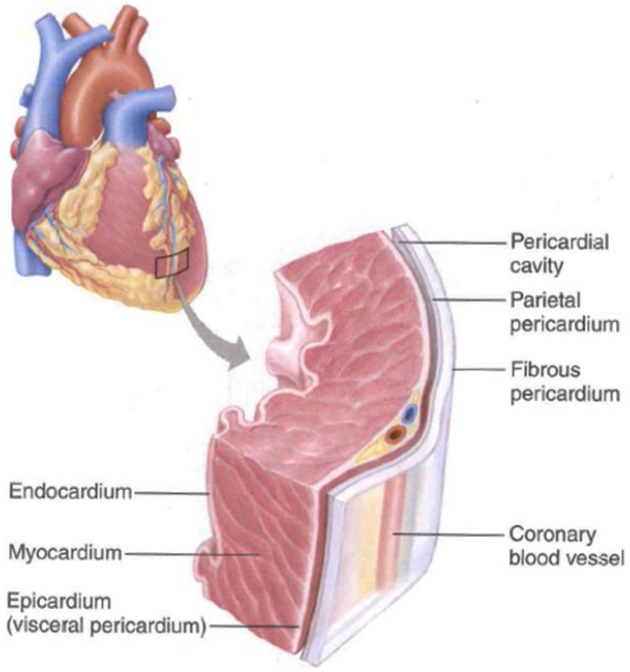

Figure 2.1. Layers of the heart wall: endocardium, myocardium, and epicardium. Cardiomyocytes make up the bulk of the myocardium [1].

2.1.2 Structure and Function

Cardiomyocytes are rod-shaped with lengths of approximately 100 µm and diameters of approximately 25 µm (Figure 2.2). In general, atrial cardiomyocytes are smaller and less structured than ventricular cardiomyocytes. The plasma membrane of a cardiomyocyte contains T-tubules, which enable depolarization to quickly penetrate the interior of the cell. Cardiomyocytes also contain sarcoplasmic reticulum (store and release calcium ions for contraction), many mitochondria (~23% of cell volume), a single spindle-shaped nucleus, and contractile elements [3, 4]. The functional contractile unit within the cell is the sarcomere, an orderly arrangement of thick filaments (myosin), thin filaments (actin), and the regulatory proteins troponin and tropomyosin [2]. Arrays of

sacromeres in series form myofilaments which are arranged in parallel to one another and give the cell a striated appearance.

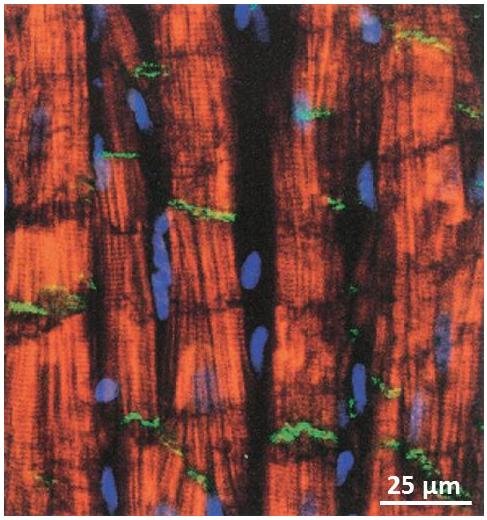

Figure 2.2. Section from adult rat heart showing cardiomyocytes *in vivo*. Cells were stained for N-cadherin (component of adherens junction within intercalated disc) (green), actin filaments (red), and nuclei (blue) [5].

Cardiomyocytes are oriented end-to-end and join to form cardiac muscle fibers that are interconnected in branching, three-dimensional networks [1]. At each cell-cell intersection, intercalated discs permit mechanical and electrical coupling [2]. Intercalated discs consist of 3 types of cell-cell interactions: adherens junctions anchor actin filaments, desmosomes anchor intermediate filaments, and gap junctions allow action potentials to propagate quickly between cells. When one portion of the cardiac muscle fiber network is stimulated, the impulse passes to other fibers and the entire structure contracts simultaneously. Cardiac muscle is also self-exciting and rhythmic, producing the regular contractions of the entire heart.

2.2 Vascular Smooth Muscle Cells

2.2.1 Location

Blood vessels are organs of the circulatory system that transport blood throughout the body. Blood flows from the ventricles of the heart, through large elastic arteries, medium-sized muscular arteries, small arteries (arterioles), capillaries, small veins (venules), medium-sized veins, and large veins, then back to the atria of the heart (Figure 2.3). The vessels differ a great deal in size and function, but all consist of three basic layers or tunics: the tunica intima, media, and adventitia. Vascular smooth muscle cells are one of the main constituents of the medial layer. The main difference between the vessel types is the relative proportion of each layer (illustrated in Figures 2.3 and 2.4).

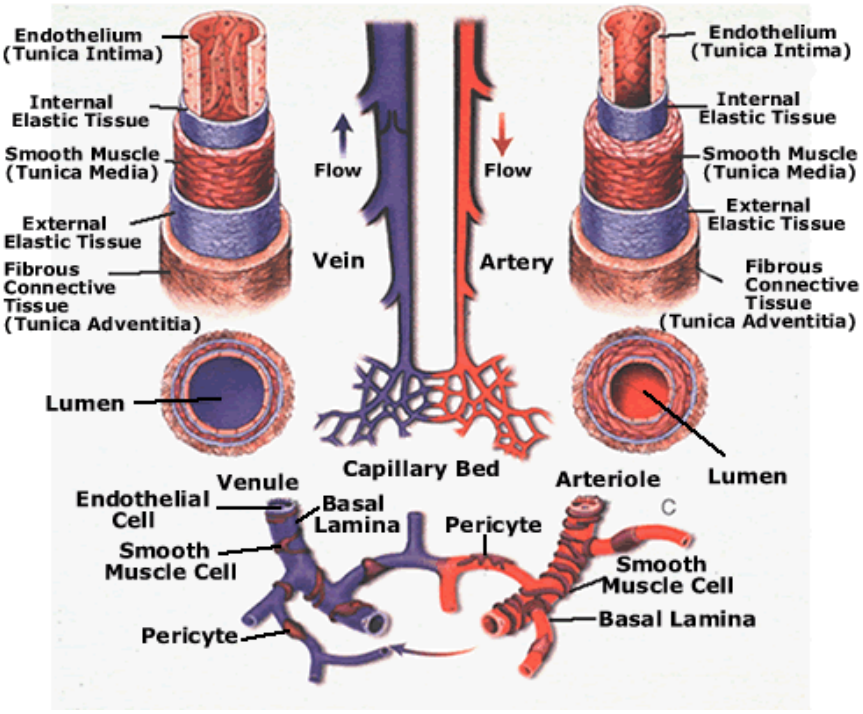

Figure 2.3. Blood vessel structure throughout circulatory system [6].

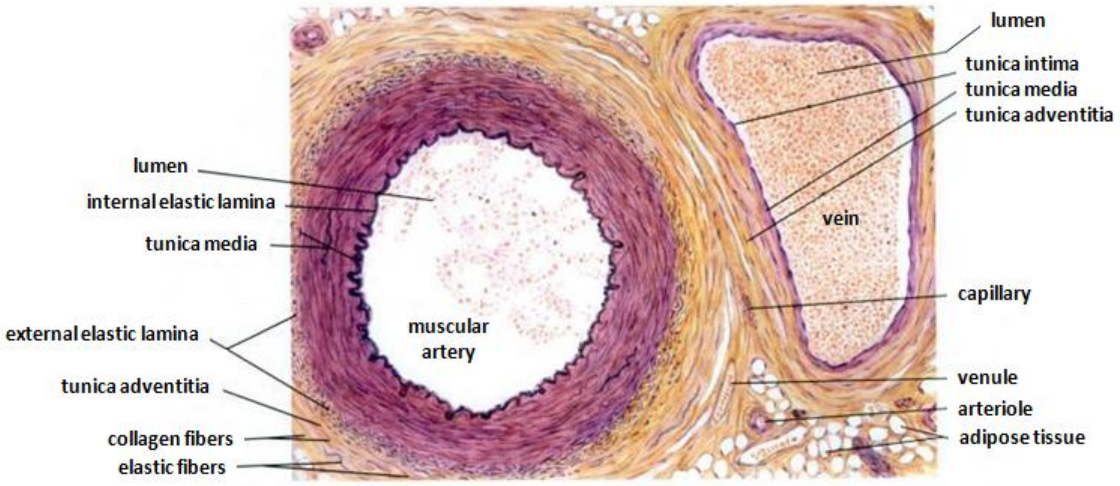

Figure 2.4. Transverse section of blood vessels with elastic stain (64x) [7].

The tunica intima is composed of a monolayer of axially oriented simple squamous epithelial cells (called endothelium) on a basement membrane, made up of type IV collagen, fibronectin, and laminin [8]. The endothelium provides a smooth surface that allows blood cells and platelets to flow without damage. The endothelial cells are highly differentiated to actively mediate the extensive bidirectional exchange of small molecules. They also secrete chemicals that inhibit platelet aggregation (clotting) and help regulate dilation and constriction of the blood vessel [9]. The internal elastic lamina, a fenestrated layer of elastic tissue, supports the endothelium and separates the tunica intima from the tunica media.

The tunica media is comprised of vascular smooth muscle cells (VSMCs) embedded in a network of collagen (types I, III, & V), elastin, and proteoglycans. The VSMCs are oriented circumferentially and organized into concentric layers separated by concentric fenestrated elastin sheets (elastic lamellae) [10]. This arrangement allows

VSMCs to regulate the lumen diameter, and thus blood flow through the vessel, by contracting and relaxing. This contraction and relaxation is regulated by autonomic nerves, local environmental changes, and circulating hormones. The elastin allows the vessel to expand with pressure while the collagen prevents excessive dilation [11]. The external elastic lamina separates the tunica media from the tunica adventitia.

The tunica adventitia consists of loose fibrous connective tissue. The fibers, primarily type I collagen and some elastin, are longitudinally arranged [10]. Sympathetic nerves, fibroblasts, and vasa vasorum (smaller blood vessels that sustain outer vascular tissue) can also be found in the tunica adventitia. The tunica adventitia anchors the vessel in place and counteracts external forces such as longitudinal stretching.

In general, arteries have thicker, more muscular walls than veins. Thus, arteries have many more VSMCs in comparison to veins of similar size. The lumen of an artery is rounder and smaller than that of a vein. The internal elastic lamina is prominent in arteries but ill-defined in veins. The tunica media is larger than the tunica adventitia in arteries and the opposite is true for veins. Veins also have valves (folds in the tunica intima) to prevent backflow and enable blood to climb against gravity, while arteries do not. Figures 2.3 and 2.4 illustrate some of these differences in vessel structure.

Large elastic arteries, such as the aorta (2.5 cm diameter), stretch in response to a bolus of blood and then passively contract in diastole [12]. They have a relatively thick tunica intima and a multi-layered internal elastic lamina. The tunica media has 40-70 elastic lamellae with VSMCs and collagen to help resist bursting. The tunica adventitia is very thin. Medium-sized muscular arteries (0.3 mm – 1 mm diameter) distribute blood

to the body. Flow is mediated by the VSMC layers of the tunica media in response to sympathetic nerve stimulation. The internal elastic lamina is prominent and the external elastic lamina is visible. There are 3-40 VSMC layers in the tunica media (very little elastic lamellae compared to VSMCs). The tunica adventitia is approximately as thick as the tunica media. Arterioles (less than 0.5 mm diameter) regulate blood flow to the capillary network by vasoconstriction and vasodilation. The internal elastic lamina is only present in arterioles with a diameter greater than 0.04 mm. There are 1-2 VSMC layers in the tunica media and the tunica adventitia is very thin. Small arterioles have a band of smooth muscle that encircles the entire vessel (precapillary sphincter) which regulates blood flow into the following capillary networks. Table 2.1 compares the relative proportions of the tunica media and adventitia constituents in different arteries.

Table 2.1. Percentage composition of the media and adventitia in several arteries at *in vivo* blood pressure (mean ± standard deviation) [13].

	Pulmonary artery	Thoracic aorta	Plantar artery
Media			
Smooth muscle	46.4 ± 7.7	33.5 ± 10.4	60.5 ± 6.5
Ground substance	17.2 ± 8.6	5.6 ± 6.7	26.4 ± 6.4
Elastin	9.0 ± 3.2	24.3 ± 7.7	1.3 ± 1.1
Collagen	27.4 ± 13.2	36.8 ± 10.2	11.9 ± 8.4
Adventitia			
Collagen	63.0 ± 8.5	77.7 ± 14.1	63.9 ± 9.7
Ground substance	25.1 ± 8.3	10.6 ± 10.4	24.7 ± 9.3
Fibroblasts	10.4 ± 6.1	9.4 ± 11.0	11.4 ± 2.6
Elastin	1.5 ± 1.5	2.4 ± 3.2	0

Capillaries (5-10 μm diameter) function to deliver nutrients, gases, and hormones to tissues and remove waste products from tissues [12]. The capillary wall is very thin (0.2 μm) and permeability is determined by the nature of the endothelium and the basal lamina. The tunica media consists of longitudinally-oriented pericytes (mesenchymal cells) and the adventitia contains sparse collagen fibers. Capillaries are classified on the basis of structure and relative permeability (continuous, fenestrated, sinusoidal). Venules (10-50 μm diameter) have walls as thin as in capillaries but much larger lumens. In postcapillary venules, the tunica media has pericytes and up to 2-4 indistinct layers of VSMCs. Small (0.2-1 mm diameter) to medium (1-9 mm diameter) sized veins have 2-4 layers of VSMCs mixed with collagen and elastic fibers in the tunica media. The vasa vasorum penetrates deeply into the media of these veins. The tunica adventitia is well developed (thicker than the tunica media) and contains some longitudinal VSMCs. Veins with a diameter greater than 2 mm contain one-way valves to prevent backflow. In large veins (diameter greater than 9 mm), the adventitia is very thick (up to 4 times thicker than the media) and contains longitudinal bundles of SMCs, in addition to collagen and elastic fibers, nerves, and vasa vasorum.

2.2.2 Structure

Like other smooth muscle cells, contractile VSMCs are fusiform, meaning they are largest at their midpoint and taper towards the ends. The nucleus of each cell is located in the center of the broadest part of the cell. VSMCs are 20 – 60 μm long and 1.5 – 5 μm wide in the nuclear region [13]. The narrow part of one cell lies adjacent to the

broad part of neighboring cells, allowing the cells to pack tightly together (Figure 2.5). Gap junctions connect neighboring cells to enable communication and simultaneous contraction. Most of the cytoplasmic organelles, including numerous mitochondria, some cisternae of the rough endoplasmic reticulum, free ribosomes, glycogen granules, and a small Golgi apparatus, are concentrated at each end of the nucleus [14]. The remaining sarcoplasm contains the cytoskeleton and contractile apparatus. VSMCs also secrete large amounts of type I collagen and elastin and divide regularly to replace damaged cells.

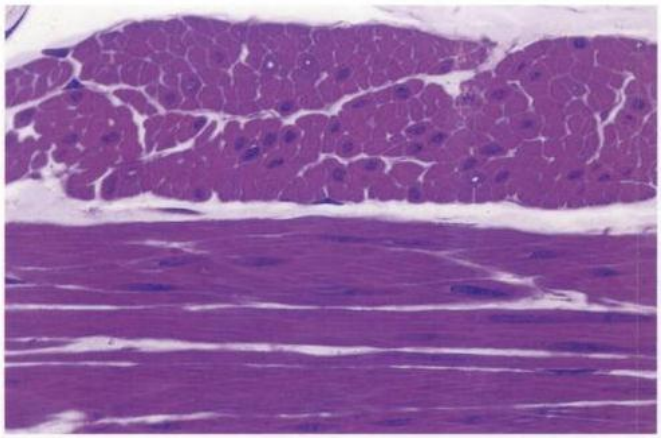

Figure 2.5. Smooth muscle cells in cross section (top) and in longitudinal section (bottom) with phosphotungstic stain [15].

While most fully mature VSMCs are contractile, synthetic VSMCs are also of interest. During vascular development, SMCs differentiate from a synthetic phenotype to a contractile phenotype (Figure 2.6). Synthetic VSMCs are highly migratory, undergo rapid cell proliferation, and exhibit very high rates of extracellular matrix (ECM)

synthesis [16]. They have a low cytoplasmic volume fraction of myofilaments and thus cannot contract. Contractile VSMCs are completely committed to carrying out their contractile function (high cytoplasmic volume fraction of myofilaments). As such, they are largely nonmigratory, have a low proliferation rate, and exhibit very low rates of ECM synthesis [16]. Modulation from synthetic to contractile phenotype is associated with increased expression and reorganization of contractile and cytoskeletal proteins (α actin, myosin heavy chain, calponin, desmin) [17]. Even in adult organisms, VSMCs are not terminally differentiated. A VSMC is capable of major changes in its phenotype in response to changes in local environmental cues including growth factors/inhibitors, mechanical influences, cell-cell and cell-matrix interactions, and various inflammatory mediators (Figure 2.6). The phenotype depends on the complex interaction of the environmental cues and may range from completely synthetic to completely contractile. In a healthy blood vessel, VSMCs exhibit extremely low synthetic activity.

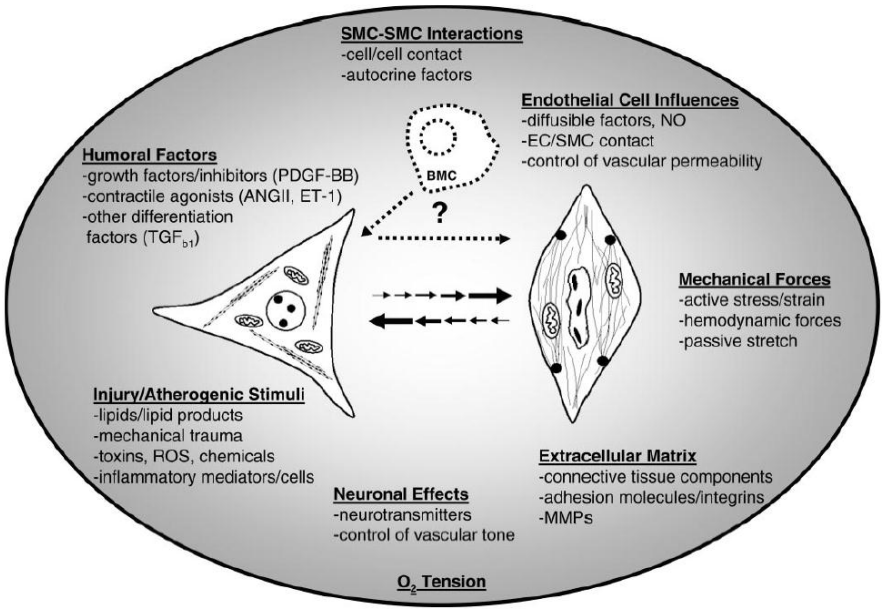

Figure 2.6. Environmental cues that are either known or believed to be important in influencing the differentiation/maturation state of the VSMC. BMC stands for bone marrow-derived progenitor cells which may or may not be capable of becoming fully differentiated SMCs (debated) [15, 16].

2.2.3 Contraction

The smooth muscle contractile apparatus is illustrated in Figure 2.7. Thin filaments contain actin, tropomyosin, and the proteins caldesmon and calponin. Actin binds to myosin II molecules on the thick filaments to generate force. Caldesmon (120-150 kilodaltons) and calponin (34 kilodaltons) are actin-binding proteins that block the myosin-binding site [14]. Thick filaments contain myosin II molecules oriented in one direction on one side of the filament and in an opposite direction on the other side of the filament. The filaments are called side-polar as the polarity of the myosin heads is the same along the entire length of one side of the filament and the opposite on the opposite side. This organization maximizes the interaction between thin and thick filaments,

allowing the thin filaments to be pulled the entire length of the thick filaments. Thin filaments are anchored to dense bodies through the attachment protein α-actinin (31 kilodaltons). Intermediate filaments, composed of desmin and vimentin filaments, also bind to α-actinin. This connection transmits contractile forces generated inside the cell to the cell surface, altering the cell shape. Upon contraction, the cell borders become scalloped and the nucleus folds into a corkscrew configuration. There are several proteins that are also associated with smooth muscle contraction. Myosin light chain kinase (MLCK) (130-150 kilodaltons) is an enzyme that initiates the contraction cycle. Calmodulin (17 kilodalton) is a calcium-binding protein that regulates the intracellular concentration of calcium. The calcium-calmodulin complex binds to and activates MLCK. It may also, with caldesmon, regulate MLCK phosphorylation and release from F-actin.

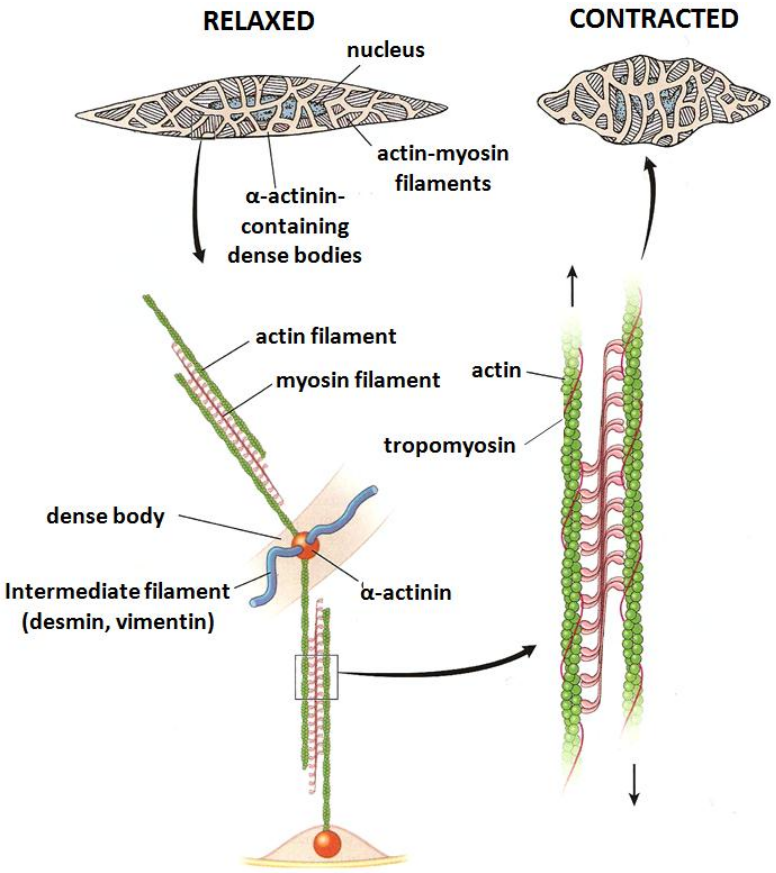

Figure 2.7. Schematic diagram of smooth muscle cell contraction [14].

Diverse signal transduction pathways initiate and control smooth muscle contraction [14]. Mechanical impulses, electrical depolarizations, and chemical stimuli can all trigger contraction. Each leads to an elevation in intracellular calcium, which is directly responsible for muscle contraction. This intracellular calcium increase is achieved either by depolarization of the cell membrane or direct activation of gated calcium-release channels in the smooth endoplasmic reticulum by a second messenger molecule (Figure 2.8). The calcium then binds calmodulin, which activates phosphorylation of the MLCK to initiate contraction. When the regulatory light chain of

myosin is phosphorylated, the actin-binding site of the myosin head is activated and it attaches to actin. In the presence of ATP, the myosin head bends, producing contraction. A long-term contraction is also possible (used often for VSMCs). For this, the myosin head attached to the actin becomes dephosphorylated, causing its ATPase activity to decrease and preventing the head from detaching from the actin filament. Once the contraction cycle is done, calcium is removed from the sarcoplasm by ATP-dependent calcium pumps and returned to the smooth endoplasmic reticulum or removed from the cell entirely. Contraction is propagated from cell to cell via gap junctions.

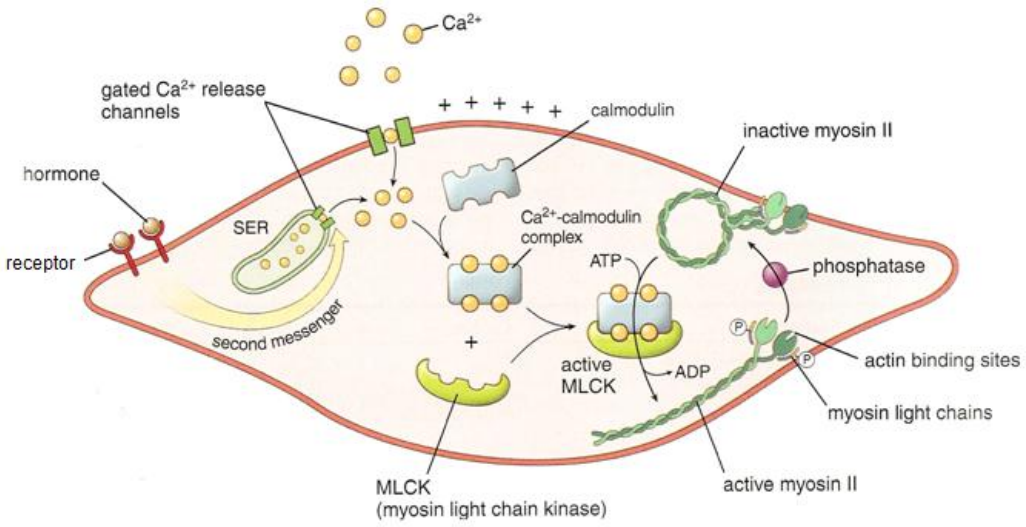

Figure 2.8. Schematic diagram illustrating steps leading to initiation of smooth muscle cell contraction [14].

2.2.4 Vascular Disease

Vascular smooth muscle cells play an integral part in vascular diseases such as atherosclerosis, the number one cause of death in the United States [18, 19]. Atherosclerosis is believed to start with injury to the blood vessel wall, caused by oxidized cholesterol (most common), free radicals, high blood pressure, homocysteine, chemicals released from fat cells, or bacteria and viruses [20]. Figure 2.9 illustrates the disease progression. Typically excessive amounts of low-density lipoprotein (LDL) accumulate beneath the endothelium, where they become oxidized by free radicals in the vasculature. In response, endothelial cells produce chemicals that attract monocytes. Once the monocytes enter the blood vessel wall (beneath the endothelium), they settle and become macrophages. These macrophages phagocytose the oxidized LDL until they become so packed with fatty droplets that they appear foamy under a microscope. Now called foam cells, these engorged macrophages accumulate beneath the endothelium to form a fatty streak (first visible bulge). The fatty streak grows by continued immigration of monocytes and lymphocytes, and SMCs migration from the tunica media to the tunica intima. The SMC migration is triggered by cytokines released at the inflammatory site. Some of the SMCs join the foam cells and even phagocytose lipids. Within the intima, they continue to divide and enlarge, producing atheromas. Others grow as a layer beneath the endothelium with reinforcing collagen, elastin, and other matrix proteins (fibrous cap). Together the lipid-rich core and overlying smooth muscle form a maturing plaque. As it continues to develop, the plaque progressively bulges into the lumen of the vessel and obscures blood flow (Figure 2.10). The oxidized LDL additionally contributes

to the vessel narrowing as it inhibits the release of nitric oxide from the endothelial cells, which normally relaxes the medial SMCs to dilate the vessel. The thickening plaque also inhibits nutrient exchange for cells in the arterial wall, leading to necrosis in the vicinity of the plaque. The damaged area is invaded by fibroblasts which contribute to the fibrous cap. In the later stages of the disease, calcium often precipitates in the plaque. The vessel becomes very hard and expansion is difficult. Figure 2.10 shows a narrowed atherosclerotic vessel.

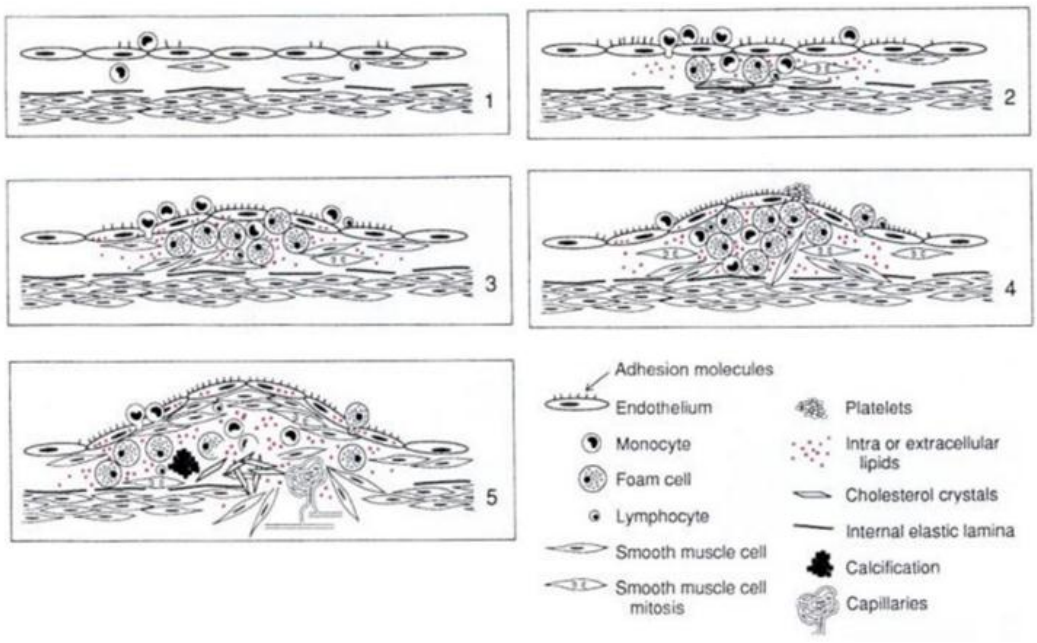

Figure 2.9. Development of atherosclerotic plaque. (1) Normal arterial wall. (2) Transendothelial passage of lipid droplets and monocytes. (3) Crowded foam cells cause the endothelium to bulge (fatty streak). SMCs arise from the tunica media. (4) Plaque growth with increasing number of foam cells and SMCs. Platelets adhere in gaps between endothelial cells. (5) Necrosis occurs in the plaque, followed by the development of cholesterol crystals, calcification, and vascularization from the adventitia [18].

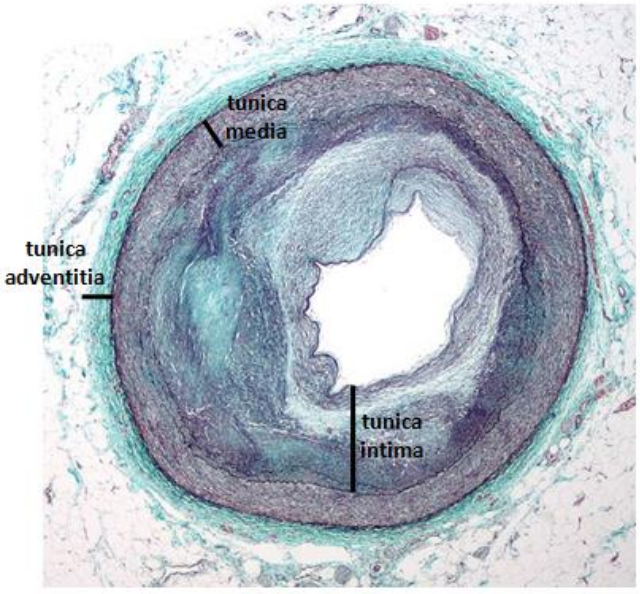

Figure 2.10. Transverse section of distal right coronary artery with complex atherosclerosis and luminal narrowing (Masson's trichrome stain). Smooth muscle cells (red/purple) have infiltrated the tunica intima.

In atherosclerosis, VSMCs undergo a phenotypic shift from a contractile to a synthetic phenotype, enabling them to migrate to the intima, divide rapidly, and secrete large amounts of extracellular matrix proteins. They are thought to play a maladaptive role in lesion development and progression but a beneficial role within the fibrous cap by stabilizing the lesion [21]. This phenotypic shift is not unique to atherosclerosis. With any vascular disease, the environmental cues acting on the VSMCs will change, resulting in altered VSMC phenotypes (Figure 2.6). In systemic hypertension, there is an increase in peripheral resistance as a result of increased vascular tone (SMC contractility) and vascular remodeling [22, 23]. The blood vessels within many cancerous tumors are often immature or defective in that they contain very few SMCs and are greatly enlarged and

leaky [24]. SMCs that are present have gross alterations in morphology and fail to express differentiation marker genes [25]. These changes in VSMC phenotype play a large part in the behavior of the diseased vasculature.

2.3 References

1. Shier, D., J. Butler, and R. Lewis, *Hole's Human Anatomy and Physiology*. 11th ed2007, New York: McGraw-Hill. 1043.

2. Walker, C.A. and F.G. Spinale, *The structure and function of the cardiac myocyte: A review of fundamental concepts.* Journal of Thoracic and Cardiovascular Surgery, 1999. **118**(2): p. 375-382.

3. Germani, A., et al., *Molecular mechanisms of cardiomyocyte regeneration and therapeutic outlook.* Trends in Molecular Medicine, 2007. **13**(3): p. 125-133.

4. Anversa, P. and B. Nadal-Ginard, *Myocyte renewal and ventricular remodelling.* Nature, 2002. **415**(6868): p. 240-243.

5. McDevitt, T.C., et al., *In vitro generation of differentiated cardiac myofibers on micropatterned laminin surfaces.* Journal of Biomedical Materials Research, 2002. **60**(3): p. 472-479.

6. Harvey, R.P. and N. Rosenthal, *Heart Development*1999, San Diego: Academic Press. 240.

7. Eroschenko, V., *Atlas of Histology with Functional Correlations*. 11th ed2008: Lippincott Williams & Wilkins. 177.

8. Silver, F.H., D.L. Christiansen, and C.M. Buntin, *Mechanical properties of the aorta - a review.* Critical Reviews in Biomedical Engineering, 1989. **17**(4): p. 323-358.

9. Shier, D., J. Butler, and R. Lewis, *Hole's Human Anatomy and Physiology*. 11th ed2007, New York: McGraw-Hill. 582.

10. Humphrey, J.D., *Mechanics of the arterial wall: Review and directions.* Critical Reviews in Biomedical Engineering, 1995. **23**(1-2): p. 1-162.

11. Glagov, S., et al. *Microarchitecture and composition of artery walls - relationship to location, diameter, and the distribution of mechanical stress*. 1992. Rapid Science Publishers.

12. Silver, M., A. Gotlieb, and F. Schoen, *Cardiovascular Pathology*. 3rd ed2001: Churchill Livingstone.

13. Fung, Y.C., *Biomechanics: Mechanical Properties of Living Tissues*. 2nd ed2004, New York: Springer Science and Business Media.

14. Ross, M.H. and W. Pawlina, *Histology: A Text and Atlas*. 5th ed2006, Baltimore: Lippincott Williams & Wilkins.

15. Junqueira, L.C. and J. Carneiro, *Basic Histology: Text and Atlas*. 11th ed2005: McGraw-Hill.

16. Owens, G.K., M.S. Kumar, and B.R. Wamhoff, *Molecular regulation of vascular smooth muscle cell differentiation in development and disease.* Physiological Reviews, 2004. **84**(3): p. 767-801.

17. Worth, N.F., et al., *Vascular smooth muscle cell phenotypic modulation in culture is associated with reorganisation of contractile and cytoskeletal proteins.* Cell Motility and the Cytoskeleton, 2001. **49**(3): p. 130-145.

18. Majno, G. and I. Joris, *Cells, Tissues, and Disease: Principles of General Pathology*. 2nd ed2004, New York: Oxford University Press.

19. Lusis, A.J., *Atherosclerosis.* Nature, 2000. **407**(6801): p. 233-241.

20. Sherwood, L., *Fundamentals of Physiology*. 3rd ed2006.

21. Owens, G.K., *Regulation of differentiation of vascular smooth muscle cells.* Physiological Reviews, 1995. **75**(3): p. 487-517.

22. Mulvany, M.J., et al., *Vascular remodeling.* Hypertension, 1996. **28**(3): p. 505-506.

23. Folkow, B., *Physiological Aspects of Primary Hypertension.* Physiological Reviews, 1982. **62**(2): p. 347-504.

24. Eberhard, A., et al., *Heterogeneity of angiogenesis and blood vessel maturation in human tumors: Implications for antiangiogenic tumor therapies.* Cancer Research, 2000. **60**(5): p. 1388-1393.

25. Morikawa, S., et al., *Abnormalities in pericytes on blood vessels and endothelial sprouts in tumors.* American Journal of Pathology, 2002. **160**(3): p. 985-1000.

CHAPTER THREE

LITERATURE REVIEW: MECHANICS

3.1 Cell Mechanics

3.1.1 Importance

All cells are subject to mechanical stimuli, such as shear stress, compression, tension, vibration, and pressure. Some cell types also exert forces on surrounding tissues (e.g., muscle cells contract). All cell types can sense and respond to forces by converting the mechanical stimuli into a biochemical response in a process known as mechanotransduction. Depending on their environment, cells continually remodel their internal structure, thereby changing their mechanical properties. Studies have shown that cell growth, differentiation, migration, contractility, and apoptosis are all influenced by changes in cell shape and structural integrity (mechanical properties) [1-4]. Any deviation in cell structural and mechanical properties can result in the breakdown of physiological function and may lead to disease [5, 6]. Table 3.1 outlines several diseases associated with abnormal mechanotransduction. Thus, it is essential to fully understand cell mechanics to explain the fundamental aspects of cell behavior and disease processes.

Table 3.1. A partial list of diseases that result from abnormal mechanotransduction. The right column indicates whether the mechanical basis of the disease is likely due to changes in cell mechanics (C), alterations in tissue structure (T), or deregulation of mechanochemical conversion (M) ("?" indicates situations where deregulation of mechanochemical conversion is likely but remains to be demonstrated) [5].

Cardiology	Angina (vasospasm)	CT
	Atherosclerosis	TM
	Atrial fibrillation	M
	Heart failure	CTM?
	Hypertension	CTM?
	Intimal hyperplasia	CTM?
	Valve disease	T
Dermatology	Scleroderma	T
Gastroenterology	Achalasia	C
	Irritable bowl syndrome	CM?
	Volvulus	CT
Nephrology	Diabetic nephropathy	CTM?
	Glomerulosclerosis	CTM?
Neurology	Cerebral edema	T
	Facial tics	C
	Hydrocephalus	TC?
	Migraine	CM?
	Stroke	CT
	Stuttering	C
Oncology	Cancer	CTM?
	Metastasis	C
Opthalmology	Glaucoma	CTM?
Orthopedics	Ankylosing spondylitis	CT
	Carpal tunnel syndrome	CT
	Chronic back pain	CT
	Dupytren's contracture	CT
	Osteoporosis	TM
	Osteoarthritis	T
	Rheumatoid arthritis	T
Pediatrics	Collagenopathies	T
	Congenital deafness	CTM
	Mucopolysaccharidoses	T
	Musculodystrophies	CTM
	Osteochondroplasias	CT
	Polycystic kidney disease	TM
	Pulmonary hypertension of newborn	CTM?
Pulmonary medicine	ARDS	CTM
	Asthma	CTM?
	Emphysema	T
	Pulmonary fibrosis	T
	Pulmonary hypertension	CTM?
	Ventilator Injury	CM
Reproductive medicine	Pre-eclampsia	CTM?
	Sexual dysfunction	CM?
Urology	Urinary frequency/incontinence	CM?

3.1.2 Cell Structure

When considering cellular mechanics, it is important to understand the structural components of a cell. The cytosol makes up approximately 70% of the cell volume and is composed of water, salts, and organic molecules [7]. However, the cytoskeleton, which maintains cell shape, enables migration, and plays important roles in intracellular transport and cell division, is most often discussed when considering cell mechanics. Numerous studies have shown that the cytoskeleton contributes substantially to cellular mechanical behavior [8-10]. It is made of three types of protein filaments – intermediate filaments, microtubules, and microfilaments (aka actin filaments), as shown in Figure 3.1.

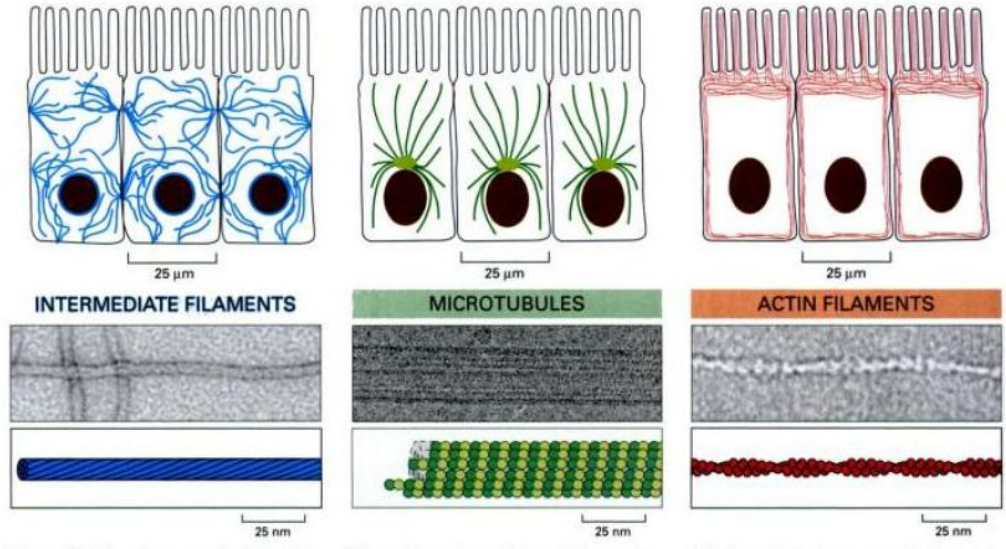

Figure 3.1. Cytoskeletal components with approximate cellular distribution indicated in epithelial cells [11].

Intermediate filaments are approximately 10 nm in diameter and have a persistence length of approximately 1 µm [12]. They have great tensile strength, enabling cells to withstand mechanical stresses associated with stretching. They typically form a network throughout the cytoplasm, anchoring organelles and serving as the main structural component of the nuclear lamina and sarcomeres. They also participate in some cell-cell and cell-matrix junctions. The subunits of intermediate filaments are elongated fibrous proteins, each composed of an N-terminal globular head, a C-terminal globular tail, and a central elongated rod domain. The rod domain consists of an extended α-helical region that enables pairs of intermediate filament proteins to wrap around each other in a coiled-coil configuration to form a stable dimer. Two dimers then bind to one another to form a tetramer, and tetramers bind end-to-end and side-by-side to

generate the ropelike intermediate filament. Because of this hierarchical structure, intermediate filaments can deform several times their initial length when needed [13].

Microtubules are approximately 25 nm in diameter and have a persistence length of approximately 1 mm [12]. They are long, straight, hollow cylinders that primarily resist tension in cells. Alpha and beta tubulin dimers polymerize end to end (α subunit of one tubulin dimer contacts the β subunit of the next) to form protofilaments, which then bundle into hollow cylindrical filaments. The protofilaments typically arrange themselves in an imperfect helix with one turn of the helix containing 13 tubulin dimers each from a different protofilament. A microtubule is said to have polarity because there is one positive end (all β tubulin dimers exposed) and one negative end (all α tubulin dimers exposed). Microtubules typically have one end attached to a single centrosome (microtubule-organizing center) and they aid in intracellular transport.

Microfilaments are approximately 7 nm in diameter and have a persistence length of approximately 17 μm [12]. They are most concentrated just beneath the plasma membrane and they serve a number of functions. They are flexible and resist tension, link transmembrane proteins to cytoplasmic proteins, anchor the centrosomes at opposite poles during mitosis, and pinch dividing cells apart during cytokinesis. The head-to-tail polymerization of actin monomers forms a fiber termed filamentous actin (F-actin). Two helical interlaced strands of F-actin make up each microfilament. Like microtubules, microfilaments are polarized.

Cells anchor to underlying extracellular matrix (ECM) scaffolds and neighboring cells by physically coupling their tensed cytoskeletal filaments to specific receptors that

cluster within localized adhesion sites (Figure 3.2). These adhesion sites are called focal adhesion complexes when they mediate cell-ECM adhesion and junctional complexes (adherens junctions, desmosomes) when they mediate cell-cell adhesion [14]. Focal adhesion complexes are comprised of clusters of transmembrane integrins bound to the ECM and actin-associated molecules. Integrins are heterodimeric proteins made up of different α and β subunits. The specific combination of the different subunits defines the molecular binding specificity. For example, integrin α5β1 binds fibronectin and α2β1 binds collagen [15]. Proteins such as talin, vinculin, α-actinin, and paxillin connect the cytoplasmic tail of integrins to microfilaments and, to a lesser extent, intermediate filaments [14]. Junctional complexes physically couple the cytoskeleton of one cell to that of its neighbor. Specialized cell-cell adhesion molecules (cadherins, selectins) use some of the same actin-associated proteins as focal adhesion complexes (vinculin, α-actinin) but not others (talin) [16]. Cantenins also connect cadherins to microfilaments within adherens junctions. Desmosomes connect intermediate filaments of neighboring cells.

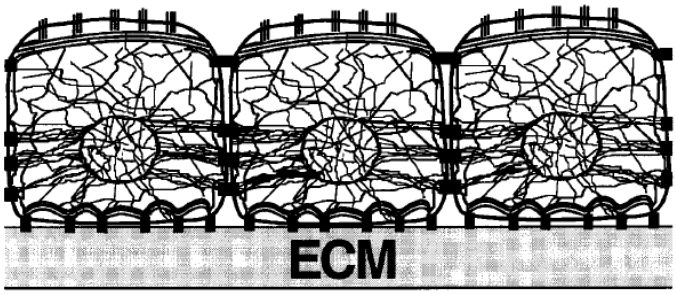

Figure 3.2. The intracellular cytoskeleton connects to the underlying extracellular matrix through focal adhesion complexes and with neighboring cells through specialized junctional complexes [17].

3.1.3 Cell Mechanical Properties

Due to their complex structure, cells have unique mechanical properties. They exhibit viscoelasticity, heterogeneity, and anisotropy. A viscoelastic material is defined as a material where the stress depends on the strain history of the material [18]. Viscoelastic materials exhibit hysteresis, stress relaxation, creep, and strain rate-dependent material properties (Figure 3.3). Hysteresis is the dissipation of energy during loading-unloading cycles. It can be visualized as the area between the loading and unloading curves on the stress-strain plot. The stress-strain behavior of a viscoelastic material depends on the strain rate. When a material is maintained at a constant strain, stress relaxation describes the reduction in stress in the material over time. Creep is defined as a continued deformation over time of a material maintained under a constant stress. Cells are described as heterogeneous and anisotropic because their material properties differ throughout the cell and are directionally dependent. This is largely due to the uneven arrangement of the cytoskeleton throughout the cytoplasm of the cell. Cells are also known to actively remodel their cytoskeleton. Therefore, their mechanical properties are dynamic in nature.

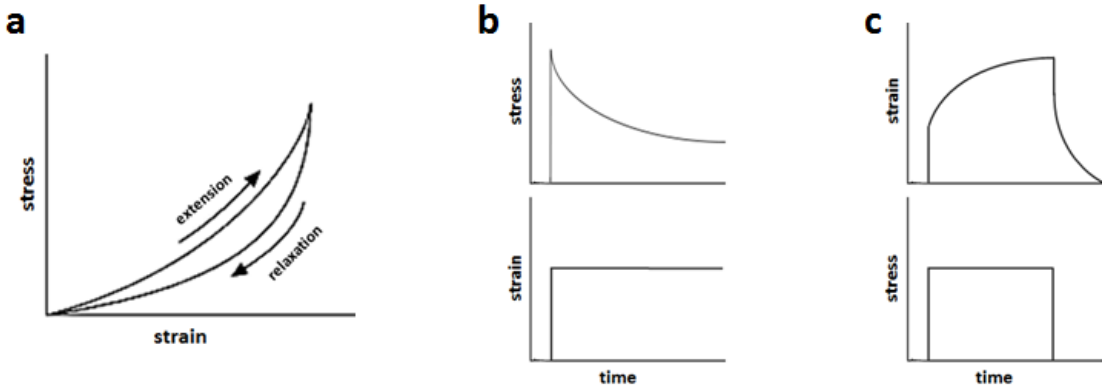

Figure 3.3. Viscoelastic material behavior. (a) Stress-strain curve. Hysteresis is area between loading and unloading curve. (b) Stress-relaxation. (c) Creep.

3.1.4 Vascular Smooth Muscle Cell Mechanics

The mechanical properties of VSMCs depend on their phenotype, which can change dramatically in development and with varying environmental cues. When individual VSMCs are studied in culture, they quickly take on a synthetic phenotype [19]. Hemmer et al. examined the role of various cytoskeletal components in determining VSMC stress relaxation behavior [20]. They found that actin depolymerization resulted in significant increases in both rate and percentage of relaxation, while microtubule stabilization caused significant decreases in rate and percentage of relaxation. Several studies have shown that VSMCs stiffen in response to stretching [21]. Sun et al. applied forces to specific extracellular matrix adhesion sites on VSMCs [22]. They discovered that this mechanical force, when applied to integrin-fibronectin binding sites, induced an actin-dependent myogenic-like event (contraction). Researchers have been able to study contractile VSMCs by starving the cells of serum in culture, which has been shown to induce a contractile phenotypic shift. In a recent study, serum starved (contractile)

VSMCs were found to be significantly stiffer (15.3 kPa) than serum fed (synthetic) cells (11.1 kPa) after five days in culture [23]. The elastic modulus of both the serum starved and fed VSMCs decreased over time in culture.

3.1.5 Heterogeneity

In several studies, researchers found a large variability in whole-cell mechanical properties between cells in a single population [8, 23-27]. This heterogeneity has been observed in many cell populations, including osteoblasts, chondrocytes, fibroblasts, endothelial cells, and smooth muscle cells, and with several measurement techniques. In particular, the coefficient of variation (COV = standard deviation/mean) values for cellular mechanical parameters within a single population are in the range of 43-103% in atomic force microscopy studies and 30-128% in micropipette aspiration studies [28]. This variability cannot be credited to the measurement techniques, as their repeatability has been statistically confirmed (repeated measurements of mechanical properties for a single cell have COV of only 5%) [24].

Hemmer et al. recently reported measures of elastic moduli for both serum-starved and serum-fed VSMCs [23]. Serum fed VSMCs take on a synthetic phenotype after a short time in culture while serum starvation induces a shift toward a contractile phenotype. For each sample, they indented fifteen cells five times each using standard AFM indentation techniques. Care was taken to choose 'spread' VSMCs for the serum-fed group and 'spindle-shaped' VSMCs for the serum-starved group to ensure all cells tested in each sample group were of a similar phenotype. Table 3.2 outlines the COV

values for the measured elastic moduli. The average COV for repeated measurements on a single cell was 6.0 ± 5.3% while the average cell-to-cell COV was much higher at 32.0 ± 9.5%.

Table 3.2. Cell-to-cell and repeated point elastic modulus coefficient of variation (COV) for VSMCs [23].

	Cell-to-cell COV (%)	Repeated point COV (%)
3 day Serum-fed	20.6	4.1
3 day Serum-starved	42.3	4.2
5 day Serum-fed	36.8	10.3
5 day Serum-starved	28.4	5.3
All (mean ± standard deviation)	32.0 ± 9.5	6.0 ± 5.3

Currently, it is not entirely clear why cells from a single population exhibit this mechanical heterogeneity. It is important to determine the source of this heterogeneity to remove confounding variables that can obscure the results of studies, such as those studying effects of disease or treatments on cellular mechanical behavior. In the experiments by Hemmer et al., cells with different phenotypes had significant differences in their mechanical properties [23]. However, the cell-to-cell COV for cells exhibiting the same phenotype were still high (Table 3.2). Thus, phenotypic differences in cells from a single population do not entirely explain the phenomenon. Jaasma et al. also explored the effects of cell phenotype, in addition to confluency and morphology [28]. They too saw a significant difference in the elastic modulus of cells with different phenotypes. They also observed that confluent cells were 1.5-1.8 times stiffer than nonconfluent cells. The projected nucleus area, cell area, and cell aspect ratio (morphology) did not correlate with mechanical behavior. These results suggest that

cytoskeleton structural parameters, such as filament density, filament crosslinking, and cell-cell and cell-matrix attachments, dominate inter-cell variability in whole-cell mechanical behavior. However, further studies must be done to gain a complete understanding of cellular mechanical heterogeneity.

3.2 Techniques for Mechanically Probing Cells

There are several techniques that apply mechanical forces to living cells in order to evaluate molecular signaling and the physical response. These methods are often conceptually simple but require the imposition of precise forces. In many methods, a group of cells are subject to a deformation or physical stress and then assayed as a group. More recently the focus has shifted to mechanically probing individual cells. The force applied can either be concentrated to one location or distributed over the entire cell. It can also be transient or dynamic. Figure 3.4 outlines the basic principles for the most common techniques.

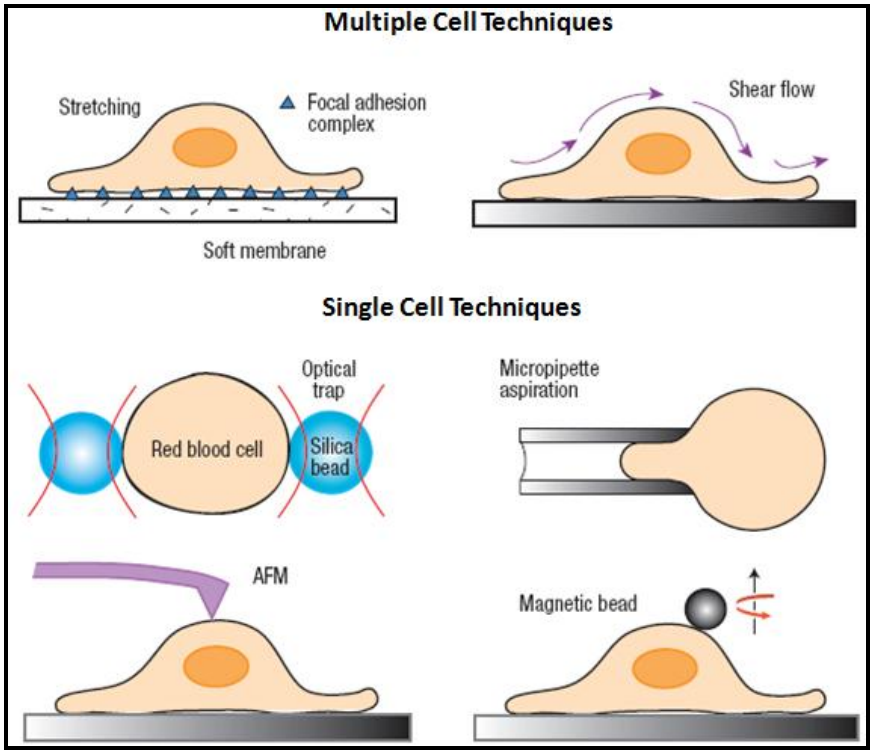

Figure 3.4. Schematic representation of experimental techniques commonly used to mechanically probe cells [29].

3.2.1 Groups of Cells

Many techniques have been developed to evaluate the physical response of groups of cells to stresses similar to what they experience in their native physiological environment. Typical stimuli applied to groups of cells include shear stress, stretch, and pressure changes. These methods have been used for nearly two decades and have many variants and combinations. They do not directly measure cellular mechanical properties but rather, asses the cellular response through various analytical techniques (e.g, Western blot to detect changes in specific protein concentration).

Membrane Stretch

Cells can be subject to a fixed strain by stretching an elastic membrane (often silicone elastomer) that the cells are cultured on. Collagens and fibronectin are often used to coat the membrane to enhance cellular adhesion. Strain rates typically range from 0.1 to 10 Hz and strain percentages range from less than 1% to greater than 30% [30]. One dimensional stretch is achieved by pulling the membrane in one direction, while leaving the membrane edges free or fixing them in place. If the edges are free, the membrane can distort freely and there will be compression in the direction perpendicular to the strain. If they are fixed, there will be no such compression. Two dimensional stretch devices strain the membrane in two directions at once, producing a more uniform strain field. A piston strain device has a piston that moves vertically relative to the membrane. In a pressure strain device, the membrane is sealed and gas is introduced and removed to vary the pressure and deform the membrane. In these devices, the strain transmitted to each cell is nearly equal in all directions (except near edges but few cells there). These stretching techniques not only impose a fixed strain on the cells; they also impose a fluid shear stress as the media above the cells flows with the deformation. This unintentional stress can be complex, difficult to predict, and may influence results [31].

Shear Stress

Shear stress can be applied to a monolayer of cells by moving fluid through a flow chamber. A pressure-driven flow chamber typically has a fully developed parabolic laminar flow profile. In a cone-and plate flow chamber, a cone is rotated relative to a

fixed plate that contains a monolayer of cells. This results in a linear flow profile with uniform shear stress. There are many possible variants on these designs. For example, the cross-section of a pressure-driven flow chamber may be circular or rectangular. Flow may be unsteady and geometric changes may be included to simulate a particular biological condition. It is important to maintain laminar flow to keep a constant level of uniform shear stress. Flow chambers are often used to study the effects of shear stress on endothelial cells, where typical shear stress levels range from 1 to 20 dynes/cm^2 [30].

Other Methods

There are several other methods to mechanically stimulate groups of cells. Elevated hydrostatic pressure can be produced with compressed air or a column of fluid above the cells. Cells may also be cultured on a stiff, porous substrate and be subjected to a transmembrane pressure (elevated pressure in sealed chamber above cells, atmospheric pressure below cells) [32]. Cells embedded in gels or tissues can be compressed by pistons linked to motors and actuators [33]. Entire blood vessels may be internally pressurized with media, thus experiencing simultaneous wall strain and hydrostatic pressure [34]. Low-intensity pulsed ultrasound, a form of mechanical energy transmitted as high-frequency acoustical pressure waves, has also been used to stimulate cells [35].

3.2.2 Single Cells

The primary advantage to mechanically probing single cells is the ability to examine the variability (heterogeneity) of data from individual cells. It is also possible to focus the applied stress on a given region of the cell. Most of the forces applied to individual cells range from 1 pN to 10 nN [30]. Many of the techniques apply precise forces to particles (0.1 to 10 μm diameter) that are attached to the cells through an adhesive ligand or antibody for a specific receptor. Local stresses can be applied to the cell by using a small number of particles while nearly global stresses may be applied by using many particles covering the entire cell surface. The force application may be either steady or vary with time. Disadvantages of particle use includes particle internalization due to phagocytosis, nonuniform particle distribution on the cell surface, variations in antibody or ligand coating, incorrect particle orientation, and nonspecific binding. Despite these limitations, the use of particles to apply highly specific forces to cells is still very popular.

Optical Traps

Optical traps (aka optical tweezers) use a laser to control the position of a particle [36]. When the particle is placed in the light gradient, the sum of all rays passing through it generates an imbalance in force, tending to push the particle towards the brighter region of light. The laser functions as a trap as strong light gradients all point towards the center at the point of focus. The gradient force in the region beyond the focus must be adequate to overcome the scattering force, which would otherwise propel the particle along the

optical axis (Figure 3.5) [37]. The main limitation with optical trapping is that only one particle can be controlled at a time with a single laser. The force acting on a particle is determined based on the distance between the center of the particle and the laser focal point. Thus, high spatial resolution of particle position and feedback control are required. Optical traps can generate tens to hundreds of piconewtons of force per particle. One adaptation of this technique uses two particles attached to the opposite ends of a cell to produce cellular deformation [38]. Optical traps are often used to study membrane and cell elasticity, local responses, and force generation by structures at the molecular scale, such as kinesin motors [39].

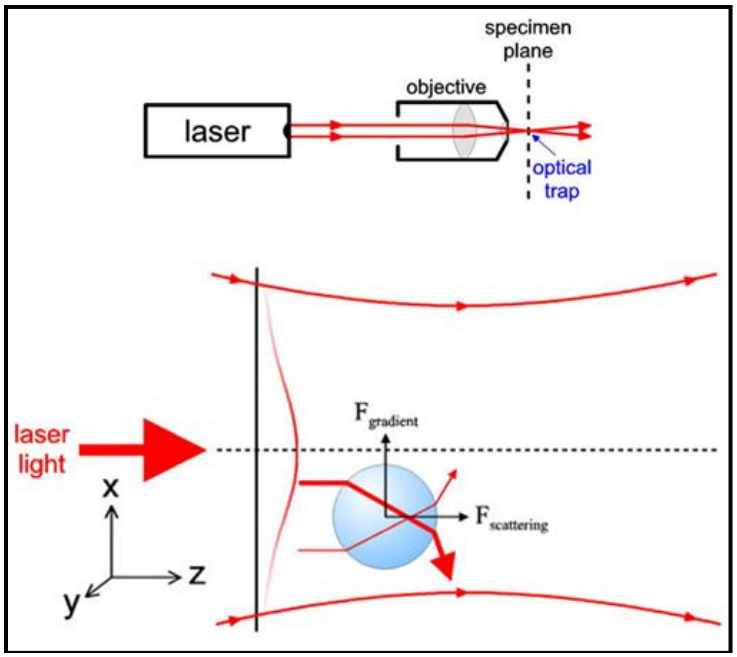

Figure 3.5. Optical trap principles. A laser beam is focused by a high-quality microscope objective to create an optical trap which is able to hold a small particle at its center (top). The particle experiences light scattering and gradient forces (bottom) [40].

Magnetic Traps

Magnets can be used to apply a linear force or a twisting torque to a particle [41, 42]. To create a linear force, one or more electromagnetic poles (wires wrapped around paramagnetic or ferromagnetic core) are used. When current is passed through the wires, the pole becomes magnetized and paramagnetic or ferromagnetic particles are attracted to the pole. This force can be amplified with a pole design that converges to a sharp tip and reduced with a blunt tip pole design. Figure 3.6 shows a typical high force cell probe design. Feedback is required to apply a fixed, specific displacement to a particle. A single pole will affect many particles simultaneously, but the forces acting on each particle will differ with particle composition, particle size, and field strength. Multiple poles, with different current amplitudes and directions, can be used to generate a nearly uniform magnetic force field in any direction over tens to hundreds of cells. The magnetic content of each particle influences the force applied to the attached cell. Ferromagnetic particles can generally exert a high force but they retain some of their magnetization each time they're exposed to the magnetic field. Paramagnetic particles exert smaller forces but are less susceptible to magnetization. Paramagnetic beads can generate hundreds of piconewtons per bead for an area magnetic trap and tens of nanonewtons per bead for a single-pole trap (assuming distance of 10 – 100 μm from cells to tip) [30]. In magnetic twisting, a brief magnetic field is pulsed on the sample to magnetize the beads with a specific orientation. A much larger counterpulse is then generated in a different direction, inflicting a rotational force on the beads as they try to realign with the new field.

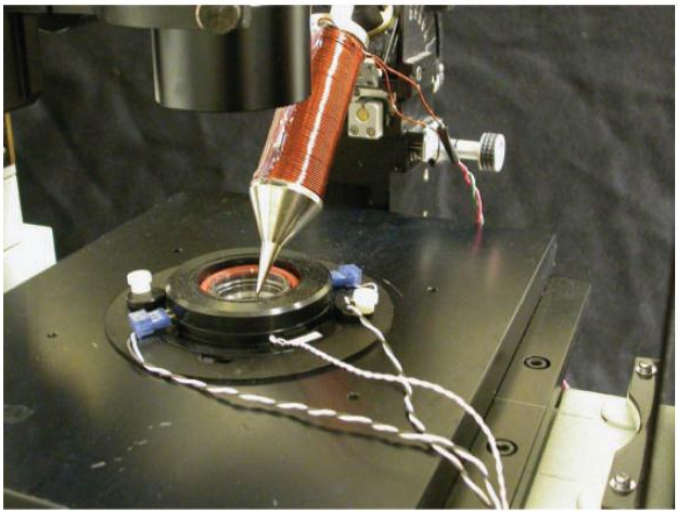

Figure 3.6. Magnetic trap for high force cell probing, composed of electromagnet with sharp tip on a micromanipulator. Imaging is performed on a microscope stage with a stage heater to maintain physiologically relevant temperatures [30].

Atomic Force Microscopy

Atomic force microscopy (AFM) is most commonly used to image samples with nanometer resolution [43]. A fine tip, attached to a small cantilever, scans the surface of the sample. The tip-cantilever assembly is typically fabricated from silicon or silicon nitride using technology similar to that used in integrated circuit fabrication [44]. The important parameters of the tip are the sharpness apex, measured by the radius of curvature, and the aspect ratio of the entire tip (Figure 3.7). In general, sharper tips yield more detailed images (better resolution). The most standard tip is a 3 μm tall pyramid with an end radius of approximately 30 nm (Figure 3.8). Tips are available in various shapes and with many coatings for optimal use in a variety of conditions. Particle tips are often used for cell indentation experiments because they have a defined geometry and are easy to model. They work well for determining average cell properties, while shaper tips

are used for measuring local properties. The cantilever may either be V shaped or have a single arm (Figure 3.7). Because of their geometric differences, each type of cantilever has different mechanical properties (spring constant and resonant frequency). The cantilever is attached to a small glass chip that allows easy handling and positioning in the AFM.

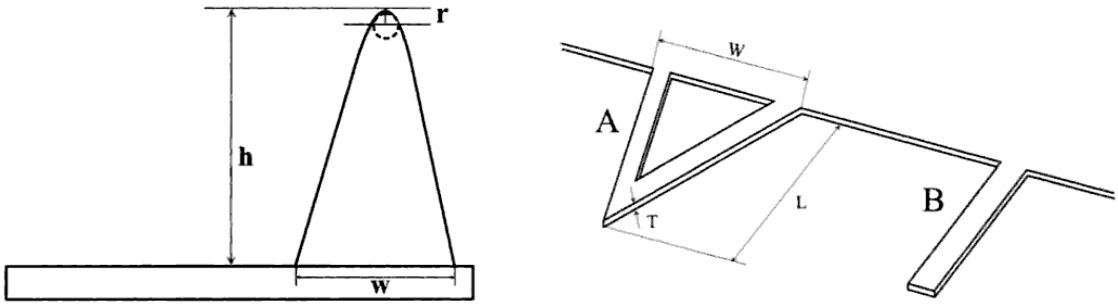

Figure 3.7. Tip and cantilevers. The essential parameters in a tip are the radius of curvature (r) and the aspect ratio (ratio of h to w) (left). Triangular (A) and single beam (B) cantilevers (right). Mechanical properties, such as the force constant and resonant frequency, depend on the values of width (W), length (L), and thickness (T) [45].

Figure 3.8 outlines operation of an atomic force microscope in contact mode imaging. As the cantilever scans the surface, it deflects vertically due to atomic interactions between the tip and the sample. A laser beam is reflected off the backside of the cantilever onto a position-sensitive 4-quadrant photodetector. The distance between the cantilever and detector is generally three orders of magnitude greater than the length of the cantilever. This allows the tip deflection to be greatly magnified, resulting in extremely high sensitivity. A feedback loop is formed as the cantilever deflection signal from the photodetector is compared to a set point and the piezoelectric scanner is told to

move up or down to follow the surface morphology while maintaining constant interaction forces. The piezoelectric scanner is an extremely accurate positioning stage that moves either the tip over the sample or the sample under the tip (depending on AFM design). A topographic image is obtained by storing the vertical control signals sent to the scanner by the feedback circuit. AFM may be operated in air or fluid and in contact or intermittent mode.

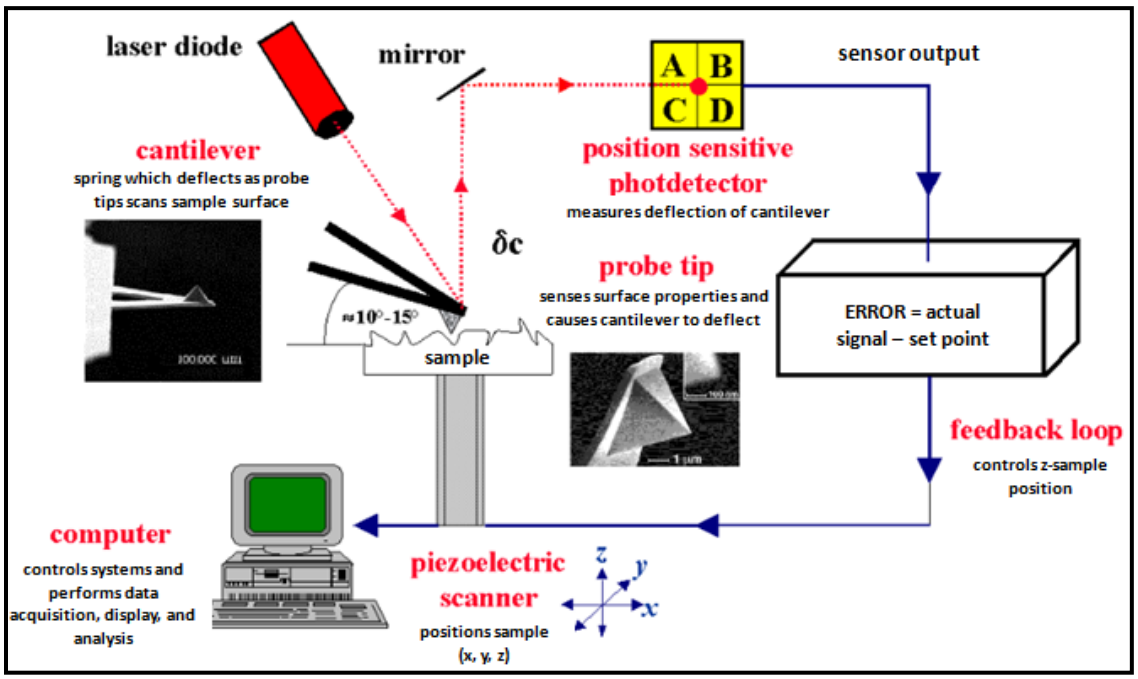

Figure 3.8. Atomic force microscope: general components and their functions [46].

Because AFM combines high sensitivity in applying and measuring forces, high precision in positioning the tip relative to the sample in all three dimensions, and the possibility to operate in liquids, it's well suited for investigating cellular mechanics [47]. The AFM can also be used in conjunction with an inverted microscope that allows the

user to visually position the tip directly over the cell to be probed. Nanoindentation experiments are performed by extending and retracting the tip into the cell surface. A "force curve" of the cantilever deflection verses the indentation depth results from each indentation (Figure 3.9). The cantilever deflection (nm) is converted to force (nN) using the spring constant of the cantilever (N/m). More recently, researchers have investigated viscoelastic (time-dependent) cell properties through indentation and hold (stress relaxation) experiments (Figure 3.10) [20].

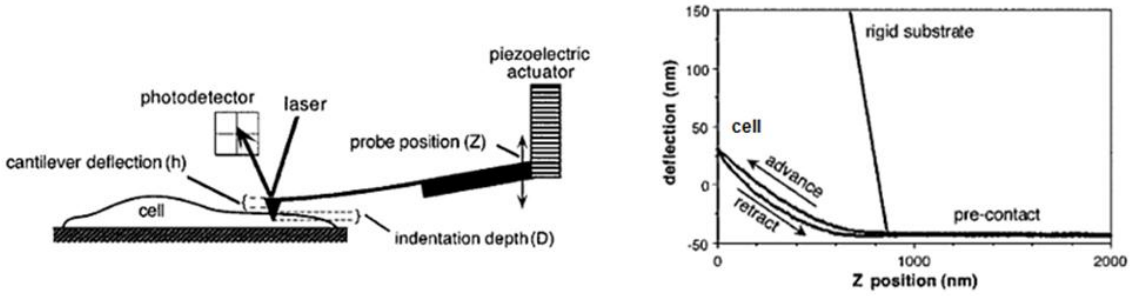

Figure 3.9. Schematic of AFM cell indentation experiment. Cantilever position is controlled by a piezoelectric ceramic actuator while probe deflection is sensed by the reflection of a laser onto a 4-quadrant photodetector (left). When the probe contacts the cell, further changes in probe position (Z) result in a combination of cantilever deflection (h) and cell indentation (D), depending on the spring constant of the probe, the geometry of the tip, and the mechanical properties of the cell. Resulting measurements of cantilever deflection (h) versus probe position (Z) during advancement and retraction of the probe yield the force curve (right) [48].

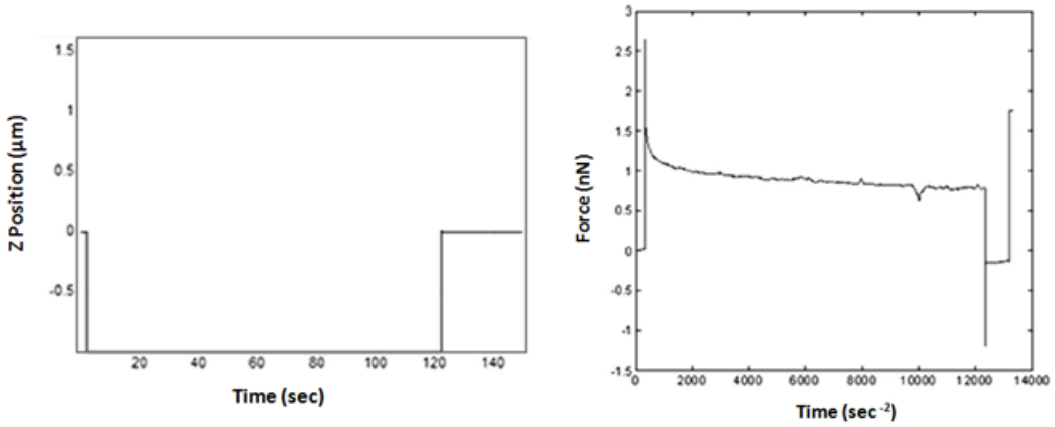

Figure 3.10. Stress relaxation data for vascular smooth muscle cell. Z-piezo movement verses time (left) and correlating cantilever deflection force versus time (right) [20].

Since AFM has the ability to both image and mechanically probe samples, it's possible to correlate cellular microstructure and mechanics [49]. Researchers have also mapped out individual cellular mechanics by probing a cell at various locations over its surface [50, 51]. There are several modifications to the traditional indentation technique which often measure adhesion forces between cells, molecules, and substrate components. In one method, adhesion forces can be measured by attaching a molecule or cell to the tip and lowering this onto a surface-bound cell, allowing them to interact, and then pulling them apart [52]. An inclined cantilever can be used to laterally dislodge a cell to measure cell-substrate adhesion forces in a technique termed manipulation force microscopy [52]. Because of the wide range of applications, AFM is the most widely used tool for studying mechanical properties of living cells [53].

Micropipette Aspiration

Micropipette aspiration produces a cellular deformation that is opposite of that produced by the AFM, in that the cell surface is extended into the pipette rather than depressed into the interior of the cell [54]. A glass micropipette, with an inner diameter smaller than the size of the cell, is brought into contact with the cell (Figure 3.11). A known suction pressure is applied within the pipette, causing the cell to deform and flow into the pipette. Several cellular mechanical properties can be estimated by measuring the length of aspiration. If the aspiration pressure is above a critical value, the cell is completely aspirated and forms a capsule shape inside the pipette. It will travel down the pipette at a velocity that depends on the pressure difference across the cell. If the cell is expelled from the pipette, it will slowly recover to its original shape.

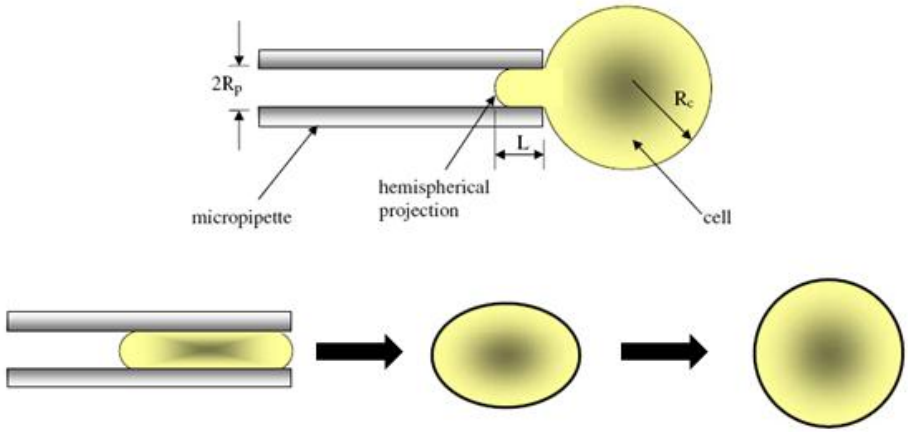

Figure 3.11. Micropipette aspiration setup where cell of radius R_c is being aspirated into a pipette of radius R_p at suction pressure ΔP (top). Once expelled from the pipette, the cell slowly recovers its original shape (bottom) [55].

Other Methods

In a less common technique, called microplate manipulation, two parallel plates squeeze, pull, or twist a cell while imaging its cytoskeleton to evaluate distortion and the mechanical response [56]. Attempts have also been made to apply controlled mechanical forces or deformations to individual cells using microfabricated or microelectromechanical systems (MEMS) devices (Figure 3.12). Finally, microfluidics and micropatterning techniques impose physical constraints rather than applying external forces to a cell. These methods demonstrate how cell geometry can influence the ability of the cell to migrate and interact with other cells.

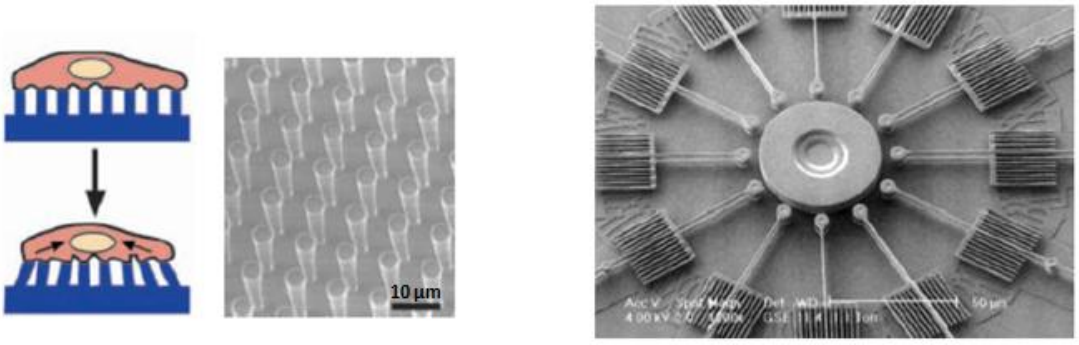

Figure 3.12. Microfabricated arrays of elastomeric, microneedle-like points (left) [57]. Microfabricated MEMS device consisting of multiple passive and active cantilever beams for measuring the forces generated by a cell at different locations, and for applying a localized shear force to a single cell that would 'sit' on the cluster of circle pads at the ends of the cantilever beams (right) [29].

3.3 Mechanical Models

3.3.1 Single Cell Models

The goal in creating a single cell mechanical model is to quantitatively evaluate the mechanical properties and responses of cells subjected to the various mechanical probing techniques described in Section 3.2. This is difficult as cells exhibit highly complex mechanical properties (Section 3.1.3). Additionally, the probing techniques have different types, magnitudes, and rates of loading applied to the cell, so they elicit different mechanical responses. Therefore, there is a wide variety of mechanical models that are used to describe these responses. In general, the models can be divided into two groups: those derived using a continuum approach and those derived using a structural approach. The continuum approach ignores the details of the microstructure and treats the cell as comprising materials with certain continuum material properties (usually elastic or viscoelastic material). From experimental observations, the appropriate constitutive material models and associated parameters are derived. This approach is advantageous in that stress distributions can be easily determined through more established methods that are commonly used for traditional materials. However, continuum models do not account for the true biological character of the cell and they make many simplifying assumptions. In the structural approach, the cytoskeleton is considered the primary structural component of the cell. A network of discrete structural elements works in harmony to respond to mechanical stimuli. These models incorporate the cell microstructure but are much more computationally intensive than continuum-based models.

Continuum-Based Models

Hertz Model

The Hertz model was originally developed to describe the elastic behavior of two spheres in contact [58]. The theory makes many assumptions including homogeneous, isotropic, linear elastic material properties, infinitesimal deformation, and infinite sample thickness and dimensions [59]. Most AFM indentation studies utilize the Hertz model to evaluate the elastic modulus of a cell according to Equation 3.1. Force and indentation data are collected by the AFM. The radius of the indenter is known and the cell's Poisson's ratio is typically assumed to be 0.5 [60].

Equation 3.1. Force of spherical indenter on sample according to Hertz model [61].

$$F = \frac{4}{3}\frac{E}{(1-\upsilon^2)}R^{\frac{1}{2}}\delta^{\frac{3}{2}}$$

F – force
E – elastic modulus
v – Poisson's ratio
R – radius of indenter
δ – indentation depth

Unfortunately, the assumptions in this model are far too simplistic to accurately describe cellular behavior. Cells have heterogeneous, anisotropic, viscoelastic material properties and the tip indentation is relatively large compared to the size of the cell. Consequently, reported values must be interpreted with caution. Elastic moduli estimated with this model are typically in the higher range of measured values (tens to hundreds of kPa compared to 0.1 to 10 kPa in other techniques) [30]. For greatest accuracy, the model should be applied for small strains (up to 10%) [23]. Despite these issues, the

Hertz model is used often to provide a simple measure of cellular mechanics. It is most useful in comparison studies when exact measurements are not required.

Viscoelastic Models

Several models of viscoelasticity are used to describe the mechanical behavior of cells. The most commonly used models are the Power Law relaxation model, the Kelvin model, the Quasilinear Viscoelastic model, and the Generalized Maxwell model [62]. The Power Law simply fits Equation 3.2 to the cellular stress relaxation data, like that seen in Figure 3.3b. Values for A and alpha are chosen to best fit the data. A is primarily chosen to match the amplitude of the stress data while alpha governs the rate of decay.

Equation 3.2. Power Law Relaxation function.

$$\sigma = At^{-\alpha}$$

The rest of the models are mechanical models that can be described as a combination of linear springs and dashpots. A linear spring produces an instantaneous deformation proportional to the load. This behavior is described by Equation 3.3 where k is the elastic modulus of the material (N/m^2). A dashpot produces a velocity proportional to the load at any instant (viscous damper). This behavior is described by Equation 3.4 where η is viscosity of the material ($N \cdot s/m^2$).

Equation 3.3. Spring equation where stress (σ) is analogous to force, strain (ε) is analogous to displacement, and the elastic modulus (k) is analogous to the spring constant.

$$\sigma = k\varepsilon$$

Equation 3.4. Dashpot equation where stress (σ) is analogous to force, the strain rate ($\dot{\varepsilon}$) is analogous to the displacement rate, and η is viscosity.

$$\sigma = \eta\dot{\varepsilon}$$

A Maxwell element is the most basic element used in all the models. It consists of a spring and a dashpot in series, as shown in Figure 3.13a. The spring and dashpot experience the same stress (analogous to force) while the total strain (analogous to displacement) is the sum of the strain from each element (Equation 3.5). This strain can be differentiated with respect to time to get the strain rate. This, combined with Equations 3.3 and 3.4 (differentiate equation 3.3), give the constitutive equation for a Maxwell element (Equation 3.6).

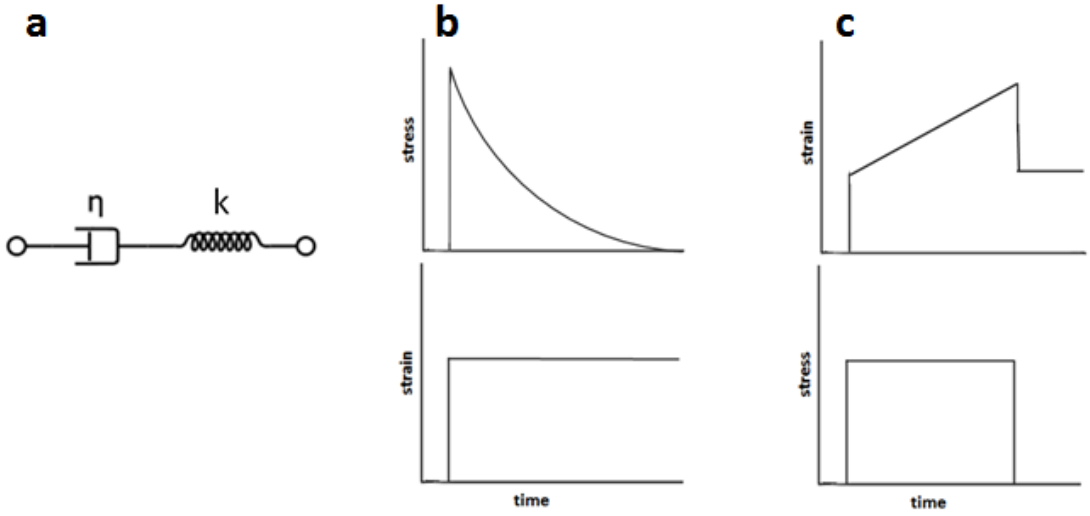

Figure 3.13. Maxwell Element. (a) Mechanical representation. (b) Stress relaxation function. (c) Creep function.

Equation 3.5. Total stress and strain in a Maxwell element.

$$\sigma = \sigma_{spring} = \sigma_{dashpot} \qquad \varepsilon = \varepsilon_{spring} + \varepsilon_{dashpot}$$

Equation 3.6. Constitutive equation for a Maxwell element.

$$\dot{\varepsilon} = \dot{\varepsilon}_{spring} + \dot{\varepsilon}_{dashpot} = \frac{\dot{\sigma}}{k} + \frac{\sigma}{\eta}$$

The constitutive equation can be applied for conditions with a constant strain (stress-relaxation experiment) and a constant stress (creep experiment). When either stimulus is applied to the Maxwell material, the spring responds immediately while the dashpot responds over time. With constant strain, $\dot{\varepsilon}$ is zero. The constitutive equation is

solved for stress to get Equation 3.7, which states that the stress will decay exponentially with time to zero (Figure 3.13b). With constant stress, $\dot{\sigma}$ is zero and the constitutive equation can be solved for strain (Equation 3.8). The strain increases at a constant rate until the stress is removed. When the stress relaxation and creep behavior of the Maxwell material (Figure 3.13b &c) are compared to that of a cell (Figure 3.3b & c), it is clear that the Maxwell model is not sufficient to model cell behavior.

Equation 3.7. Maxwell element relaxation function (constant strain).

$$\sigma(t) = \sigma_0 + e^{\frac{-kt}{\eta}}$$

Equation 3.8. Maxwell element creep function (constant stress).

$$\varepsilon(t) = \sigma\left(\frac{1}{k} + \frac{t}{\eta}\right)$$

The Kelvin model, also known as the Standard Linear Solid model, is the simplest mechanical model for viscoelastic cell behavior. It is represented by a Maxwell element in parallel with a linear spring (Figure 3.14a). The elastic modulus of the additional spring is termed k_e as it provides the system with an equilibrium stiffness. Within the Kelvin model, the Maxwell element and the spring experience equal strain while the total stress is the sum of the stress in each arm (Maxwell element and spring) (Equation 3.9).

Combining the constitutive equation for a Maxwell element (Equation 3.6) with these relationships gives the constitutive equation for the Kelvin body (Equation 3.10).

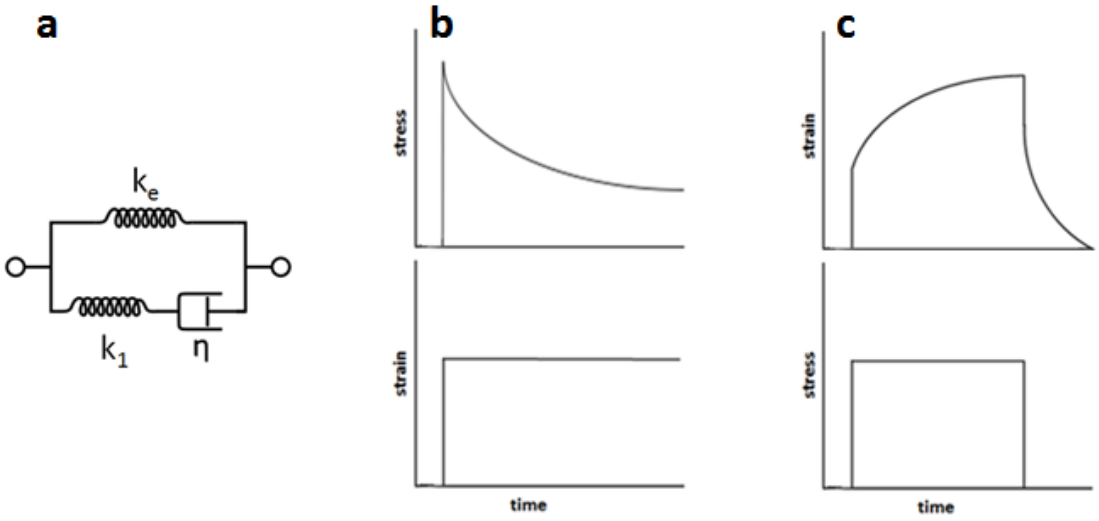

Figure 3.14. Kelvin Model. (a) Mechanical representation. (b) Stress relaxation function. (c) Creep function.

Equation 3.9. Total stress and strain in a Kelvin body.

$$\sigma = \sigma_{Maxwell\ \ Element} + \sigma_{Spring}$$
$$\varepsilon = \varepsilon_{Maxwell\ \ Element} = \varepsilon_{Spring}$$

Equation 3.10. Constitutive equation for a Kelvin body.

$$\dot{\varepsilon} = \frac{\frac{k_1}{n}\left(\frac{n}{k_1}\dot{\sigma} + \sigma - k_e\varepsilon\right)}{k_e + k_1}$$

Like the Maxwell model constitutive equation, the constitutive equation for the Kelvin model can be solved for conditions of constant strain and constant stress. Figure 3.14b & c shows the system responses to these conditions. Under a constant stress, the material instantaneously deforms to some strain (elastic portion of model). It continues to deform and asymptotically approach a steady-state strain (viscous portion of model). When the stress is released, there is an instantaneous (elastic) and viscous response to return the strain to zero. With a constant strain, the stress in the material approaches an equilibrium value over time as the dashpot relaxes. The plots very closely resemble those for a cell (Figure 3.3b & c), making the Kelvin model a popular model for single cell viscoelasticity.

An even better fit is commonly obtained through the use of the Quasilinear Viscoelastic model or the Generalized Maxwell model. The Quasilinear Viscoelastic model is represented by an infinite series of Kelvin bodies (Figure 3.15). The Generalized Maxwell model is represented by a spring in parallel with an infinite series of Maxwell elements (Figure 3.16). It is possible to use any number of elements in either model. The number of elements should be chosen to match the number of rates of decay in the model with those produced by the data (cells typically exhibit a fast and slow decay) [20].

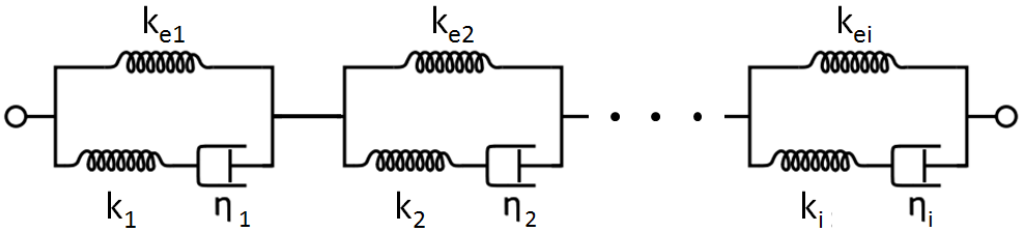

Figure 3.15. Mechanical representation of the Quasilinear Viscoelastic model.

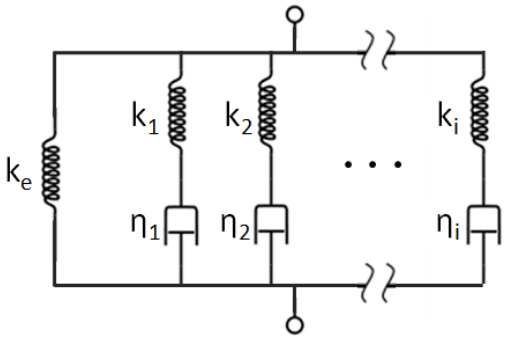

Figure 3.16. Mechanical representation of the Generalized Maxwell model.

Structure-Based Models

Molecular Networks

Molecular network models are based on cross-linked biopolymer networks that, like cells, stiffen with increasing strain [63]. These models are comprised of an infinite number of cytoskeletal protein filaments (microfilaments, microtubules, or intermediate filaments) in a fluid unit cell, like that seen in Figure 3.17. The filaments are arranged in an open cross-linked mesh and they distort in an affine manner as the sample is deformed. The structure has been shown to stiffen at low strains without requiring a specific architecture or multiple elements with different intrinsic stiffness [64]. The 3D

network behavior depends on filament concentration, cross-link density, and network architecture (connectivity, filament length) [65]. Molecular networks are limited in accurately modeling cellular behavior as they typically only model one type of filament in a free solution rather than a combination of filaments anchored to a substrate.

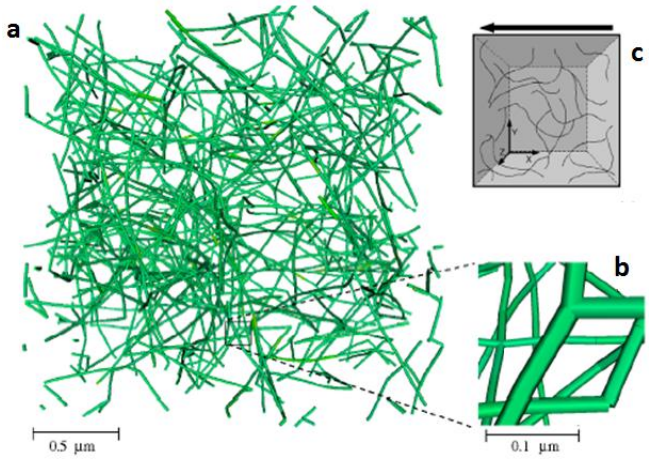

Figure 3.17. 3D discrete network model of cross-linked filaments. (a) View of filaments in network. (b) Magnification to see element cross-linking. (c) Schematic representation of network with arrow indicating direction of applied shear displacement to the xy plane [65].

Tensegrity Model

Tensegrity is a building principle where structures stabilize their shape by continuous tension rather than continuous compression [66]. A tensed network of structural members that resist shape distortion is stabilized by other support elements that resist compression, as seen in Figure 3.18. The joints are held in position as a result of 'prestress' (pre-existing tensile stress or isometric tension) within the structure. Donald Ingber first proposed that tensegrity could be used to describe cellular mechanics [17, 67-

69]. In his model, cytoskeletal microfilaments and intermediate filaments resist tension while microtubules and extracellular matrix adhesions resist compression (Figure 3.18). The tensional prestress that stabilizes the entire cell is generated actively by the contractile actomyosin apparatus and passively through adhesions to the ECM and other cells, osmotic forces acting on the cell membrane, and forces exerted by filament polymerization. The model also includes a viscous cytosol surrounding the cytoskeleton and a semipermeable surface membrane.

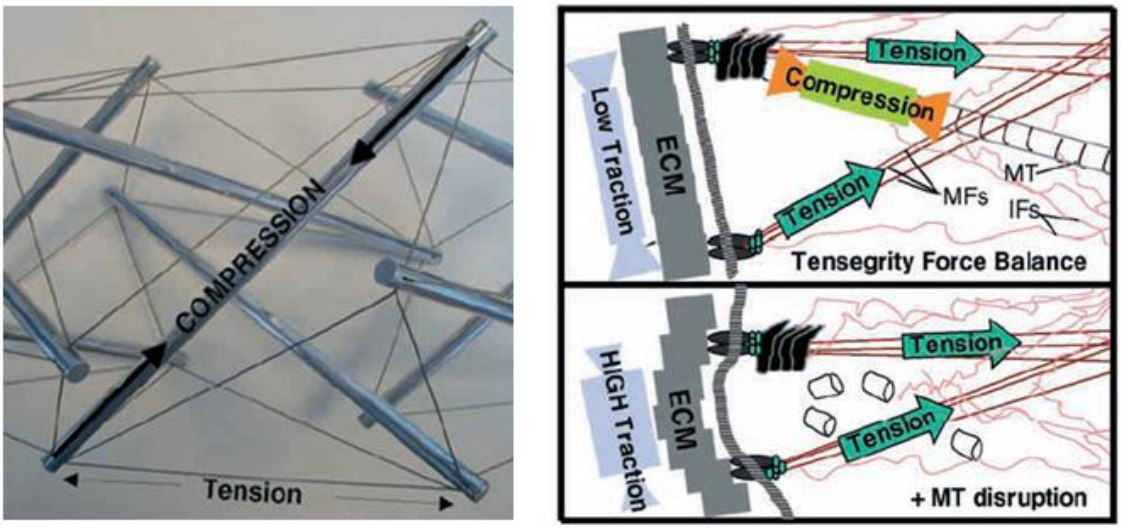

Figure 3.18. Tensegrity structure with members under tension and compression (left). Schematic diagram of tensed microfilaments (MFs) and intermediate filaments (IFs), compressed microtubules (MTs), and extracellular matrix (ECM) in a cell tensegrity model (right). Compressive forces borne by microtubules (top) are transferred to ECM adhesions when microtubules are disrupted (bottom), increasing substrate traction [67].

There are several experimental results that support Ingber's cellular tensegrity model. Studies with isolated cytoskeletal filaments revealed that microfilaments are

better at resisting tension while microtubules are much more effective at withstanding compression [70]. In solution, microtubules are rigid and straight while microfilaments and intermediate filaments are bent [71]. In cells, however, microtubules often appear curved while microfilaments are almost always linear (Figure 3.19). This is consistent with the engineering rule that tension straightens and compression buckles [67]. Additionally, researchers observed the viscoelastic recoil of a single living actin stress fiber when it was cut with a laser, indicating that it was under tension as proposed in the model [72]. Various studies have shown that cell shape stability, both in culture and *in vivo*, depends on a balance of microtubules and opposing contractile microfilaments or intermediate filaments [1, 73-76]. Cells are also known to exert tensional forces on their extracellular matrix substrate [77].

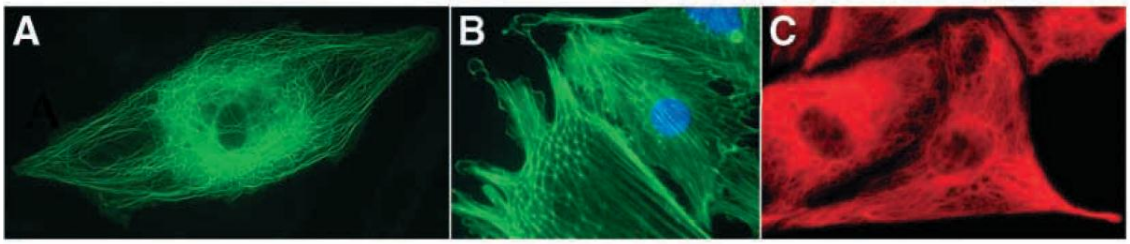

Figure 3.19. Microtubules (A), microfilaments (B), and intermediate filaments (C) within the cytoskeleton of endothelial cells visualized with GFP-tubulin, rhodaminated-phalloidin, and antibodies to vimentin respectively [67].

3.3.2 Vascular Models

It is important to model the mechanical properties of vasculature to understand its response to physiologic loads in both health and disease. Mechanical models can help to

understand disease processes such as atherosclerosis and aid in the development of clinical therapies such as angioplasty and stenting. Modeling the mechanical behavior of entire blood vessels is similar in many ways to modeling single cell mechanics. Like individual cells, vasculature is known to be nonlinear, anisotropic, and viscoelastic [78-80]. Blood vessels are also heterogeneous through the wall and along their length, stressed in the unloaded state, and experience smooth muscle contraction and pressure-related dynamic wall motion. In addition, they have the ability to actively remodel their structure when stress and strain differ from their homeostatic values.

There are many types of experiments that are used to collect data to fit to a model's constitutive equation. Several *in vitro* studies inflate intact blood vessels while applying forces such as axial stretch and torsion [81-83]. A broad range of loading conditions is necessary to fully characterize the tissue [84, 85]. Torsional loading experiments provide data on shear tissue properties [86, 87]. Often times a vessel will be loaded repeatedly in cycles. With this cyclically varying strain, the hysteresis loop tends to decrease with succeeding cycles until it reaches a steady state (Figure 3.20). Mechanical measurements are only taken on a sample that has been preconditioned (at steady state). To get a measure of the residual stress in the vessel, it is often cut open axially and the angle is measured (opening angle) [88, 89]. Pharmacological agents have been incorporated into experiments to differentiate between passive and active tissue responses [90]. Bioreactors are especially useful as they have been shown to maintain cell viability and vascular tone within an excised artery for up to seven days [91]. *In vivo* studies are also possible through the use of imaging techniques such as ultrasound,

angiography, and magnetic resonance imaging. Although *in vivo* studies do not allow for the same experimental control and measurement opportunities as *in vitro* studies, researchers can study blood pressure, changes in vessel geometry, the state of a disease, and responses to outside stimuli such as exercise and pharmacological agents [92, 93].

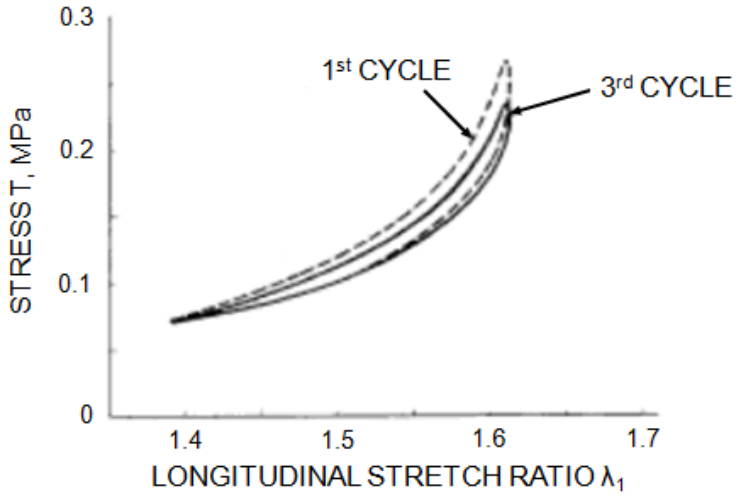

Figure 3.20. Preconditioning. Cyclic stress response of a dog's carotid artery which was maintained in a cylindrical configuration and stretched longitudinally. λ_1 is the stretch ratio referred to the zero-stress length of the segment [94].

No constitutive equation is able to account for all of the complex characteristics blood vessels display. Similar to single cell models, there are both continuum-based models and structure-based models of entire blood vessels. Structure-based models take the vascular microstructure (cells, fibers in different layers) into account while continuum approaches assume average vascular properties. Most models are continuum-based. In general, blood vessels are treated as pseudoelastic, randomly elastic, poroelastic, or viscoelastic materials. Table 3.3 outlines each type of model.

Table 3.3. Comparison of blood vessel mechanical models [95].

Type	Assumptions	Major Limitation	Benefit	Vessels Modeled
Pseudoelastic	The vessel is treated as one hyperelastic material in loading and another in unloading.	The equation separately models loading or unloading data. Data multicollinearity leads to unstable parameters and protocol dependence if incremental loading methods are used.	The approach is simple and captures vessel deformation. Pseudoelastic models form the backbone for other model types.	Aorta (human, porcine, rabbit, rat) Carotid bifurcation (human, porcine) Carotid (canine, porcine) Coronary (bovine) Rat tail artery
Randomly Elastic	The strain response is centered around a definite value that lies on a well-defined curve.	Data is noisier than when separately modeling loading or unloading values.	The equation models both loading and unloading data simultaneously.	Saphenous vein (canine) Coronary (porcine)
Poroelastic	The tissue is treated as a fluid-saturated porous medium.	The movement of fluid through the porous tissue may be irrelevant within the timescale of the experiment. Nonlinear models include many unknown parameters.	The equation models the fluid contribution to tissue properties.	Aorta (rabbit, bovine)
Viscoelastic	The strain response is a function of the stress history.	The response is usually modeled using a discrete number of elements. Data from one viscoelastic test may be insufficient to model characteristics from other viscoelastic tests.	The equation models observed viscoelastic behavior (creep, hysteresis, and stress relaxation).	Aorta (canine, human) Coronary (porcine)

Pseudoelastic models treat a material as one elastic material in loading and as another elastic material in unloading [62]. After preconditioning biological tissue, the stress-strain relationship generally does not vary much with the strain rate [96]. If the strain-rate effect is ignored altogether then the loading curve and the unloading curve can be treated separately with unique stress-strain relationships. Therefore, elastic theory, applied separately to the loading and unloading curves, may be used to describe a single inelastic material. This is termed pseudoelasticity as a reminder that the material is not actually elastic. Strain energy density functions (SEDFs) are a convenient, commonly used way to derive a constitutive equation for a biological tissue that is subject to a finite deformation [62]. Elastic materials that have a SEDF are termed hyperelastic. The strain

energy per unit mass of tissue (W) is expressed in terms of nine strain components E_{11}, E_{22}, E_{33}, E_{12}, E_{21}, E_{23}, E_{32}, E_{31}, and E_{13}, which are each treated as independent variables when partial derivatives of the strain density are formed (Equation 3.11).

Equation 3.11. Stress if strain energy density function exists [62].

$$S_{ij} = \frac{\partial(\rho_0 W)}{\partial E_{ij}}$$

S – stress
W – strain energy per unit mass of tissue
ρ_0 – density in the zero-stress state

Most of the pseudoelastic constitutive models for blood vessels build upon SEDFs developed by earlier researchers. Chuong and Fung introduced a seven-parameter exponential SEDF while Takamizawa and Hayashi introduced a four-parameter logarithmic SEDF [97, 98]. The exponential form offers a better fit for certain arteries, has more stable material parameters, but tends to be overparameterized [99]. The logarithmic model and reduced parameter exponential model cannot fully describe anisotropic behavior [100]. Within the SEDF approach, models differ in simplifying assumptions and whether analytical results are available or numerical methods, such as the finite element method, are required [95]. In general, pseudoelastic models are limited by the neglect of the unloading data and the statistical difficulties (multicollinearity) that result from the incremental method of loading (couples large strains and large stresses) used by most researchers [95].

Randomly elastic models use data from both the loading and unloading curves. Although the results of this type of model are typically noisier than those for a model of a single curve, this type of model avoids the multicollinearity seen in pseudoelastic models. The derivation of the randomly elastic constitutive equation assumes the existence of a SEDF. Randomly elastic models also make use of the complementary energy density function (CEDF), which was first described by Fung for use in modeling soft biological tissue [101]. Under quasistatic conditions, the energy differential of the volume inside an artery is related to the total change in strain energy in the artery. The derivation by Brossollet and Vito yields strain energy density and complementary energy density relationships (Equation 3.12) [84]. Randomly elastic models also assume that the strain response for a given load is centered around a definite value that lies on a well-defined curve (e = e(F,P)). This allows loading and unloading data to be fit simultaneously.

Equation 3.12. Strain energy density and complementary energy density functions [95].

$$dW' = Fde_z + \pi R^2 Pde_v + Td\theta'$$

$$dW'_c = e_z dF + e_v \pi R^2 dP + \theta' dT$$

W' – strain energy density function (SEDF) normalized to specimen length
W'_c – complementary energy density function (CEDF) normalized to specimen length
e_z – axial engineering strain
F – measured force
e_v – volume strain $((1+e_z)x(1+e_l)^2-1)$
P – internal pressure
Θ' – twist per unit length
T – applied torque

Poroelastic models treat the blood vessel as a fluid-saturated porous medium and are best suited to model wall transport. They include measures of both the solid and fluid components in the kinematic and conservation equations [95]. In the kinematic equations, strain is related to the effective stress rather than the total stress. The conservation equations require knowledge of the velocities of both the fluid and the solid phase, the density of the solid, the ratio of the solid to fluid volume, and the hydraulic conductivity describing the interaction of the fluid and solid phases. Due to this complexity, poroelastic models are well suited for finite element methods.

Viscoelastic models include time-dependent responses in the constitutive equation and are useful for modeling creep, stress relaxation, and hysteresis. The same viscoelastic models that were previously described for single cells are often used to describe whole-vessel mechanical behavior. Quasilinear viscoelasticity, with time and strain-dependent components, is most commonly used as it can model strain rate insensitivity and is simpler to implement than fully nonlinear viscoelastic models [95].

There have been many attempts to incorporate the complex mechanical behavior of blood vessels in the different types of models. In some studies, researchers modeled a vessel that was cut through the entire wall to account for residual stress and strain [102]. Different stress equations can be assigned for active (SMC contraction) and passive vessel responses while sinusoidal equations are used to account for wall motion with blood flow [103, 104]. Heterogeneity has been modeled using approaches of increasing complexity. Von Maltzahn et al. created a model with a two-layered cross section representing the tunica media and adventitia (each layer assigned different material

properties) [105]. Kilpatrick et al. created finite element models to account for healthy and diseased components in a atherosclerosis model [106]. In particular, they examined the change in magnitude and distribution of stress in the vessel at different stages of disease. Incompressible, isotropic, bilinear elastic material properties were used to define the constitutive behavior of the media, calcified regions, fibrous cap, and necrotic lipid cores. Holzapfel et al. modeled an artery as a two-layer fiber-reinforced composite [107]. They used histological sections to determine the content and directional organization of the collagen fibers in both the media and adventitia. Some models specifically incorporate smooth muscle mechanical properties in addition to those of collagen and elastin fibers [108, 109]. However, no model currently considers cellular mechanical heterogeneity but rather, they assume averaged mechanical properties.

3.4 References

1. Maniotis, A.J., C.S. Chen, and D.E. Ingber, *Demonstration of mechanical connections between integrins cytoskeletal filaments, and nucleoplasm that stabilize nuclear structure.* Proceedings of the National Academy of Sciences of the United States of America, 1997. **94**(3): p. 849-854.

2. Boudreau, N. and M.J. Bissell, *Extracellular matrix signaling: integration of form and function in normal and malignant cells.* Current Opinion in Cell Biology, 1998. **10**(5): p. 640-646.

3. Huang, S. and D.E. Ingber, *The structural and mechanical complexity of cell-growth control.* Nature Cell Biology, 1999. **1**(5): p. E131-E138.

4. Schwartz, M.A. and M.H. Ginsberg, *Networks and crosstalk: integrin signalling spreads.* Nature Cell Biology, 2002. **4**(4): p. E65-E68.

5. Ingber, D.E., *Mechanobiology and diseases of mechanotransduction.* Annals of Medicine, 2003. **35**(8): p. 564-577.

6. Costa, K.D., *Single-cell elastography: Probing for disease with the atomic force microscope.* Disease Markers, 2003. **19**(2-3): p. 139-154.

7. Shier, D., J. Butler, and R. Lewis, *Hole's Human Anatomy and Physiology*. 11th ed2007, New York: McGraw-Hill. 582.

8. Charras, G.T. and M.A. Horton, *Single cell mechanotransduction and its modulation analyzed by atomic force microscope indentation.* Biophysical Journal, 2002. **82**(6): p. 2970-2981.

9. Rotsch, C. and M. Radmacher, *Drug-induced changes of cytoskeletal structure and mechanics in fibroblasts: An atomic force microscopy study.* Biophysical Journal, 2000. **78**(1): p. 520-535.

10. Wu, H.W., T. Kuhn, and V.T. Moy, *Mechanical properties of l929 cells measured by atomic force microscopy: Effects of anticytoskeletal drugs and membrane crosslinking.* Scanning, 1998. **20**(5): p. 389-397.

11. Alberts, B., et al., *Essential Cell Biology*. 2nd ed2004, New York: Garland Science.

12. Kasza, K.E., et al., *The cell as a material.* Current Opinion in Cell Biology, 2007. **19**(1): p. 101-107.

13. Herrmann, H., et al., *Intermediate filaments: from cell architecture to nanomechanics.* Nature Reviews Molecular Cell Biology, 2007. **8**(7): p. 562-573.

14. Geiger, B., S. YehudaLevenberg, and A.D. Bershadsky, *Molecular interactions in the submembrane plaque of cell-cell and cell-matrix adhesions.* Acta Anatomica, 1995. **154**(1): p. 46-62.

15. Albelda, S.M. and C.A. Buck, *Integrins and Other Cell-Adhesion Molecules.* Faseb Journal, 1990. **4**(11): p. 2868-2880.

16. Yoshida, M., et al., *Leukocyte adhesion to vascular endothelium induces E-selectin linkage to the actin cytoskeleton.* Journal of Cell Biology, 1996. **133**(2): p. 445-455.

17. Ingber, D.E., *Tensegrity: The architectural basis of cellular mechanotransduction.* Annual Review of Physiology, 1997. **59**: p. 575-599.

18. Athanasiou, K.A. and R.M. Natoli, *Introduction to Continuum Biomechanics*, ed. J.D. Enderle2008: Morgan and Claypool.

19. Poliseno, L., et al., *Resting smooth muscle cells as a model for studying vascular cell activation.* Tissue & Cell, 2006. **38**(2): p. 111-120.

20. Hemmer, J.D., et al., *Role of Cytoskeletal Components in Stress-Relaxation Behavior of Adherent Vascular Smooth Muscle Cells.* Journal of Biomechanical Engineering-Transactions of the Asme, 2009. **131**(4): p. 9.

21. Na, S., G.A. Meininger, and J.D. Humphrey, *A theoretical model for F-actin remodeling in vascular smooth muscle cells subjected to cyclic stretch.* Journal of Theoretical Biology, 2007. **246**(1): p. 87-99.

22. Sun, Z., et al., *Extracellular matrix-specific focal adhesions in vascular smooth muscle produce mechanically active adhesion sites.* American Journal of Physiology-Cell Physiology, 2008. **295**(1): p. C268-C278.

23. Hemmer, J.D., et al., *Effects of serum deprivation on the mechanical properties of adherent vascular smooth muscle cells.* Proceedings of the Institution of Mechanical Engineers Part H-Journal of Engineering in Medicine, 2008. **222**(H5): p. 761-772.

24. Jaasma, M.J., W.M. Jackson, and T.M. Keaveny, *Measurement and characterization of whole-cell mechanical behavior.* Annals of Biomedical Engineering, 2006. **34**(5): p. 748-758.

25. Jones, W.R., et al., *Alterations in the Young's modulus and volumetric properties of chondrocytes isolated from normal and osteoarthritic human cartilage.* Journal of Biomechanics, 1999. **32**(2): p. 119-127.

26. Mahaffy, R.E., et al., *Scanning probe-based frequency-dependent microrheology of polymer gels and biological cells.* Physical Review Letters, 2000. **85**(4): p. 880-883.

27. Sato, M., et al., *Application of the micropipette technique to the measurement of cultured porcine aortic endothelial cell viscoelstic properties.* Journal of Biomechanical Engineering-Transactions of the Asme, 1990. **112**(3): p. 263-268.

28. Jaasma, M.J., W.M. Jackson, and T.M. Keaveny, *The effects of morphology, confluency, and phenotype on whole-cell mechanical behavior.* Annals of Biomedical Engineering, 2006. **34**(5): p. 759-768.

29. Bao, G. and S. Suresh, *Cell and molecular mechanics of biological materials.* Nature Materials, 2003. **2**(11): p. 715-725.

30. Huang, H.D., R.D. Kamm, and R.T. Lee, *Cell mechanics and mechanotransduction: pathways, probes, and physiology.* American Journal of Physiology-Cell Physiology, 2004. **287**(1): p. C1-C11.

31. Brown, T.D., et al. *Loading paradigms, Intentional and unintentional, for cell culture mechanostimulus*. 1998. Lippincott Williams & Wilkins.

32. Ressler, B., et al., *Molecular responses of rat tracheal epithelial cells to transmembrane pressure.* American Journal of Physiology-Lung Cellular and Molecular Physiology, 2000. **278**(6): p. L1264-L1272.

33. Tanaka, S.M., et al., *Effects of broad frequency vibration on cultured osteoblasts.* Journal of Biomechanics, 2003. **36**(1): p. 73-80.

34. Lemarie, C.A., et al., *Pressure-induced vascular activation of nuclear factor-kappa B - Role in cell survival.* Circulation Research, 2003. **93**(3): p. 207-212.

35. Naruse, K., et al., *Distinct anabolic response of osteoblast to low-intensity pulsed ultrasound.* Journal of Bone and Mineral Research, 2003. **18**(2): p. 360-369.

36. Henon, S., et al., *A new determination of the shear modulus of the human erythrocyte membrane using optical tweezers.* Biophysical Journal, 1999. **76**(2): p. 1145-1151.

37. Svoboda, K. and S.M. Block, *Biological applications of optical forces.* Annual Review of Biophysics and Biomolecular Structure, 1994. **23**: p. 247-285.

38. Dao, M., C.T. Lim, and S. Suresh, *Mechanics of the human red blood cell deformed by optical tweezers (vol 51, pg 2259, 2003).* Journal of the Mechanics and Physics of Solids, 2005. **53**(2): p. 493-494.

39. Kuo, S.C. and M.P. Sheetz, *Force of single kinesin molecules measured with optical tweezers.* Science, 1993. **260**(5105): p. 232-234.

40. Block, S.M. *Optical Tweezers: An Introduction*. 2009.

41. Lo, C.M., et al., *Cell-substrate separation: effect of applied force and temperature.* European Biophysics Journal with Biophysics Letters, 1998. **27**(1): p. 9-17.

42. Wang, N., J.P. Butler, and D.E. Ingber, *Mechanotransduction across the cell-surface and through the cytoskeleton.* Science, 1993. **260**(5111): p. 1124-1127.

43. Binnig, G., C.F. Quate, and C. Gerber, *Atomic Force Microscope.* Physical Review Letters, 1986. **56**(9): p. 930-933.

44. Tortonese, M., *Cantilevers and tips for atomic force microscopy.* Ieee Engineering in Medicine and Biology Magazine, 1997. **16**(2): p. 28-33.

45. Braga, P.C. and D. Ricci, *Methods in Molecular Biology: Atomic Force Microscopy - Biomedical Methods and Applications*. Vol. 242. 2004, Totowa: Humana Press.

46. Ortiz, C. *Nanomechanics Links - Atomic Force Microscopy*. 2009.

47. Hoh, J.H. and C.A. Schoenenberger, *Surface morphology and mechanical properties of mdck monolayers by atomic force microscopy.* Journal of Cell Science, 1994. **107**: p. 1105-1114.

48. Costa, K.D., *Imaging and Probing Cell Mechanical Properties With the Atomic Force Microscope*, in *Cell Imaging Techniques: Methods and Protocols*2006, Humana Press: Totowa. p. 331-335.

49. Radmacher, M., *Studying the mechanics of cellular processes by atomic force microscopy*, in *Cell Mechanics*2007, Elsevier Academic Press Inc: San Diego. p. 347-372.

50. Radmacher, M., et al., *Mapping interaction forces with the atomic force microscope.* Biophysical Journal, 1994. **66**(6): p. 2159-2165.

51. A-Hassan, E., et al., *Relative microelastic mapping of living cells by atomic force microscopy.* Biophysical Journal, 1998. **74**(3): p. 1564-1578.

52. Simon, A. and M.C. Durrieu, *Strategies and results of atomic force microscopy in the study of cellular adhesion.* Micron, 2006. **37**(1): p. 1-13.

53. Moore, J. and G. Zouridakis, *Biomedical Technology and Devices Handbook*2004: CRC Press.

54. Hochmuth, R.M., *Micropipette aspiration of living cells.* Journal of Biomechanics, 2000. **33**(1): p. 15-22.

55. Lim, C.T., E.H. Zhou, and S.T. Quek, *Mechanical models for living cells - A review.* Journal of Biomechanics, 2006. **39**(2): p. 195-216.

56. Thoumine, O., et al., *Microplates: a new tool for manipulation and mechanical perturbation of individual cells.* Journal of Biochemical and Biophysical Methods, 1999. **39**(1-2): p. 47-62.

57. Tan, J.L., et al., *Cells lying on a bed of microneedles: An approach to isolate mechanical force.* Proceedings of the National Academy of Sciences of the United States of America, 2003. **100**(4): p. 1484-1489.

58. Hertz, H., *On the Contact of Elastic Solids.* J. Reine Angew. Math., 1881. **92**: p. 156-171.

59. Costa, K.D., A.J. Sim, and F.C.P. Yin, *Non-Hertzian approach to analyzing mechanical properties of endothelial cells probed by atomic force microscopy.* Journal of Biomechanical Engineering-Transactions of the Asme, 2006. **128**(2): p. 176-184.

60. Smith, B.A., et al., *Probing the viscoelastic behavior of cultured airway smooth muscle cells with atomic force microscopy: Stiffening induced by contractile agonist.* Biophysical Journal, 2005. **88**(4): p. 2994-3007.

61. Rico, F., et al., *Probing mechanical properties of living cells by atomic force microscopy with blunted pyramidal cantilever tips.* Physical Review E, 2005. **72**(2): p. 10.

62. Fung, Y.C., *Biomechanics: Mechanical Properties of Living Tissues*. 2nd ed2004, New York: Springer Science and Business Media.

63. Mackintosh, F.C., J. Kas, and P.A. Janmey, *Elasticity of semiflexible biopolymer networks.* Physical Review Letters, 1995. **75**(24): p. 4425-4428.

64. Storm, C., et al., *Nonlinear elasticity in biological gels.* Nature, 2005. **435**(7039): p. 191-194.

65. Huisman, E.M., et al., *Three-dimensional cross-linked F-actin networks: Relation between network architecture and mechanical behavior.* Physical Review Letters, 2007. **99**(20): p. 4.

66. Fuller, B., *Tensegrity.* Portfolio Art News Annual, 1961. **4**: p. 112-127.

67. Ingber, D., *Tensegrity 1. Cell structure and hierarchical systems biology.* Journal of Cell Science, 2003. **116**: p. 1157-1173.

68. Ingber, D.E., *Tensegrity II. How structural networks influence cellular information processing networks.* Journal of Cell Science, 2003. **116**(8): p. 1397-1408.

69. Ingber, D.E., *Cellular Tensegrity - Defining new rules of biological design that govern the cytoskeleton.* Journal of Cell Science, 1993. **104**: p. 613-627.

70. Mizushimasugano, J., T. Maeda, and T. Mikinoumura, *Flexural rigidity of singlet microtubules estimated from statistical analysis of their contour lengths and end to end distances.* Biochimica Et Biophysica Acta, 1983. **755**(2): p. 257-262.

71. Janmey, P.A., et al., *Viscoelastic properties of vimentin compared with other filamentous biopolymer networks.* Journal of Cell Biology, 1991. **113**(1): p. 155-160.

72. Kumar, S., et al., *Viscoelastic retraction of single living stress fibers and its impact on cell shape, cytoskeletal organization, and extracellular matrix mechanics.* Biophysical Journal, 2006. **90**(10): p. 3762-3773.

73. Domnina, L.V., et al., *Effect of microtubule-destroying drugs on the spreading and shape of cultured epithelial cells.* Journal of Cell Science, 1985. **74**(MAR): p. 267-282.

74. Madreperla, S.A. and R. Adler, *Opposing microtubule-dependent and actin-dependent forces in the development and maintenance of structural polarity in retinal photoreceptors.* Developmental Biology, 1989. **131**(1): p. 149-160.

75. Bailly, E., C. Celati, and M. Bornens, *The Cortical Actomyosin System of Cytochalasin D-Treated Lymphoblasts.* Experimental Cell Research, 1991. **196**(2): p. 287-293.

76. Brown, M.J., et al., *Rigidity of circulating lymphocytes is primarily conferred by vimentin intermediate filaments.* Journal of Immunology, 2001. **166**(11): p. 6640-6646.

77. Harris, A.K., P. Wild, and D. Stopak, *Silicone-rubber substrata - new wrinkle in the study of cell locomotion.* Science, 1980. **208**(4440): p. 177-179.

78. Levy, B.I., *Mechanics of the large artery vascular wall.* Pathologie Biologie, 1999. **47**(6): p. 634-640.

79. McVeigh, G.E., P.K. Hamilton, and D.R. Morgan, *Evaluation of mechanical arterial properties: clinical, experimental and therapeutic aspects.* Clinical Science, 2002. **102**(1): p. 51-67.

80. Shadwick, R.E., *Mechanical design in arteries.* Journal of Experimental Biology, 1999. **202**(23): p. 3305-3313.

81. Patel, D.J. and J.S. Janicki, *Static elastic properties of left coronary circumflex artery and common carotid artery in dogs.* Circulation Research, 1970. **27**(2): p. 149-&.

82. Vito, R.P., *The mechanical properties of soft tissues. 1. A mechanical system for bi-axial testing.* Journal of Biomechanics, 1980. **13**(11): p. 947-950.

83. Humphrey, J.D., et al., *Computer-aided vascular experimentation - a new electromechanical test system.* Annals of Biomedical Engineering, 1993. **21**(1): p. 33-43.

84. Brossollet, L.J. and R.P. Vito, *A new approach to mechanical testing and modeling of biological tissues, with application to blood vessels.* Journal of Biomechanical Engineering-Transactions of the Asme, 1996. **118**(4): p. 433-439.

85. Dixon, S.A., R.G. Heikes, and R.P. Vito, *Constitutive modeling of porcine coronary arteries using designed experiments.* Journal of Biomechanical Engineering-Transactions of the Asme, 2003. **125**(2): p. 274-279.

86. Deng, S.X., et al., *New Experiments on Shear Modulus of Elasticity of Arteries.* American Journal of Physiology, 1994. **266**(1): p. H1.

87. Vorp, D.A., et al., *A device for the application of cyclic twist and extension on perfused vascular segments.* American Journal of Physiology-Heart and Circulatory Physiology, 1996. **39**(2): p. H787-H795.

88. Vaishnav, R.N. and J. Vossoughi, *Residual stress and strain in aortic segments.* Journal of Biomechanics, 1987. **20**(3): p. 235.

89. Van Dyke, T.J. and A. Hoger, *A new method for predicting the opening angle for soft tissues.* Journal of Biomechanical Engineering-Transactions of the Asme, 2002. **124**(4): p. 347-354.

90. Joannides, R., et al. *Chronic ACE inhibition enhances the endothelial control of arterial mechanics and flow-dependent vasodilatation in heart failure*. 2001. Lippincott Williams & Wilkins.

91. Han, H.C. and D.N. Ku, *Contractile responses in arteries subjected to hypertensive pressure in seven-day organ culture.* Annals of Biomedical Engineering, 2001. **29**(6): p. 467-475.

92. Bank, A.J., *Intravascular ultrasound studies of arterial elastic mechanics.* Pathologie Biologie, 1999. **47**(7): p. 731-737.

93. Cameron, J., *Estimation of arterial mechanics in clinical practice and as a research technique.* Clinical and Experimental Pharmacology and Physiology, 1999. **26**(4): p. 285-294.

94. Lee, J.S., W.G. Frasher, and Y.C. Fung, *Two-Dimensional Finite-Deformation on Experiments on Dog's Arteries and Veins*, 1967: San Diego.

95. Vito, R.P. and S.A. Dixon, *Blood vessel constitutive models-1995-2002.* Annual Review of Biomedical Engineering, 2003. **5**: p. 413-439.

96. Dunn, F., *Ultrasound*, in *Biological Engineering*1969, McGraw-Hill: New York.

97. Chuong, C.J. and Y.C. Fung, *3-Dimensional Stress-Distribution in Arteries.* Journal of Biomechanical Engineering-Transactions of the Asme, 1983. **105**(3): p. 268-274.

98. Takamizawa, K. and K. Hayashi, *Strain energy density function and uniform strain hypothesis for arterial mechanics.* Journal of Biomechanics, 1987. **20**(1): p. 7-17.

99. Fung, Y.C., K. Fronek, and P. Patitucci, *Pseudoelasticity of arteries and the choice of its mathematical expression.* American Journal of Physiology, 1979. **237**(5): p. H620-H631.

100. Humphrey, J.D., *An evaluation of pseudoelastic descriptors used in arterial mechanics.* Journal of Biomechanical Engineering-Transactions of the Asme, 1999. **121**(2): p. 259-262.

101. Fung, Y.C., *Inversion of a class of non-linear stress-strain relationships of biological soft-tissues.* Journal of Biomechanical Engineering-Transactions of the Asme, 1979. **101**(1): p. 23-27.

102. Matsumoto, T. and K. Hayashi, *Stress and strain distribution in hypertensive and normotensive rat aorta considering residual strain.* Journal of Biomechanical Engineering-Transactions of the Asme, 1996. **118**(1): p. 62-73.

103. Demiray, H. and R.P. Vito, *On Large Periodic Motions of Arteries.* Journal of Biomechanics, 1983. **16**(8): p. 643-648.

104. Rachev, A. and K. Hayashi, *Theoretical study of the effects of vascular smooth muscle contraction on strain and stress distributions in arteries.* Annals of Biomedical Engineering, 1999. **27**(4): p. 459-468.

105. Vonmaltzahn, W.W., R.G. Warriyar, and W.F. Keitzer, *Experimental measures of elastic properties of media and adventitia of bovine carotid arteries.* Journal of Biomechanics, 1984. **17**(11): p. 839-847.

106. Kilpatrick, D., et al., *Effect of plaque composition on fibrous cap stress in carotid endarterectomy specimens.* Journal of Biomechanical Engineering-Transactions of the Asme, 2001. **123**(6): p. 635-638.

107. Holzapfel, G.A., T.C. Gasser, and M. Stadler, *A structural model for the viscoelastic behavior of arterial walls: Continuum formulation and finite element analysis.* European Journal of Mechanics a-Solids, 2002. **21**(3): p. 441-463.

108. Wuyts, F.L., et al., *Elastic properties of human aortas in relation to age and atherosclerosis - a structural model.* Physics in Medicine and Biology, 1995. **40**(10): p. 1577-1597.

109. Armentano, R.L., et al., *Arterial-wall mechanics in conscious dogs - assessment of viscous, inertial, and elastic-moduli to characterize aortic-wall behavior.* Circulation Research, 1995. **76**(3): p. 468-478.

CHAPTER FOUR

CREATING ALIGNED COLLAGEN AND FIBRONECTIN MATRICES USING INKJET PRINTER TECHNOLOGY

4.1 Introduction

In cell culture experiments, it is important to mimic *in vivo* physiological conditions in the *in vitro* environment as closely as possible. The extracellular matrix (ECM) has been shown to affect cell growth, adhesion, differentiation, morphology, and signaling and is thus an important part of the cellular environment that should be replicated in cell culture [1, 2]. The proteins collagen and fibronectin are major constituents of many extracellular matrices and have long been used in cell culture as an approximation to the ECM. Collagen is a triple helical protein with a diameter of 1.5 nm and length of 300 nm. It undergoes self-assembly into fibrils with a diameter of 36 nm, which in turn form larger fibers and fiber bundles [3, 4]. Although fibrils have a persistence length of approximately 130 nm, fiber bundles are known to have much greater stiffness and appear straight over long distances, particularly in tissue [5]. Fibronectin is a high-molecular weight (440 kDa) glycoprotein, consisting of two nearly identical monomers linked by a pair of disulfide bonds [6]. When fully extended in solution, fibronectin is 120 to 140 nm long, 2 to 3 nm in diameter, and has a persistence length of 20 to 30 nm [7]. Under physiological conditions, it generally folds up into a more compact, tangled structure.

Collagen and fibronectin fibers are organized in different orientations in different tissues in the body, which affects the overall tissue properties. For example, collagen

fibers organize into extensive parallel arrays in tendons and ligaments, regular sheets of varying fiber orientation in the transparent cornea of the eye, and randomly in isotropic connective tissues [8]. Aligned fibers are also believed to play a role in cell signaling and development as well as directing cell proliferation and migration after injury [9, 10]. Therefore, it is often important to orient the fibers in cell culture to match the *in vivo* environment for the particular cell type under investigation. For example, some cell types, including cardiomyocytes, require matrix alignment to maintain their *in vivo*-like phenotype *in vitro* [11, 12]. Randomly oriented collagen and fibronectin matrices are easily prepared. However, it is more difficult to create aligned fiber arrays for cells that require aligned ECM for normal functioning.

Current techniques used to align collagen and fibronectin include mechanical scraping and gravity, microfluidics, and magnetic field alignment. For the first method, a matrix solution is applied to the top edge of a tilted culture dish and a cell scraper draws the solution downward across the dish. The tilted dish is stored while gravity works to further align the fibers [13]. While this method is inexpensive and quick, it lacks consistency and precise alignment. In microfluidic alignment, fibers align along the direction of flow as the solution polymerizes inside a channel up to 100 μm in width [14]. Finally, a collagen solution may be exposed to a strong static magnetic field on the order of 1 T during gelation. Each collagen molecule has a slightly negative diamagnetic susceptibility so fibrils align perpendicular to the magnetic field [15-18]. An alternative magnetic alignment technique has recently been established in which magnetic beads are used within collagen gels, requiring a much smaller magnet [19]. These techniques

produce well aligned matrix fibers but require specialized equipment. In addition to these mechanical alignment methods, substrate-directed collagen fibrillogenesis methods have been developed. Although quite useful for specific tissue culture applications (e.g., bone), these methods require special substrates (e.g., hydroxyapatite) and produce composite materials in 3D [20].

In this work, we describe an alternative matrix alignment technique based on inkjet printer technology that is precise, repeatable, inexpensive, and easy to use. Inkjet printers have been utilized in tissue engineering to construct three-dimensional synthetic polymer tissue scaffolds one layer at a time while integrating pores and channels. Researchers have more recently proven the feasibility of printing biological materials [21]. Although printing has previously been used to arrange individual cells in culture, there has been little investigation into the alignment of ECM fibers [22]. Our work takes advantage of this established tool to develop a new collagen and fibronectin alignment technique that can work on a variety of underlying substrates. The success of the alignment was determined not only by inspection of the printed fibers, but also by inspection of cardiomyocytes grown on the aligned collagen and fibronectin substrates. Cardiomyocytes are known to bind well to collagen and fibronectin in culture and require ECM alignment to maintain their *in vivo* phenotype [11].

4.2 Materials and Methods

4.2.1 Substrate Preparation

Glass slides (Fisher Scientific, Pittsburgh, PA, USA) with ~0.17 mm thickness and 18 mm diameter were used as substrates for the collagen and fibronectin matrices. The slides were plasma cleaned for fifteen minutes and then placed in a seventy percent ethanol solution. They were UV sterilized for at least one hour and subsequently used. Following cleaning and sterilization, some slides were additionally treated with 95% 3-amioproplytrimethoxysilane (APTES, Sigma-Aldrich, St. Louis, MO, USA) and a 1 mM bis(sulfosuccinimidyl)suberate (BS^3, Pierce, Rockford, IL, USA) linker to covalently bind the matrix proteins to the glass substrates.

4.2.2 Matrix Solution Preparation

Rat tail collagen type I (BD Biosciences, Bedford, MA, USA) was received at a concentration of 9.44 mg/ml in acid. Fibronectin from human plasma (BD Biosciences) was received in a lyophilized form and was allowed to resuspend in sterile distilled water for 30 minutes before use. Both matrix solutions were diluted to concentrations ranging from 0.25 mg/ml to 5 mg/ml using deionized water and printed within 2 hours. Each concentration was tested to determine the optimal concentration for printing.

4.2.3 Printing

The pattern, as shown in Figure 4.1, was designed in Word (Microsoft, Redmond, WA, USA) and printed using a modified HP DeskJet 500 printer (C2106A, Hewlett-

Packard, Palo Alto, CA, USA). The printer was modified with new gear mount pillars with closer tolerances, as described previously (Figure 4.2) [23]. Black Inkjet cartridges (26, Hewlett-Packard) were emptied and thoroughly rinsed with deionized water 50 to 100 times to ensure no ink was left in the reservoir. The cartridges were then rinsed with ethanol and sterile water before use in the printer. Deionized water was printed first to ensure that the cartridge nozzles were clear and to locate the proper position for centering the slide. The water was then removed from the cartridge and another print was completed to ensure that nothing printed, indicating a completely empty cartridge. 100 μl of the matrix solution was then added to the cartridge and a slide was positioned for printing. The pattern was printed three successive times on the slide. In normal ambient conditions, the patterned collagen solution visibly dried within seconds of printing. However, one can maintain hydration by increasing environmental humidity (e.g., using the printer in an incubator). Each slide was stored in a 22 mm diameter well of a 12 well plate after printing. The well plate was stored in an incubator until cardiomyocytes were plated on the matrices. Cartridges were rinsed in ethanol and sonicated in deionized water for at least 20 minutes between uses to remove protein buildup clogging the nozzles.

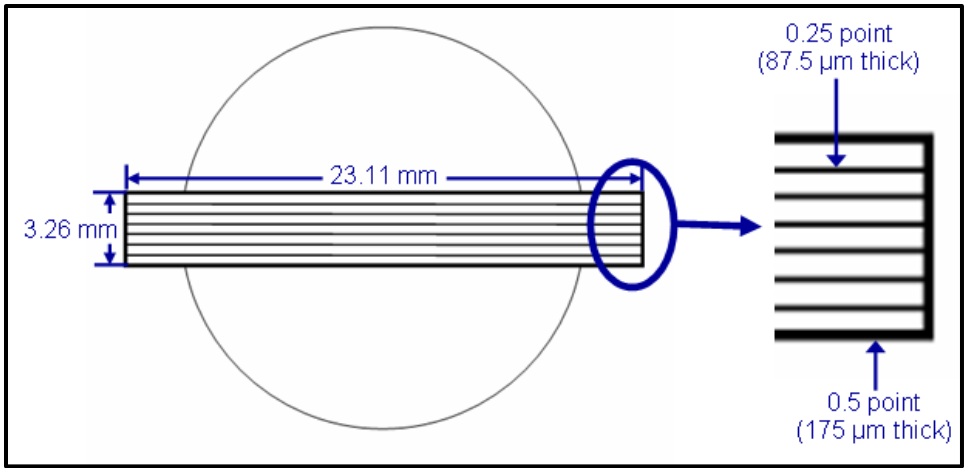

Figure 4.1. Schematic of printed pattern location on slide with line dimensions labeled.

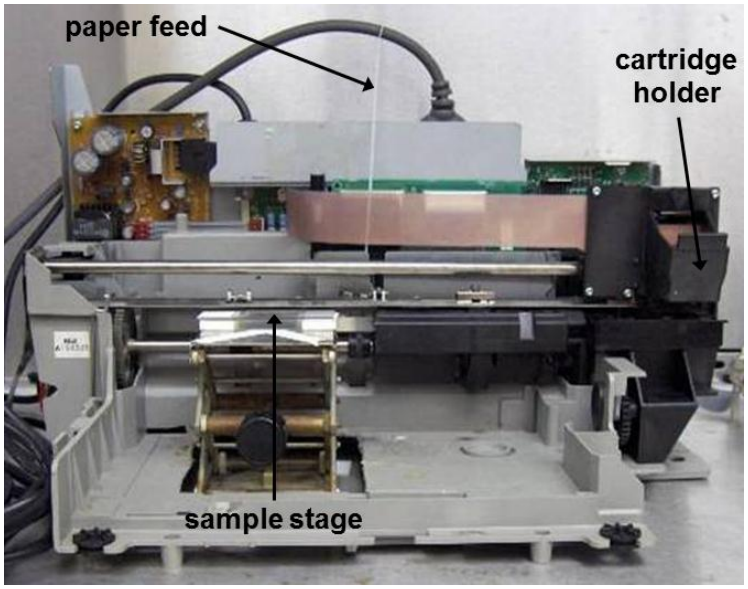

Figure 4.2. Modified HP DeskJet 500 printer in sterile biohazard hood. Glass slides are first placed on top of the sample stage. Cartridges containing matrix "ink" are then loaded in the cartridge holder. Immediately following the command to print in Microsoft Word, the paper feed lever is pulled upward to bypass the paper feed mechanism. The pattern is printed three consecutive times onto each slide in this manner.

4.2.4 Cell Culture

To isolate neonatal rat cardiomyocytes, the hearts of 3 day old pups were removed, minced, and subjected to collagenase dissociation as described previously [11-13]. The isolated cardiomyocytes were plated on the slides containing the aligned collagen or fibronectin within 2 hours of printing. Each slide received approximately 250,000 cardiomyocytes to create a near-confluent layer of cells. The cardiomyocytes were cultured under standard conditions (37ºC, 5% CO_2) in Dulbecco's modified Eagle's medium (DMEM) supplemented with 8% horse serum, 5% newborn bovine serum, 1% penicillin/streptomycin, sodium bicarbonate, HEPES (pH 7.4), amphotericin B, and proliferative cell inhibitor Cytosin β-D-arabinofuranoside to prevent fibroblast growth. The media was changed every 48 hours and the cells were monitored daily via light microscopy.

4.2.5 Imaging

A light microscope was used to observe the lines of printed collagen and the cardiomyocytes cultured on the printed matrices. The printed collagen was additionally stained using mouse monoclonal anti-collagen type I (Clone Col-1, Sigma-Aldrich) as the primary antibody and donkey anti-mouse TRITC IgG (Jackson ImmunoResearch, West Grove, PA, USA) as the secondary antibody. This primary antibody does not bind to heat denatured collagen and was used to confirm that the printing process did not modify the collagen type I molecule. To image the fibers within the printed lines, both polarized

light microscopy and atomic force microscopy (Dimension 3100, Veeco, Plainview, NY, USA) were used.

4.3 Results and Discussion

4.3.1 Optimal Preparation Techniques

Slides prepared by plasma cleaning and UV sterilization alone showed equivalent collagen and fibronectin attachment as those that were additionally treated with APTES and BS^3 linker to covalently bind the printed matrix proteins. Thus, this additional step was deemed unnecessary and omitted in subsequent preparations. Matrix protein solutions at concentrations greater than 3 mg/ml clogged the print head nozzles and did not allow any transfer of the solution to the substrate. A concentration of 1 mg/ml allowed for three to five printing passes before the cartridge had to be cleaned so this concentration became the standard for subsequent samples.

4.3.2 Matrix Fiber Alignment

The printed samples, viewed under a light microscope, showed clear stripes and indicated alignment in the printed pattern (Figures 4.3 and 4.4a). While a line diameter of 87.5 μm was specified in the design, the diameters of the printed lines were consistently closer to 20 μm after polymerization (Figures 4.1 and 4.3). This is most likely because the drops coalesced along the line, contracting in width as they were pulled in length along the printed line. There was a remaining concern over the state of the printed collagen and fibronectin as printing exposes the proteins to high temperatures

that could potentially cause denaturation. To test if the collagen was denatured, the printed collagen samples were stained using a primary antibody which has been shown not to react with thermally-denatured collagen [21]. This antibody did in fact bind to the printed collagen, as well as to a control sample that was not printed (Figure 4.3).

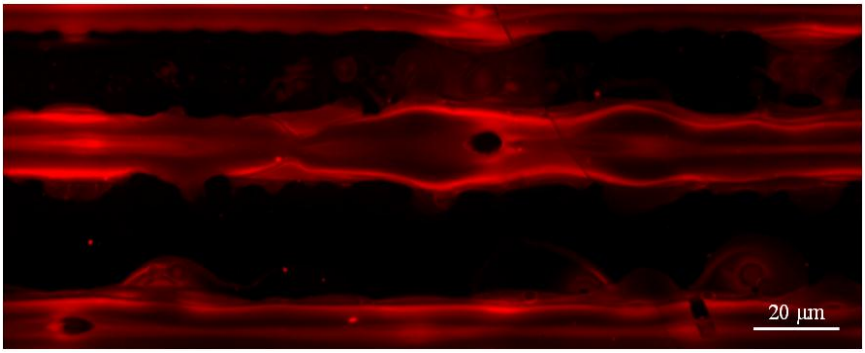

Figure 4.3. Fluorescently stained lines of printed collagen.

Both polarized light microscopy and AFM were utilized to verify fiber alignment within the lines of printed collagen. AFM scans confirmed proper collagen fiber formation and small degrees of fiber alignment at 10 μm scan size. The polarized light images clearly indicated alignment over the bulk of the printed line section. In crossed polarized illumination, isotropic gels remain permanently dark when the stage is rotated through 360 degrees while anisotropic gels (with fiber alignment) will brighten with rotation. Figure 4.4a shows a typical printed line before complete polymerization (line decreases in width with polymerization). Figure 4.4b shows the edge of this line under polarized light after polymerization. This image indicates that the degree of alignment is high at the edge of the printed line while it decreases towards the center of the line. As

the fibers polymerize, the line will become thinner and further alignment throughout is possible. Perfect fiber alignment would be indicated by illumination of the entire line. While the fibers may not all be perfectly aligned, this method shows significant alignment compared to a random collagen film showing no alignment (Figure 4.4c) or matrix proteins that were mechanically scraped, which look dark between cross polarizers.

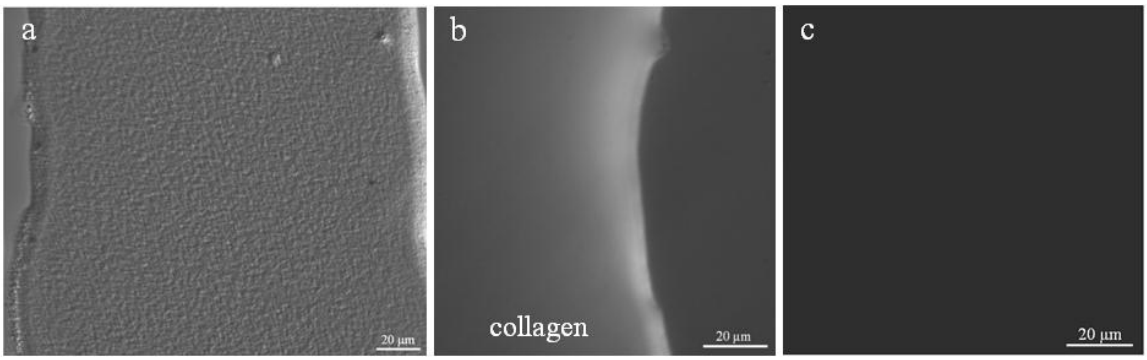

Figure 4.4. Images of collagen under light microscopy. a) Collagen within printed line. b) Polarized light image of collagen within printed line. c) Polarized light image of randomly oriented collagen fibers (control).

4.3.3 Cardiomyocyte Morphology

During development *in vivo*, cardiomyocytes elongate into a rod-like shape with parallel arrays of myofibrils. Contraction is synchronized through the intercalated discs that connect the cells [10]. This structure is lost when the cells are placed in two dimensional culture as the cardiomyocytes take on a spread-morphology and lack connections with neighboring cells. When cultured on the printed collagen and fibronectin samples, the *in vivo* morphology was restored (Figure 4.5). The lines of cells

beat in unison unlike cardiomyocytes on randomly oriented matrix substrates where individual cells beat occasionally. Thus, the printed collagen and fibronectin matrices simulated the *in vivo* ECM well enough for cardiomyocytes to take on their *in vivo* phenotype *in vitro*.

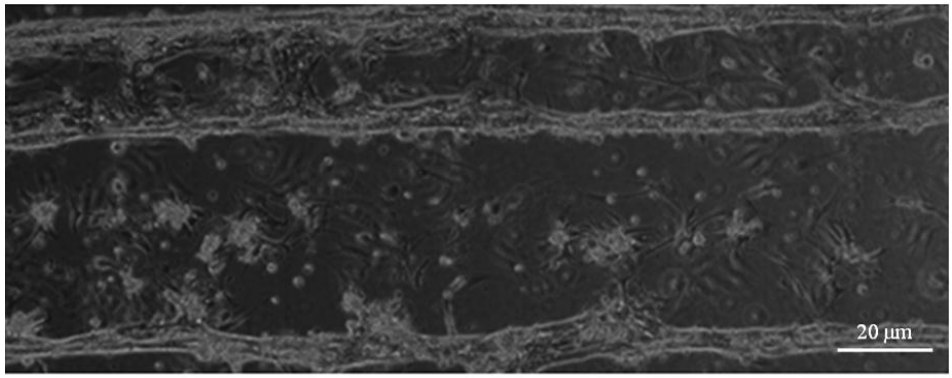

Figure 4.5. Cardiomyocytes aligned on printed collagen.

4.4 Conclusions

A novel inkjet printing technique for aligning ECM proteins was outlined. Collagen and fibronectin solutions were printed onto glass substrates in a designated line pattern without significant heat denaturation. Within the printed lines, the ECM fibers show alignment, particularly at the edges of the printed lines. Cardiomyocytes attached to the lines of printed ECM fibers and were therefore able to sustain their *in vivo*-like phenotype. This alignment technique combines the best aspects of the methods currently in use – accuracy, simplicity, and low cost. Distinct advantages to the printing technique are the ability to print on any type of substrate and to build a three dimensional construct with varying collagen alignment by printing layer upon layer. This technique may also

be used to print other extracellular matrix proteins such as laminin, elastin, and other types of collagen. Thus, this printing alignment technique may be useful in many broader tissue engineering and biomaterial applications in the future. For our purposes, this technique was used to create a more uniform extracellular matrix for cellular interactions (Chapter 5), within the overall goal of determining the sources of cellular mechanical heterogeneity.

4.5 References

1. Kleinman, H.K., et al., *Use of extracellular-matrix components for cell-culture.* Analytical Biochemistry, 1987. **166**(1): p. 1-13.

2. Martin, G.R. and H.K. Kleinman, *Extracellular-matrix proteins give new life to cell-culture.* Hepatology, 1981. **1**(3): p. 264-266.

3. Kadler, K.E., et al., *Collagen fibril formation.* Biochemical Journal, 1996. **316**: p. 1-11.

4. Ottani, V., et al., *Hierarchical structures in fibrillar collagens.* Micron, 2002. **33**(7-8): p. 587-596.

5. Gelman, R.A., B.R. Williams, and K.A. Piez, *Collagen fibril formation - evidence for a multistep process.* Journal of Biological Chemistry, 1979. **254**(1): p. 180-186.

6. Pankov, R. and K.M. Yamada, *Fibronectin at a glance.* Journal of Cell Science, 2002. **115**(20): p. 3861-3863.

7. Uitto, J. and A. Perejda, *Connective tissue disease: molecular pathology of the extracellular matrix*1986, New York, NY: Marcel Dekker, Inc.

8. Komai, Y. and T. Ushiki, *The 3-dimensional organization of collagen fibrils in the human cornea and sclera.* Investigative Ophthalmology & Visual Science, 1991. **32**(8): p. 2244-2258.

9. Glass-Brudzinski, J.T., D. Perizzolo, and D.M. Brunette, *Effects of substratum surface topography on the organization of cells and collagen fibers in collagen gel cultures.* Journal of Biomedical Materials Research, 2002. **61**(4): p. 608-618.

10. Matsumoto, N., et al., *Effect of alignment of the transplanted graft extracellular matrix on cellular repopulation and newly synthesized collagen.* Archives of Orthopaedic and Trauma Surgery, 1998. **117**(4-5): p. 215-221.

11. Borg, T.K., et al., *Recognition of extracellular-matrix components by neonatal and adult cardiac myocytes.* Developmental Biology, 1984. **104**(1): p. 86-96.

12. Simpson, D.G., et al., *Modulation of cardiac myocyte phenotype in-vitro by the composition and orientation of the extracellular-matrix.* Journal of Cellular Physiology, 1994. **161**(1): p. 89-105.

13. Walsh, K.B., et al., *Modulation of outward potassium currents in aligned cultures of neonatal rat ventricular myocytes during phorbol ester-induced hypertrophy.* Journal of Molecular and Cellular Cardiology, 2001. **33**(6): p. 1233-1247.

14. Lee, P., et al., *Microfluidic alignment of collagen fibers for in vitro cell culture.* Biomedical Microdevices, 2006. **8**(1): p. 35-41.

15. Guido, S. and R.T. Tranquillo, *A methodology for the systematic and quantitative study of cell contact guidance in oriented collagen gels - correlation of fibroblast orientation and gel birefringence.* Journal of Cell Science, 1993. **105**: p. 317-331.

16. Dickinson, R.B., S. Guido, and R.T. Tranquillo, *Biased cell-migration of fibroblasts exhibiting contact guidance in oriented collagen gels.* Annals of Biomedical Engineering, 1994. **22**(4): p. 342-356.

17. Kotani, H., et al., *Magnetic orientation of collagen and bone mixture.* Journal of Applied Physics, 2000. **87**(9): p. 6191-6193.

18. Torbet, J. and M.C. Ronziere, *Magnetic alignment of collagen during self-assembly.* Biochemical Journal, 1984. **219**(3): p. 1057-1059.

19. Guo, C. and L.J. Kaufman, *Flow and magnetic field induced collagen alignment.* Biomaterials, 2007. **28**(6): p. 1105-1114.

20. Hartgerink, J.D., E. Beniash, and S.I. Stupp, *Self-assembly and mineralization of peptide-amphiphile nanofibers.* Science, 2001. **294**(5547): p. 1684-1688.

21. Roth, E.A., et al., *Inkjet printing for high-throughput cell patterning.* Biomaterials, 2004. **25**(17): p. 3707-3715.

22. Nakamura, M., et al., *Biocompatible inkjet printing technique for designed seeding of individual living cells.* Tissue Engineering, 2005. **11**(11-12): p. 1658-1666.

23. Pardo, L., W.C. Wilson, and T.J. Boland, *Characterization of patterned self-assembled monolayers and protein arrays generated by the ink-jet method.* Langmuir, 2003. **19**(5): p. 1462-1466.

CHAPTER FIVE

EFFECTS OF MATRIX COMPOSITION AND ORIENTATION ON CARDIOMYOCYTE AND VASCULAR SMOOTH MUSCLE CELL MECHANICAL PROPERTIES

5.1 Introduction

All cells in the body are subjected to mechanical stimuli in their surrounding environment. These stimuli are transmitted through the cell's intracellular signal transduction pathways to the nucleus, ultimately resulting in altered growth, differentiation, migration, contractility, and apoptosis [1-4]. Any deviation in cell structural and mechanical properties will alter the way the cell responds to mechanical stimuli, which may result in the breakdown of physiological function and possibly lead to disease [5, 6]. Therefore, the study of cellular mechanics is important for understanding cell behavior and disease progression.

Many researchers who have investigated cellular mechanical properties have noted the high level of heterogeneity they observed in whole-cell mechanical properties between cells from a single population [7-11]. This heterogeneity has been observed in many cell populations and with several measurement techniques. In particular, the coefficient of variation (COV = standard deviation / mean) values for cellular mechanical parameters within a single population are in the range of 43-103% in atomic force microscopy studies and 30-128% in micropipette aspiration studies [12]. This variability cannot be credited to the measurement techniques, as their repeatability has been

statistically confirmed (repeated measurements of mechanical properties for a single cell have COV of only 5%) [9].

It is important to fully understand the sources of this heterogeneity to remove confounding variables that can obscure the results of studies, such as those investigating effects of disease or treatments on cellular mechanical behavior. Additionally, understanding the causes of cellular mechanical heterogeneity in an *in vitro* environment will allow researchers to better predict cellular mechanical behavior *in vivo*. In previous experiments, researchers found that cellular phenotype and confluency affected cell mechanical properties, while morphology did not [7, 12]. This work was done on multiple cell populations, but it suggests that variations in cellular phenotype and confluency throughout a single population could account for the variability in measured mechanical properties from cells throughout the sample.

In most cell culture studies, extracellular matrix (ECM) proteins are used to promote cell attachment. These proteins are randomly oriented throughout the sample and the concentration varies throughout the sample. We hypothesized that this variation in the cellular microenvironment was significant enough to lead to variations in cellular structure and, in turn, cellular mechanical properties. In order to limit this type of variability in the cellular microenvironment, aligned matrices were created (Chapter 4) and used as substrates for cells in culture.

The main objective of this study was to determine if culturing cells on aligned matrices resulted in a more mechanically homogeneous population. For this, we cultured both cardiomyocytes and vascular smooth muscle cells on aligned and unaligned collagen

and fibronectin matrices for a period of 1 to 15 days. Cellular mechanical properties were measured using AFM techniques and the cells were visualized using immunofluorescence staining. In doing this, we not only satisfied our main objective. We were also able to draw conclusions about the effects of time (days 1 – 15) and extracellular matrix composition (collagen vs. fibronectin) on cellular mechanical properties in 2D culture.

5.2 Materials and Methods

5.2.1 Substrates

Twelve millimeter diameter glass slides (Fisher Scientific, Pittsburgh, PA, USA) were plasma cleaned for 10 minutes, followed by UV sterilization in 70% ethanol for at least 1 hour. The slides were then dried and coated with thin layers of 1 mg/ml type I collagen and fibronectin solutions (BD Biosciences, Rockville, MD, USA). Each matrix solution was applied in both aligned and unaligned orientations to produce 4 samples: aligned collagen, unaligned collagen, aligned fibronectin, and unaligned fibronectin. A modified inkjet printer was utilized to align the substrate fibers within thin printed lines, as described in Chapter 4 [13]. The unaligned samples were simply prepared by spreading 5 µl of the matrix solution over the slide surface. The matrix-coated slides were incubated at 37°C for approximately 24 hours before plating cells on them.

5.2.2 Cells

To isolate neonatal rat cardiomyocytes, the hearts of 3 day old pups were removed, minced, and subjected to collagenase dissociation as described previously [14-16]. Each matrix-coated slide received approximately 57,000 cardiomyocytes (50,000 cells/cm^2) to create a near-confluent layer of cells. All samples were maintained in 24-well plates under standard conditions (37ºC, 5% CO_2). The cardiomyocytes were maintained in Dulbecco's modified Eagle's medium (DMEM) (Fisher), supplemented with 8% horse serum (Invitrogen Life Technologies, Chicago, IL, USA), 5% newborn bovine serum (Invitrogen), 1% penicillin/streptomycin (Fisher), sodium bicarbonate (Sigma-Aldrich, St. Louis, MO, USA), HEPES (pH 7.4) (Sigma-Aldrich), amphotericin B (Fisher), and proliferative cell inhibitor Cytosin β-D-arabinofuranoside (Sigma-Aldrich) to prevent fibroblast growth. The media was changed every 48 hours and cell growth was monitored daily via light microscopy. After 24 hours in culture, most cells had started contracting at a frequency of approximately 1 Hz. Figure 5.1 illustrates the structural differences between the cardiomyocytes on unaligned and aligned substrates after 5 days in culture.

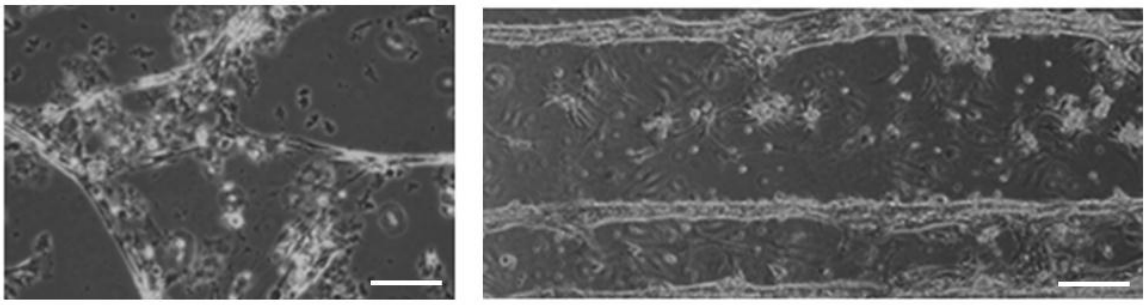

Figure 5.1. Brightfield microscopy images of day 5 cardiomyocytes on unaligned (left) and aligned (right) collagen matrices (scale bar = 20 μm).

Aortic smooth muscle cells were isolated from week 12 Sprague-Dawley rats as outlined in Appendix A. The isolated primary cells were allowed to culture in T75 flasks under standard conditions (37ºC, 5% CO_2) with media (DMEM (Fisher), 10% FBS (Sigma-Aldrich), 1% antibiotic/antimycotic solution (Sigma-Aldrich)) exchanges every 48 hours. Once the cells reached approximately 80% confluency, they were passaged and divided into new T75 flasks until reaching approximately 80% confluency again. This process was replicated several times to increase the total cell number. The vascular smooth muscle cells (VSMCs) were utilized for experimentation between passages 5 and 8. These cells were seeded on the substrates at 20,000 cells/cm^2 (subconfluent layer) and maintained in culture under standard conditions for 5 days before testing. On day 5, the VSMCs were typically at approximately 80% confluency. Figure 5.2 illustrates the structural differences between the VSMCs on unaligned and aligned substrates.

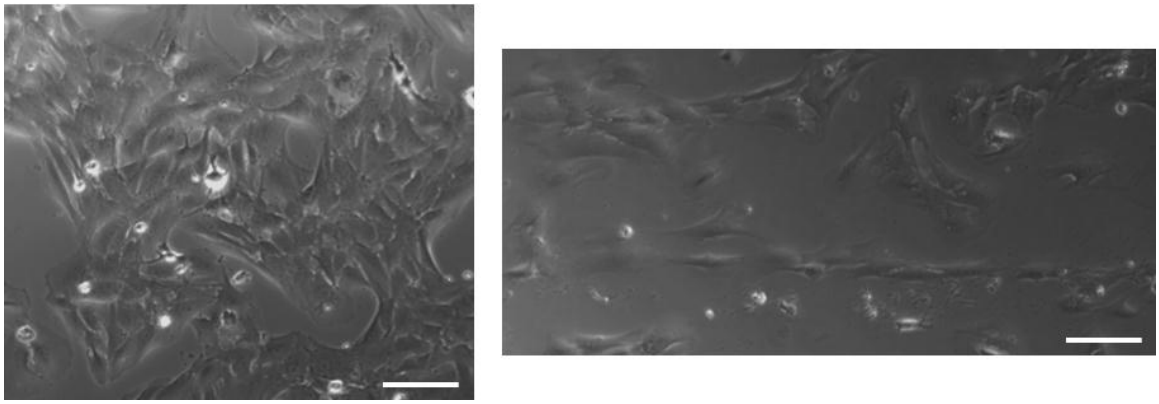

Figure 5.2. Brightfield microscopy images of day 5 vascular smooth muscle cells on unaligned (left) and aligned (right) fibronectin matrices (scale bar = 100 μm).

5.2.3 AFM Indentation

Atomic force microscopy (AFM) cytoindentation experiments were performed 1 to 15 days after the cells were seeded on the slides. Specifically, a cardiomyocyte sample was tested each day on days 1, 2, 3, 5, 7, 9, and 15. The vascular smooth muscle cell samples were only tested on day 5. For all AFM experiments, an Asylum Research MFP-3D AFM (Asylum Research, Santa Barbara, CA, USA) was operated in contact mode with a fluid cell. The cells remained on their slides throughout the study, with warm (37°C) media exchanged every 30 minutes. A 5 μm diameter borosilicate spherical-tipped AFM probe on a silicon-nitride cantilever with a spring constant of 0.12 N/m (Novascan, Ames, IA, USA) was used to mechanically probe individual cells. Before each experiment, the deflection sensitivity (nm/V) was determined by indenting onto a clean glass slide with media present. The AFM optical microscope (10x) was used to position the tip of the cantilever over the center of a cell before data was collected. For cardiomyocyte samples, each cell was indented five times to approximately 1 μm depth

at 5 μm/sec (5 force curves). Each indentation was done immediately following cell contraction to ensure the force measurements represented relaxed cells, as cardiomyocytes have been shown to exhibit different elastic moduli in contraction and relaxation [17]. The vascular smooth muscle cells were indented in the same manner, but at a reduced speed of 1 μm/sec. Each cell was also subjected to two-1 μm step indentation and 60 second hold experiments (2 stress relaxation curves). For each sample, 20 cells from throughout the culture area were probed in this manner.

5.2.4 Force Curve Analysis

The force curves were exported from the AFM software and a custom MATLAB script (MathWorks, Natick, MA, USA) was used to normalize and shift the curves to a common zero point. The contact point was determined as the point where the slope of the curve changes by fitting the curve to a 2-region model [9]. To obtain a measure of individual cell stiffness, the apparent elastic modulus of each cell was calculated by fitting the Hertz model to the data. This model was fit to the first 500 nm of cardiomyocyte data and the first 300 nm of VSMC data. This indentation depth was chosen as approximately 10 percent of the average cell height as measured by contact mode AFM imaging (average cardiomyocyte height ≈ 5 μm, average VSMC height ≈ 3 μm), because the Hertz model only remains accurate within the 10 percent strain range [18]. The Hertz model for a spherical indenter is defined by the following equation:

$$F = \frac{4}{3}\frac{E}{(1-\upsilon^2)} R^{\frac{1}{2}} \delta^{\frac{3}{2}}$$

In this equation, F is the measured force (N), E is the apparent elastic modulus (Pa), υ is Poisson's ration (0.5), R is the radius of the spherical indenter (2.5 µm), and $\boldsymbol{\delta}$ is the indentation depth (m). All MATLAB scripts that were used to calculate the apparent elastic modulus can be found in Appendix B. Figure 5.3 shows a typical force curve with the overlying Hertz model fit to the first 500 nm of indentation.

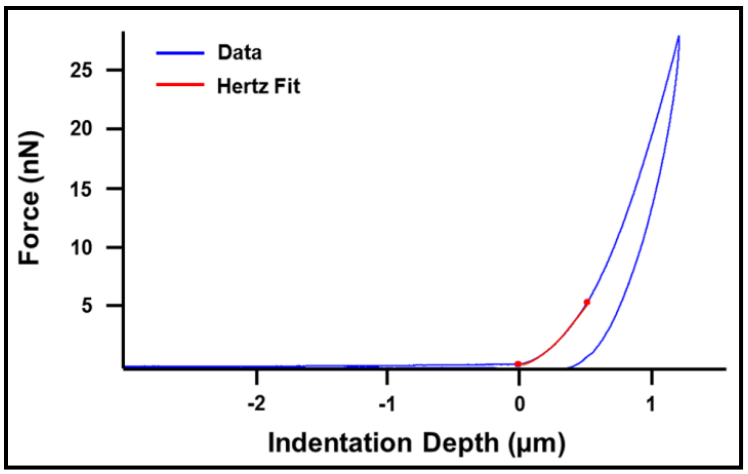

Figure 5.3. Sample force curve with Hertz model fit to the first 500 nm of indentation.

5.2.5 Stress Relaxation Curve Analysis

The stress relaxation curves were also exported from the AFM software and analyzed using custom MATLAB scripts (Appendix C). All curves were first shifted along the y-axis to move the baseline (minimum) force to zero. The curves were then normalized by setting the maximum force value to one, meaning all the relaxation data fell in the zero to one normalized force range. The normalized data can be described as a reduced relaxation function (G (t)) and the percentage of relaxation can be calculated as:

Percent Relaxation = 1 – G (t = 60 sec)

The percent relaxation during the 60 second hold was calculated in this manner for each stress relaxation curve. Each curve was also fit with two relaxation models: the Quasilinear Viscoelastic (QLV) model and the Standard Linear Solid (SLS) model. The QLV reduced relaxation function G (t) contains 3 parameters (c, τ_1, and τ_2) with a continuous relaxation spectrum ($S(\tau) = c/\tau$) between τ_1 and τ_2:

$$G(t) = \frac{1 + c\int_{\tau_1}^{\tau_2} \frac{e^{\frac{-t}{\tau}}}{\tau} d\tau}{1 + c\int_{\tau_1}^{\tau_2} \frac{1}{\tau} d\tau}$$

The constant c is unitless and represents a relative measure of viscous energy dissipation while τ_1 and τ_2 are time constants governing short and long term relaxation behavior, respectively. The SLS reduced relaxation function is:

$$G(t) = E_R\left[1 - \left(1 - \frac{\tau_\sigma}{\tau_\varepsilon}\right) e^{\frac{-t}{\tau_\varepsilon}}\right]$$

In this equation, E_R is the reduced-relaxation modulus, τ_σ is the relaxation time for constant stress, and τ_ε is the relaxation time for constant strain. Figures 5.4 and 5.5 show typical cardiomyocyte and vascular smooth muscle cell stress relaxation data with QLV and SLS model fits.

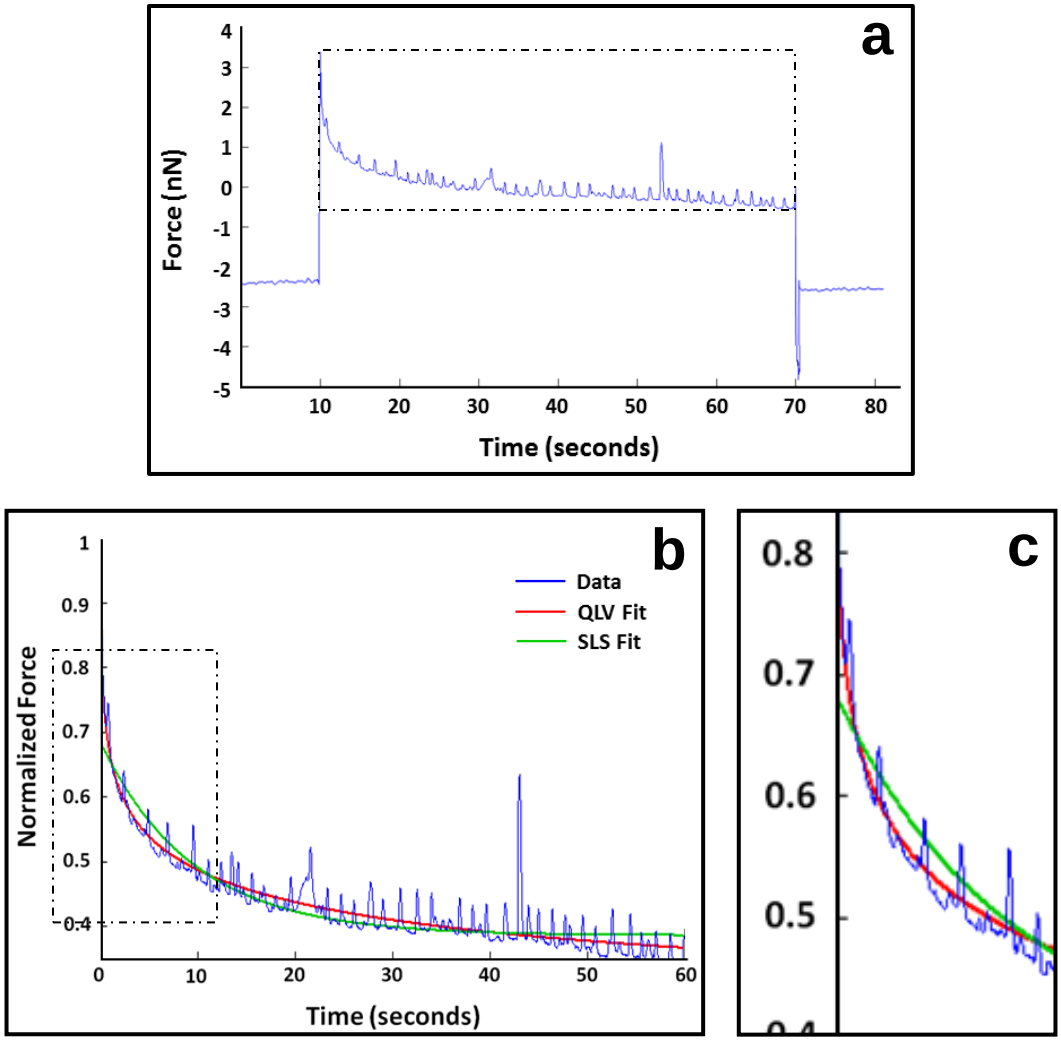

Figure 5.4. Sample cardiomyocyte stress relaxation curve. Spikes in data represent cellular contractions (beating). Raw data (a) and the relaxation portion of the data after normalization with overlying QLV and SLS model fits (b). Zoomed in section (c) shows how the SLS model fails to fit the fast initial relaxation in the data.

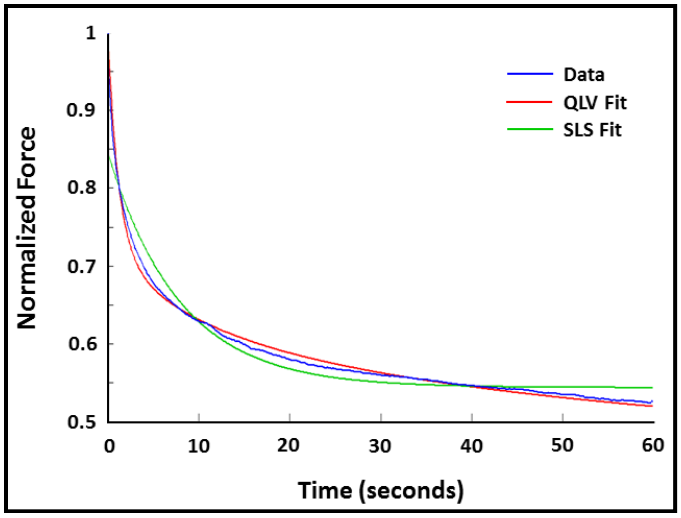

Figure 5.5. Sample vascular smooth muscle cell stress relaxation data with overlying QLV and SLS model fits.

5.2.6 Statistics

For both the elastic modulus and percent relaxation measures, Student's t-tests were used to determine any statistically significant differences between samples on a given day and within samples across time points. P-values less than 0.05 were considered statistically significant. Additionally, the coefficient of variation (COV = standard deviation / mean) was calculated within each sample as a measure of cell-to-cell variation and within each cell-loading session as a measure of data repeatability on a single point of indentation. The accuracy of the QLV and SLS models in predicting cellular stress relaxation behavior was accessed by calculating the coefficient of determination (R^2) for each model fit.

5.2.7 Immunofluorescence

Day 5 cardiomyocytes on each sample were fixed and stained for nuclei, filamentous actin, and N-cadherin. Specifically, cells were fixed in 4 percent paraformaldehyde at room temperature for 10 minutes. Following 2 – 15 minute rises with PBS, the samples were incubated with a solution of 0.01M glycine and 0.1% Triton-X in PBS for 30 minutes, 5% bovine serum albumin (BSA) in PBS for 15 minutes, then 5% normal donkey serum / 1% BSA in PBS for 15 minutes. The samples were then treated with a mouse N-cadherin monoclonal primary antibody (1:100 in 1% BSA/PBS, Sigma-Aldrich) overnight at 4° C. The samples were rinsed with 1% BSA/PBS (2 x 15 minutes) and 5% normal donkey serum in 1% BSA/BPS (15 minutes) before application of a secondary donkey anti-mouse rhodamine (TRITC)-conjugated antibody (1:100 in 1% BSA/PBS, Jackson ImmunoResearch, West Grove, PA, USA) for 2 hours. Next, the samples were rinsed with 1% BSA/PBS (15 minutes) and twice with PBS. They were then incubated with Alexa Fluor 488 phalloidin (1:100 in PBS, Invitrogen) for 15 minutes. Finally, the samples were rinsed 3 times with PBS and mounted on microscope slides with SlowFade Gold antifade reagent with DAPI (Invitrogen).

Day 5 VSMCs were fixed and stained for nuclei, filamentous actin, and microtubules. The same protocol was followed with a different primary antibody: monoclonal anti-α-tubulin antibody produced in mouse (1:100 in 1% BSA/PBS, Sigma-Aldrich). All samples were stored in the dark before microscopy. The samples were viewed using an Olympus IX81 spinning disk confocal microscope (Olympus, Tokyo,

Japan) and digital images were collected and processed using MetaMorph Image Analysis software (Molecular Devices, Sunnyvale, CA, USA).

5.3 Results

5.3.1 Cardiomyocytes

Elastic Modulus

The mean apparent elastic moduli measures for cardiomyocytes on each substrate throughout the 15 day study are outlined in Figure 5.6. On day 1 in culture, the mean apparent elastic moduli for cells on each substrate ranged from 4.0 kPa to 6.8 kPa, with a significant difference between the cells on unaligned and aligned collagen substrates ($p = 0.045$). On days 2 and 3, cellular elastic modulus measures increased for each sample, with significant increases from day 1 to day 3 for each sample ($p \leq 0.005$). On both of these days, cells on unaligned collagen were significantly less stiff than cells on the other substrates ($p \leq 0.015$), which did not significantly differ from one another. Elastic moduli measures continued to increase from day 3 to day 5 (significant for all samples except aligned collagen, $p \leq 0.003$). On day 5, the cells on unaligned collagen remained significantly less stiff than cells on all the other substrates ($p \leq 0.036$). Additionally, the aligned collagen sample exhibited a significantly lower mean elastic modulus than the aligned fibronectin sample ($p = 0.041$). Within each sample, no more significant differences in elastic moduli measures with time were observed from day 5 through day 15. On day 7, aligned fibronectin samples remained significantly stiffer than unaligned and aligned collagen samples ($p \leq 0.0003$). On both days 9 and 15, the unaligned and

aligned collagen samples were significantly less stiff than the unaligned and aligned fibronectin samples ($p \leq 0.004$). The final (day 15) mean elastic moduli measures were 13.7 kPa for unaligned collagen, 17.5 kPa for aligned collagen, 34.4 kPa for unaligned fibronectin, and 38.0 kPa for aligned fibronectin.

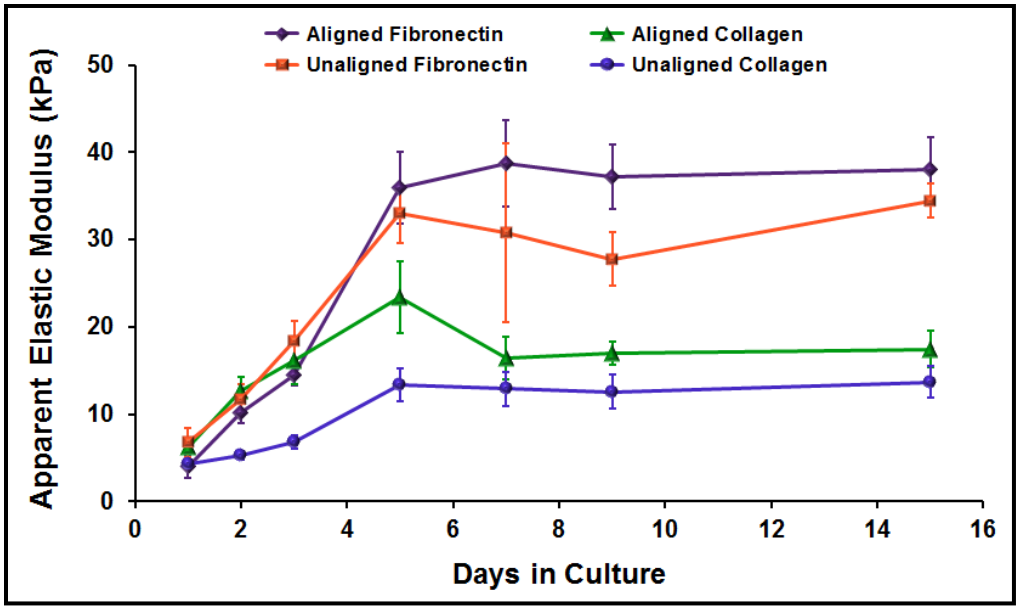

Figure 5.6. Apparent elastic moduli of cardiomyocytes on different substrates over 15 day culture period. Data presented as mean ± standard error.

The average cell-to-cell and repeated point elastic modulus COV measures for cardiomyocytes on each of the 4 sample types can be found in Table 5.1. The level of variation both from cell-to-cell and within repeated measures on a single cell was consistent across sample types (no significant differences). The average cell-to-cell COV for elastic moduli measures was relatively high at 57.2% for all samples. The average repeated point COV for elastic moduli measures was much smaller at 14.1%, indicating

that the variation that was observed among elastic moduli measurements on different cells in a single sample was not due to the measurement technique, but was in fact due to differences in the cellular mechanical properties.

Table 5.1. Cardiomyocyte cell-to-cell and repeated point coefficients of variation (COV) for elastic modulus and percent relaxation measures. Data from all days were averaged to get a measure for the average variation within each sample (substrate type).

	Samples	Average Cell-to-Cell COV (%)	Average Repeated Point COV (%)
Elastic Modulus	Unaligned Collagen	53.9	13.9
	Aligned Collagen	51.3	14.9
	Unaligned Fibronectin	68.2	15.5
	Aligned Fibronectin	55.5	12.1
	All (mean ± standard error)	**57.2 ± 6.2**	**14.1 ± 1.5**
Percent Relax	Unaligned Collagen	37.3	7.3
	Aligned Collagen	32.8	4.6
	Unaligned Fibronectin	39.3	7.4
	Aligned Fibronectin	40.2	6.3
	All (mean ± standard error)	**37.4 ± 1.5**	**6.4 ± 0.6**

Stress Relaxation

The mean percent relaxation measures for cardiomyocytes on each substrate throughout the 15 day study are outlined in Figure 5.7. On day 1 in culture, the mean percent relaxation measures for cells on each substrate ranged from 62.0% to 68.8%, with no significant differences between the different samples. Between days 1 and 2, the percent relaxation measures for all samples decreased (cells exhibited less relaxation during 60 second hold), but the drop was only significant for the cells on aligned fibronectin ($p = 0.003$). On day 2, the average percent relaxation measure for cells on

unaligned collagen was significantly higher than that for aligned collagen ($p = 0.017$). From day 2 to day 3, percent relaxation measures continued to decrease, significantly for unaligned collagen ($p = 0.040$). The drop in percent relaxation measures between days 1 and 3 was significant for all samples ($p \leq 0.011$). On day 3, there were no significant differences in percent relaxation measures among the different samples. Within each sample, no more significant differences in percent relaxation measures with time were observed from day 3 through day 15. On day 5, the unaligned collagen sample exhibited a significantly greater percent relaxation than the aligned collagen and aligned fibronectin samples ($p \leq 0.036$). The only remaining statistically significant differences were between aligned and unaligned collagen on day 7 ($p = 0.013$) and aligned collagen and unaligned fibronectin on day 15 ($p = 0.015$). The final (day 15) mean percent relaxation measures during the 60 second hold were 52.6% for unaligned collagen, 46.0% for aligned collagen, 54.1% for unaligned fibronectin, and 50.6% for aligned fibronectin.

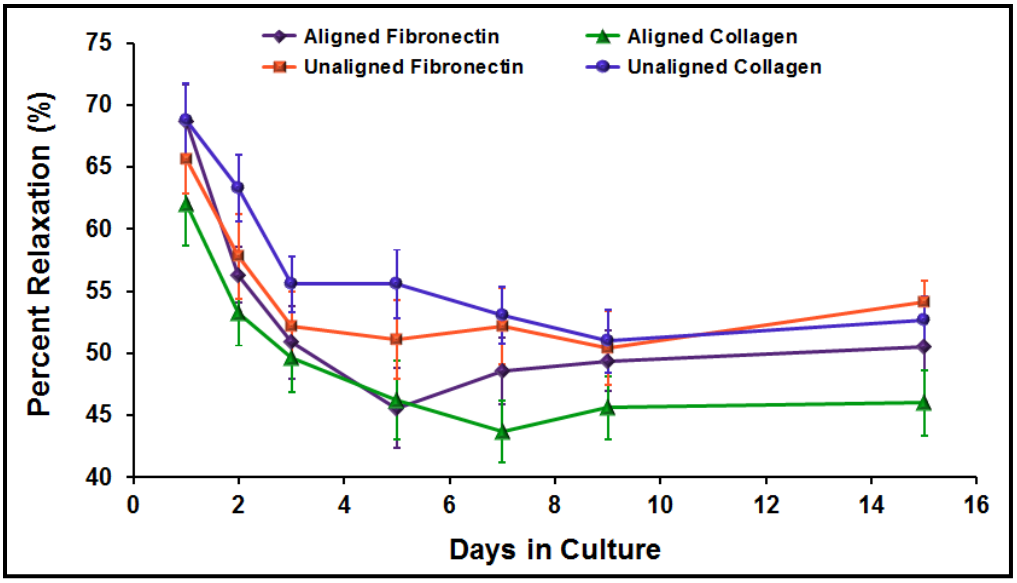

Figure 5.7. Percent relaxation during 60 second hold for cardiomyocytes on different substrates over 15 day culture period. Data presented as mean ± standard error.

The average cell-to-cell and repeated point percent relaxation COV measures for cardiomyocytes on each of the 4 sample types can be found in Table 5.1. The level of variation both from cell-to-cell and within repeated measures on a single cell was consistent across sample types (no significant differences). The average cell-to-cell COV for percent relaxation measures (37.4%) was lower than that for elastic moduli measures (57.2%) for all samples. The average repeated point COV for percent relaxation measures was very low at 6.4%, indicating that the variation that was observed among percent relaxation measurements on different cells in a single sample was not due to the measurement technique, but was in fact due to differences in the cellular mechanical properties.

In general, the QLV model fit the cardiomyocyte relaxation data very well (Figure 5.4). The mean coefficient of determination (R^2) for QLV fits to all cardiomyocyte relaxation data was 0.89 ± 0.14 (standard deviation). The SLS model did not fit the data as well, with a mean R^2 of 0.84 ± 0.13 for SLS fits to all relaxation data. The SLS model failed to fit the initial fast relaxation and then alternately overshot and undershot the remaining data (Figure 5.4). The R^2 values would have been higher if the myocytes were in a relaxed state during the hold (not contracting).

Immunofluorescence

Native cardiomyocytes are highly aligned and combine to form cardiac muscle fibers. These cells contain myofibrils aligned parallel to the long axis of the cardiac muscle fibers and intercalated discs between cells that transmit electrochemical signals [19]. The cardiomyocytes cultured on the aligned collagen and fibronectin matrices typically lined up end-to-end and took on a phenotype similar to cells found *in vivo*. The immunofluorescence staining revealed that the actin fibers (components of myofibrils) were highly aligned within these cells and N-cadherin (component of intercalated discs) was concentrated at the intersection between neighboring cells (Figure 5.8). In contrast to this, the cardiomyocytes on unaligned collagen and fibronectin matrices were typically spread in all directions with variable cell-cell interactions. Within these cells, the actin fibers were oriented in all directions and the N-cadherin was not more concentrated in any region. Thus, it can be concluded that both the aligned collagen and fibronectin

matrices promote a much more *in vivo*-like cardiomyocyte phenotype in 2D culture than the unaligned collagen and fibronectin matrices.

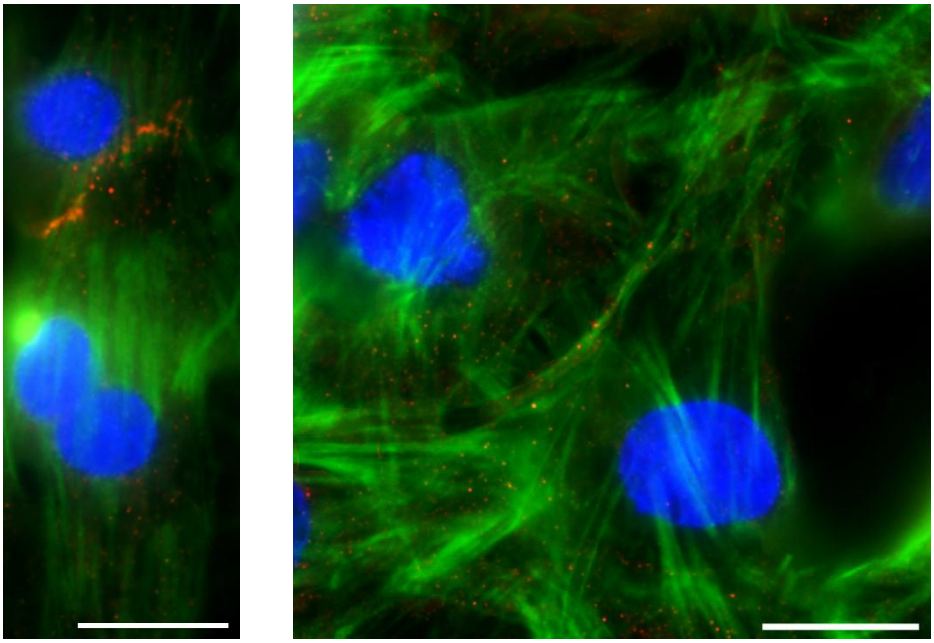

Figure 5.8. Representative immunofluorescence images of day 5 cardiomyocytes on an aligned matrix (left) and an unaligned matrix (right) (scale bar = 20 μm). Cells are stained for nuclei (blue), filamentous actin (green), and N-cadherin (red).

5.3.2 Vascular Smooth Muscle Cells

Elastic Modulus

The mean apparent elastic moduli measures for day 5 VSMCs ranged from 9.2 kPa for the unaligned collagen sample to 13.3 kPa for the aligned fibronectin sample (Figure 5.9). For both aligned and unaligned samples, cells on collagen matrices were less stiff than cells on fibronectin matrices. For both collagen and fibronectin samples, cells on unaligned matrices were less stiff than cells on aligned matrices. The change

from collagen to fibronectin samples or unaligned to aligned samples was fairly uniform, increasing the average cellular elastic modulus by approximately 2 kPa. However, these differences were not large enough to be considered statistically significant ($p \geq 0.161$).

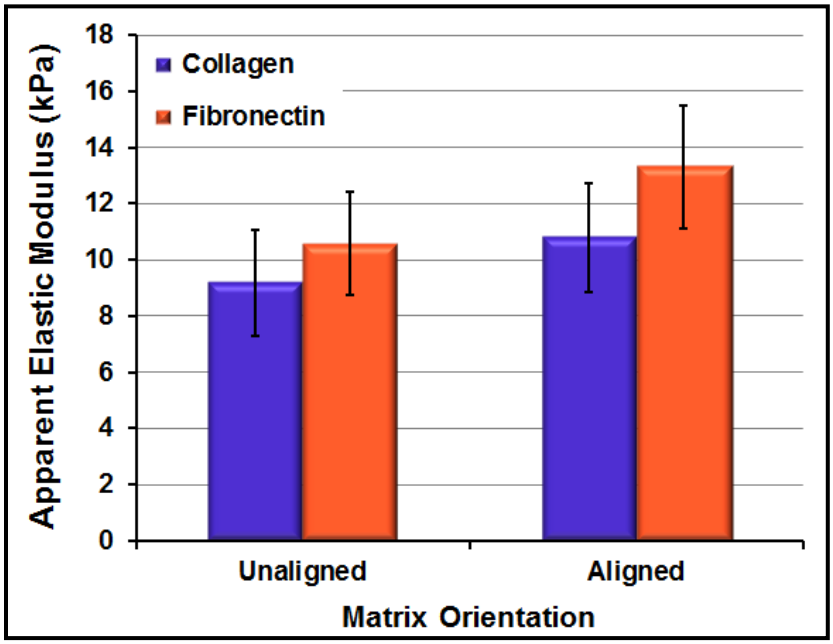

Figure 5.9. Apparent elastic moduli of day 5 VSMCs on different substrates. Data presented as mean ± standard error.

The average cell-to-cell and repeated point elastic modulus COV measures for day 5 VSMCs on each of the 4 sample types can be found in Table 5.2. The average cell-to-cell COV for elastic moduli measures was 70.3%, slightly higher than the average level of variation that was found within elastic moduli measures for cardiomyocytes (57.2%). The COV measures for aligned samples were 10.1% (collagen) and 3.6% (fibronectin) lower than the COV measures for unaligned samples. This suggests that there was less variation within elastic moduli measures for cardiomyocytes on the aligned

substrates, but this drop in variation was not large. The average repeated point COV for elastic moduli measures was low (16.9%) as expected, confirming that the cell-to-cell variation was in fact due to differences in the cellular mechanical properties.

Table 5.2. VSMC (day 5) cell-to-cell and repeated point coefficients of variation (COV) for elastic modulus and percent relaxation measures.

	Sample	Average Cell-to-Cell COV (%)	Average Repeated Point COV (%)
Elastic Modulus	Unaligned Collagen	79.7	16.5
	Aligned Collagen	69.6	15.7
	Unaligned Fibronectin	67.7	18.4
	Aligned Fibronectin	64.1	17.1
	All (mean ± standard error)	**70.3 ± 3.3**	**16.9 ± 0.6**
Percent Relax	Unaligned Collagen	59.1	6.1
	Aligned Collagen	70.9	8.0
	Unaligned Fibronectin	81.0	6.0
	Aligned Fibronectin	65.7	6.4
	All (mean ± standard error)	**69.2 ± 4.6**	**6.6 ± 0.5**

Stress Relaxation

The mean percent relaxation measures for day 5 VSMCs ranged from 33.6% for the aligned fibronectin sample to 40.3% for the unaligned collagen sample (Figure 5.10). For both aligned and unaligned samples, cells on collagen matrices relaxed more than cells on fibronectin matrices. For both collagen and fibronectin samples, cells on unaligned matrices relaxed more than cells on aligned matrices. The drop in percent relaxation measures from collagen to fibronectin samples was approximately 5%, while

the drop from unaligned to aligned samples was approximately 2%. No differences between samples were considered statistically significant ($p \geq 0.483$).

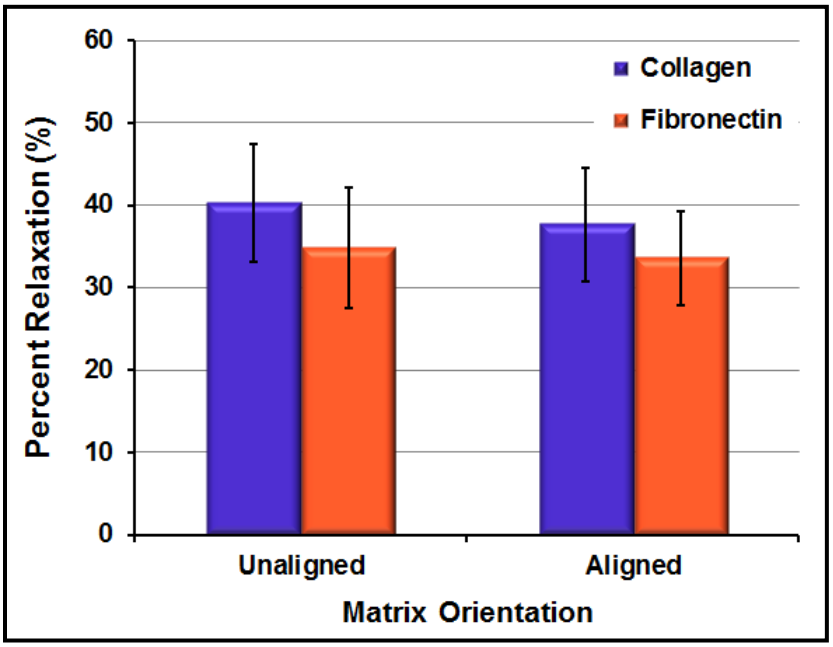

Figure 5.10. Percent relaxation during 60 second hold for day 5 VSMCs on different substrates. Data presented as mean ± standard error.

The average cell-to-cell and repeated point percent relaxation COV measures for day 5 VSMCs on each of the 4 sample types can be found in Table 5.2. The average cell-to-cell COV for percent relaxation measures was 69.2%, very close to the COV for elastic moduli measures (70.3%) and significantly higher than the average percent relaxation COV for cardiomyocytes (37.4%). This indicates that cardiomyocytes from a single sample were more uniform in their relaxation behavior than VSMCs from a single sample. The percent relaxation COV measures for aligned VMCS samples were 11.8% higher (collagen) and 15.3% lower (fibronectin) than the COV measures for unaligned

samples. These changes are not large and are conflicting, so we cannot draw the conclusion that aligned matrices promote more uniform cellular mechanical properties. The average repeated point COV for percent relaxation measures was low (6.6%) as expected, confirming that the cell-to-cell variation was in fact due to differences in the cellular mechanical properties.

The VSMC relaxation behavior during the 60 second hold was very similar to the cardiomyocyte relaxation behavior (similar shape to relaxation curves – Figures 5.4 and 5.5). As such, the QLV model fit the relaxation data very well while the SLS model did not fit the data as well, just as they had for the cardiomyocytes. The mean coefficient of determination for the QLV model fit to the VSMC relaxation data was 0.99 while the mean R^2 for the SLS model fit was 0.95.

Immunofluorescence

In a healthy blood vessel, VMSCs are almost entirely contractile. Contractile VSMCs cells are fusiform in shape, with the narrow part of one cell lying adjacent to the broad part of neighboring cells [20, 21]. These cells have a very high cytoplasmic volume fraction of myofilaments to allow for contraction. Synthetic VSMCs are present primarily during vascular development and can be found to a greater degree in unhealthy blood vessels. These cells spread in all directions and contain very few myofilaments.

In culture, the VSMCs exhibited a continuum of phenotypes, rather than purely contractile or synthetic cells. However, in general, VSMCs on both of the aligned matrices took on a more contractile phenotype, as they were generally long and narrow

and each cell contained actin fibers that were highly aligned along the long axis of the cell (Figure 5.11). Because they were in 2D culture, they were spread out flat (wider than native cells) and positioned end-to-end (rather than alternating as seen *in vivo*). The VSMCs on both unaligned matrices generally took on a more synthetic phenotype, which is typical for VSMCs in culture [22]. The cytoskeletal elements (actin, microtubules) within these cells exhibited no clear organization. No phenotypical differences were evident between cells on collagen and cells on fibronectin samples.

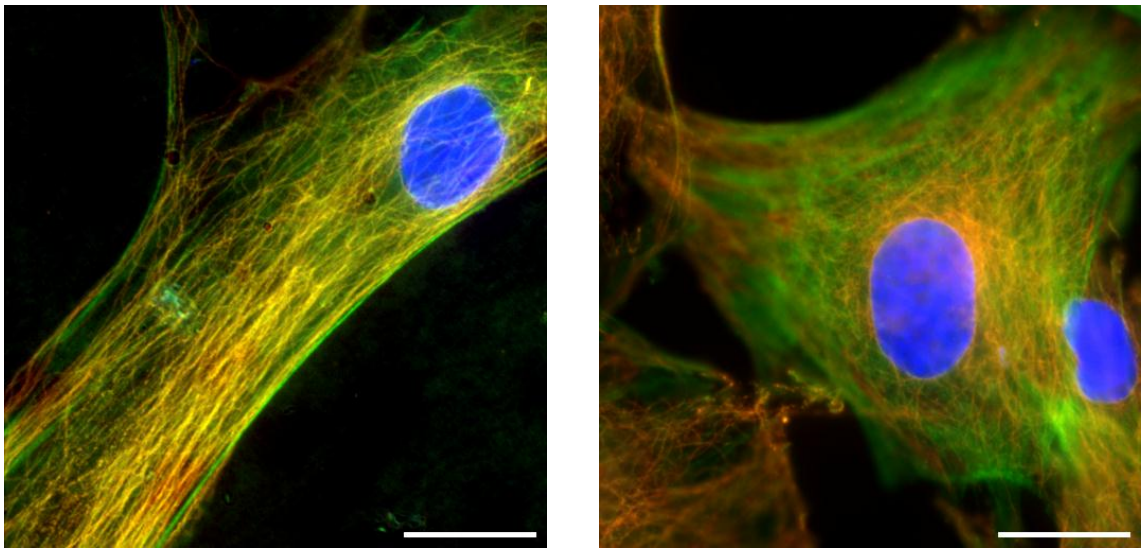

Figure 5.11. Representative immunofluorescence images of day 5 VSMCs on an aligned matrix (left) and an unaligned matrix (right) (scale bar = 20 μm). Cells are stained for nuclei (blue), filamentous actin (green), and microtubules (red).

5.4 Discussion

In this study, the cellular microenvironment was limited by reducing the variation within the extracellular matrix upon which the cells were cultured. Printed ECM proteins

have been shown to be much more uniform in their distribution and orientation than the randomly oriented proteins that are easily prepared and often used in cell culture [13]. The main objective of this study was to determine if, and to what extent, culturing cells on these more uniform printed matrices affected the level of cell-to-cell variability in mechanical properties. To this end, the mechanical properties of two different cell types (cardiomyocytes and VSMCs) on two different matrix materials (collagen and fibronectin) were investigated.

For the cardiomyocytes, elastic moduli measures increased over the first five days in culture for cells on all four sample types (aligned collagen, unaligned collagen, aligned fibronectin, unaligned fibronectin). The elastic moduli of the cells generally reached a plateau at day five. From this point on (day 5 – day 15), the cells were the most stiff on aligned fibronectin (~37 kPa), followed by unaligned fibronectin (~32 kPa), aligned collagen (~18 kPa), and lastly unaligned collagen (~13 kPa) (Figure 5.6). These measures are on par with other AFM measurements of neonatal cardiomyocyte elastic moduli [17, 23]. Azeloglu et al. recently looked at the elastic moduli of neonatal cardiomyocytes on scraped (aligned) cardiomyocytes, and found a non-significant increase in elastic moduli between days 5 and 20 [17]. This also correlates well with our data, as we did not observe significant changes in elastic moduli measures after day 5 in culture. The level of heterogeneity (COV) found in cell-to-cell elastic moduli measures (57%) was in the typical range for AFM studies (30 – 128%), while the repeated point elastic moduli measures (14%) were a bit higher than in other studies (5%) (Table 5.1) [9, 12]. The cardiomyocytes on the aligned matrices not only positioned themselves end-to-

end on the aligned matrices, but immunofluorescence staining revealed that the N-cadherin and actin within the cells appeared very similar to native cells [19]. Such highly oriented actin fibers have been shown to promote cellular stiffness, as was found here [24].

The cardiomyocyte percent relaxation measures decreased over the first five days in culture for cells on all four sample types before reaching a plateau. On day 15, the cells on unaligned fibronectin exhibited the highest percentage of relaxation (54%), followed by unaligned collagen (53%), aligned fibronectin (51%), and lastly aligned collagen (46%) (Figure 5.7). Researchers have previously investigated viscoelastic mechanical properties of adherent cells using AFM stress relaxation techniques, but this was the first time measurements were taken on cardiomyocytes [25-29]. The QLV model has been used extensively to model tissue behavior, but was only recently applied to cellular data [29-32]. The SLS model has previously been applied to both cells and tissues [29, 33, 34]. As in other studies, the QLV model provided the best fit to the cardiomyocyte relaxation data with R^2 of 0.89 (higher when cells not contracting). The level of heterogeneity (COV) found in cell-to-cell percent relaxation measures (37%) was on the low end of COV measures for all AFM studies (30 – 128%), while the repeated point percent elastic moduli measures (6%) were very close to repeated point measures in other studies (5%) (Table 5.1) [9, 12].

Overall, the cell-to-cell COV measures for both cardiomyocyte elastic modulus and percent relaxation measures did not decrease for cells on the aligned samples, as we had hypothesized (Table 5.1). Recently, measures of cardiomyocyte mechanical

properties have been shown to vary with the timing of the measurement in the cellular contraction cycle [17]. Even though we were consistent in our indentation timing immediately after contraction, we decided to replicate this study and focus our future studies on another cell type (VSMCs) to remove any potential extra variation that this factor (contraction) could have caused. Nevertheless, the cardiomyocyte study provided us with several valuable insights. To our knowledge, this is the first study where the effects of different matrix compositions and orientations on cellular mechanical properties were compared. These results should be considered for researchers planning cell culture studies where cell mechanics is an important factor.

The VSMCs were only tested on day 5. This was the point when the cardiomyocyte mechanical properties reached a steady state and there was previous VSMC mechanics work done at this time point that we could refer to for comparison [7, 29]. VSMC elastic moduli measurements averaged approximately 10 kPa, with non-significant increases in elastic moduli measures going from unaligned to aligned samples and collagen to fibronectin samples (Figure 5.9). These measurements were similar to day 5 elastic moduli measurements made by Hemmer et al. (~11.1 kPa for indenter speed of 0.5 μm/sec) [7]. The level of heterogeneity (COV) found in cell-to-cell elastic moduli measures (70.3%) was in the typical range for AFM studies (30 – 128%), while the repeated point elastic moduli measures (17%) were slightly higher than in other studies (5%) (Table 5.2) [9, 12]. As seen in the cardiomyocyte study, the VSMCs lined up on along the lines of printed ECM and contained highly oriented actin fibers. In fact, the overall morphology and actin organization with both cell types was similar for cells on

aligned (elongated morphology, oriented fibers) and unaligned matrices (spread morphology, randomly oriented fibers).

The VSMCs exhibited non-significant decreases in percent relaxation measures going from unaligned to aligned samples and collagen to fibronectin samples (Figure 5.10). The QLV and SLS models fit the relaxation data very well with R^2 of 0.99 and 0.95, respectively. The level of heterogeneity (COV) found in cell-to-cell percent relaxation measures (69%) was typical for COV measures for all AFM studies (30 – 128%), while the repeated point percent elastic moduli measures (7%) were very close to repeated point measures in other studies (5%) (Table 5.2) [9, 12].

Overall, the cell-to-cell COV measures for both VSMC elastic modulus and percent relaxation measures did not decrease for cells on the aligned samples, as we had hypothesized (Table 5.2). This was the same result as in the cardiomyocyte study. Therefore, it was concluded that limiting cellular microenvironment variability via matrix alignment did not decrease cellular mechanical heterogeneity as expected. This suggested to us that creating aligned matrices might not have been enough of a microenvironment limitation to affect cellular mechanical heterogeneity. Therefore, in the next study we took a larger step by blocking cell-matrix interactions entirely.

5.5 Conclusions

For both cardiomyocytes and vascular smooth muscle cells, aligned matrices were shown to promote cells with higher elastic moduli and lower percent relaxation measures. In a similar fashion, fibronectin matrices were shown to promote the same trends in

comparison to collagen matrices. Within each sample, however, the level of variation in cellular mechanical properties (for both elastic modulus and percent relaxation) did not decrease for cells on aligned matrices in comparison to cells on unaligned matrices. Therefore, other techniques to limit variability in the cellular microenvironment were investigated in hopes of determining the causes of the high level of mechanical heterogeneity that is observed in cellular mechanical properties.

5.6 References

1. Maniotis, A.J., C.S. Chen, and D.E. Ingber, *Demonstration of mechanical connections between integrins cytoskeletal filaments, and nucleoplasm that stabilize nuclear structure.* Proceedings of the National Academy of Sciences of the United States of America, 1997. **94**(3): p. 849-854.

2. Boudreau, N. and M.J. Bissell, *Extracellular matrix signaling: integration of form and function in normal and malignant cells.* Current Opinion in Cell Biology, 1998. **10**(5): p. 640-646.

3. Huang, S. and D.E. Ingber, *The structural and mechanical complexity of cell-growth control.* Nature Cell Biology, 1999. **1**(5): p. E131-E138.

4. Schwartz, M.A. and M.H. Ginsberg, *Networks and crosstalk: integrin signalling spreads.* Nature Cell Biology, 2002. **4**(4): p. E65-E68.

5. Ingber, D.E., *Mechanobiology and diseases of mechanotransduction.* Annals of Medicine, 2003. **35**(8): p. 564-577.

6. Costa, K.D., *Single-cell elastography: probing for disease with the atomic force microscope.* Disease Markers, 2003. **19**(2-3): p. 139-154.

7. Hemmer, J.D., et al., *Effects of serum deprivation on the mechanical properties of adherent vascular smooth muscle cells.* Proceedings of the Institution of Mechanical Engineers Part H-Journal of Engineering in Medicine, 2008. **222**(H5): p. 761-772.

8. Charras, G.T. and M.A. Horton, *Single cell mechanotransduction and its modulation analyzed by atomic force microscope indentation.* Biophysical Journal, 2002. **82**(6): p. 2970-2981.

9. Jaasma, M.J., W.M. Jackson, and T.M. Keaveny, *Measurement and characterization of whole-cell mechanical behavior.* Annals of Biomedical Engineering, 2006. **34**(5): p. 748-758.

10. Jones, W.R., et al., *Alterations in the Young's modulus and volumetric properties of chondrocytes isolated from normal and osteoarthritic human cartilage.* Journal of Biomechanics, 1999. **32**(2): p. 119-127.

11. Mahaffy, R.E., et al., *Scanning probe-based frequency-dependent microrheology of polymer gels and biological cells.* Physical Review Letters, 2000. **85**(4): p. 880-883.

12. Jaasma, M.J., W.M. Jackson, and T.M. Keaveny, *The effects of morphology, confluency, and phenotype on whole-cell mechanical behavior.* Annals of Biomedical Engineering, 2006. **34**(5): p. 759-768.

13. Deitch, S., et al., *Collagen matrix alignment using inkjet printer technology*. Materials Research Society Symposium Proceedings, 2008. **1094**.

14. Borg, T.K., et al., *Recognition of extracellular-matrix components by neonatal and adult cardiac myocytes.* Developmental Biology, 1984. **104**(1): p. 86-96.

15. Simpson, D.G., et al., *Modulation of cardiac myocyte phenotype in-vitro by the composition and orientation of the extracellular-matrix.* Journal of Cellular Physiology, 1994. **161**(1): p. 89-105.

16. Walsh, K.B., et al., *Modulation of outward potassium currents in aligned cultures of neonatal rat ventricular myocytes during phorbol ester-induced hypertrophy.* Journal of Molecular and Cellular Cardiology, 2001. **33**(6): p. 1233-1247.

17. Azeloglu, E.U. and K.D. Costa, *Cross-bridge cycling gives rise to spatiotemporal heterogeneity of dynamic subcellular mechanics in cardiac myocytes probed with atomic force microscopy.* American Journal of Physiology-Heart and Circulatory Physiology, 2010. **298**(3): p. H853-H860.

18. Dimitriadis, E.K., et al., *Determination of elastic moduli of thin layers of soft material using the atomic force microscope.* Biophysical Journal, 2002. **82**(5): p. 2798-2810.

19. McDevitt, T.C., et al., *In vitro generation of differentiated cardiac myofibers on micropatterned laminin surfaces.* Journal of Biomedical Materials Research, 2002. **60**(3): p. 472-479.

20. Fung, Y.C., *Biomechanics: Mechanical Properties of Living Tissues*. 2nd ed2004, New York: Springer Science and Business Media.

21. Junqueira, L.C. and J. Carneiro, *Basic Histology: Text and Atlas*. 11th ed2005: McGraw-Hill.

22. Poliseno, L., et al., *Resting smooth muscle cells as a model for studying vascular cell activation.* Tissue & Cell, 2006. **38**(2): p. 111-120.

23. Akiyama, N., et al., *Transverse stiffness of myofibrils of skeletal and cardiac muscles studied by atomic force microscopy.* Journal of Physiological Sciences, 2006. **56**(2): p. 145-151.

24. Nagayama, K., et al., *Effiect of actin filament distribution on tensile properties of smooth muscle cells obtained from rat thoracic aortas.* Journal of Biomechanics, 2006. **39**(2): p. 293-301.

25. Darling, E.M., S. Zauscher, and F. Guilak, *Viscoelastic properties of zonal articular chondrocytes measured by atomic force microscopy.* Osteoarthritis and Cartilage, 2006. **14**(6): p. 571-579.

26. Darling, E.M., et al., *A thin-layer model for viscoelastic, stress-relaxation testing of cells using atomic force microscopy: Do cell properties reflect metastatic potential?* Biophysical Journal, 2007. **92**(5): p. 1784-1791.

27. Okajima, T., et al., *Stress relaxation of HepG2 cells measured by atomic force microscopy.* Nanotechnology, 2007. **18**(8).

28. Smith, B.A., et al., *Probing the viscoelastic behavior of cultured airway smooth muscle cells with atomic force microscopy: stiffening induced by contractile agonist.* Biophysical Journal, 2005. **88**(4): p. 2994-3007.

29. Hemmer, J.D., et al., *Role of cytoskeletal components in stress-relaxation behavior of adherent vascular smooth muscle cells.* Journal of Biomechanical Engineering-Transactions of the Asme, 2009. **131**(4): p. 9.

30. Tanaka, T.T. and Y.C. Fung, *Elastic and inelastic properties of canine aorta and their variation along aortic tree.* Journal of Biomechanics, 1974. **7**(4): p. 357-370.

31. Doehring, T.C., E.O. Carew, and I. Vesely, *The effect of strain rate on the viscoelastic response of aortic valve tissue: A direct-fit approach.* Annals of Biomedical Engineering, 2004. **32**(2): p. 223-232.

32. Toms, S.R., et al., *Quasi-linear viscoelastic behavior of the human periodontal ligament.* Journal of Biomechanics, 2002. **35**(10): p. 1411-1415.

33. Engler, A.J., et al., *Surface probe measurements of the elasticity of sectioned tissue, thin gels and polyelectrolyte multilayer films: Correlations between substrate stiffness and cell adhesion.* Surface Science, 2004. **570**(1-2): p. 142-154.

34. Bao, G. and S. Suresh, *Cell and molecular mechanics of biological materials.* Nature Materials, 2003. **2**(11): p. 715-725.

CHAPTER SIX

EFFECTS OF CELL-CELL AND CELL-MATRIX INTERACTIONS ON VASCULAR SMOOTH MUSCLE CELL MECHANICAL PROPERTIES

6.1 Introduction

In Chapter 5, it was found that limiting the cellular microenvironment by culturing cells on a highly organized aligned matrix did not lead to a reduction in cellular mechanical heterogeneity. In a further effort to discover the root causes of this heterogeneity, diversified cell-cell and cell-matrix interactions were investigated. We reasoned that throughout a sample the cell-cell and cell-matrix interactions vary a great deal. For example, one cell may have an abundance of matrix proteins to adhere to while another may have more neighboring cells to interact with. Since confluent cells (more neighboring contacts) have been shown to be 1.5 – 1.8 times stiffer than nonconfluent cells (no neighbors), this difference could account of some of the heterogeneity that is observed across a sample [1]. In general, cell-cell and cell-matrix interactions are strongly tied to cytoskeletal structure and, therefore, cellular mechanical properties.

Cells anchor to underlying extracellular matrix scaffolds through focal adhesion complexes and to neighboring cells through adherens junctions (Figure 6.1) [2]. Through these interactions, the tensed cytoskeletal filaments within the cell are physically coupled to the matrix and cells in their environment. Focal adhesion complexes are comprised of clusters of transmembrane integrins. Integrins are heterodimeric proteins made up of different α and β subunits. The specific combination of the different subunits defines the molecular binding specificity. Integrin $\beta 1$ mediates cellular interactions with collagen

through α2β1 and fibronectin through α5β1 [3]. Proteins such as talin, vinculin, α-actinin, and paxillin connect the cytoplasmic tail of integrins to microfilaments and, to a lesser extent, intermediate filaments [2]. N-cadherin-based adherens junctions help to physically couple the cytoskeleton of one cell to that of its neighbor. Cadherins use some of the same actin-associated proteins as focal adhesion complexes (vinculin, α-actinin) but not others (talin). Cantenins also connect cadherins to microfilaments within adherens junctions [4].

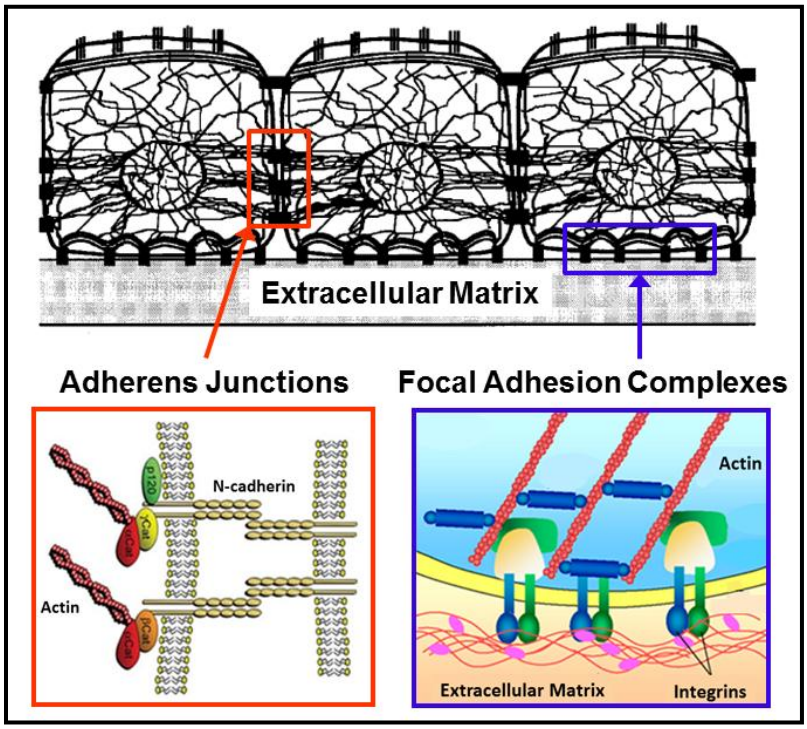

Figure 6.1. Cellular cytoskeleton is physically coupled to neighboring cells through adherens junctions and to underlying matrix scaffolds through focal adhesion complexes [5, 6].

The main objective of this study was to determine if culturing cells under N-cadherin and integrin β1 blocking conditions resulted in a more mechanically homogeneous population. By blocking these interactions, we essentially took any variation in the cellular microenvironment that was due to diversified cellular adhesions out of the equation. For this, we cultured vascular smooth muscle cells on unaligned collagen and fibronectin matrices for a period of 5 days. Cellular media was supplemented with antibodies to N-cadherin and integrin β1, which have previously been shown to block functionality [7, 8]. Cellular mechanical properties were measured using AFM techniques and the cells were visualized using immunofluorescence staining.

6.2 Materials and Methods

Many of the methods for this study are similar to the methods outlined in Chapter 5. Materials and methods that were previously discussed in detail are briefly outlined here, while new concepts are explained in detail.

6.2.1 Samples

Unaligned collagen and unaligned fibronectin substrates were prepared as outlined in section 5.2.1. Vascular smooth muscle cells were isolated, passaged, and plated on the substrates as outlined in section 5.2.2.

Some of the media that was used throughout the 5 day culture period in this study was supplemented with antibodies to test the effects of blocking cell-cell (N-cadherin) and/or cell-matrix (integrin β1) interactions. Specifically, there were 5 different media

conditions: regular VSMC media, VSMC media with 50 μg/ml integrin β1 antibody (Fisher), VSMC media with 50 μg/ml N-cadherin antibody (Sigma-Aldrich), VSMC media with 50 μg/ml integrin β1 antibody and 50 μg/ml N-cadherin antibody (both antibodies), and VSMC media with 50 μg/ml of a non-immune IgG (Sigma-Aldrich). The non-immune IgG served as a control as it was not expected to affect cellular interactions or mechanical properties. The antibody concentration of 50 μg/ml was chosen as it has been demonstrated as an effective blocking concentration in other studies [9, 10]. In total there were 10 samples in this study: 5 media conditions on unaligned collagen and 5 media conditions on unaligned fibronectin. The different media conditions were applied to the cells immediately upon seeding on the substrates and were used continuously throughout the 5 day culture period (media changed every 48 hours) and during AFM testing.

6.2.2 AFM Testing and Data Analysis

The same AFM cytoindentation experiments and data analysis as outlined in sections 5.2.3 through 5.2.6 were performed on the samples in this study. In short, day 5 VSMCs from each sample were mechanically probed using AFM indentation-(hold)-retraction techniques. On each sample, 20 cells were repeatedly probed in this manner at a speed of 1 μm/sec, resulting in 5 force curves and 2 stress relaxation curves per cell. The Hertz model was fit to the first 300 nm of indentation in each force curve to estimate the apparent elastic modulus for the cells. The stress relaxation data was normalized and the percent relaxation over the 60 second hold was calculated. The QLV model was also

fit to this data and R^2 values for this fit were assessed. Student's t-tests were used to determine any statistically significant differences between elastic moduli and percent relaxation measures for the different samples. Cell-to-cell and repeated point coefficients of variation were calculated to access the variation within each sample.

6.2.3 Immunofluorescence

In order to visualize structural differences between day 5 cells on the different samples, all samples were fixed and stained for nuclei, filamentous actin, and microtubules, as outlined in section 5.2.7. Additionally, the anti-N-cadherin and anti-integrin β1 samples were stained to confirm antibody blocking. For these stains, nuclei and filamentous actin (N-cadherin samples) or the plasma membrane (integrin β1 samples) were also stained as a reference of cellular structure. The primary N-cadherin antibody that was present in the media throughout the study was produced in mouse so a donkey anti-mouse rhodamine (TRITC)-conjugated secondary antibody (Jackson ImmunoResearch) was used to stain these samples. The primary integrin β1 antibody was produced in hamster so a mouse anti-hamster FITC-conjugated secondary antibody (Fisher) was used to stain these samples. Positive and negative controls were also done to rule out non-specific binding of these secondary antibodies. All samples were mounted on microscope slides and stored in the dark before and during imaging.

6.3 Results

6.3.1 Elastic Modulus

The mean apparent elastic moduli for the day 5 VSMCs with the different media conditions on both collagen and fibronectin matrices are shown in Figure 6.2. The cells under control conditions (no antibodies, IgG control) had elastic moduli ranging from 8.6 kPa to10.6 kPa. For both the collagen and fibronectin samples, there was not a significant difference between these control samples (no antibodies, IgG control) ($p \geq 0.386$). The cells under test conditions (antibodies) had elastic moduli ranging from 2.3 kPa to 5.3 kPa. This drop in comparison to the control samples was considered statistically significant in most cases. When comparing the "no antibodies" control sample to the test (antibodies) samples, all test samples exhibited significantly lower elastic moduli than the control ($p \leq 0.025$) except for the anti-N-cadherin sample on collagen ($p = 0.070$). Within the antibody samples, the "both antibodies" sample was the least stiff. This difference was considered statistically significant for cells on both collagen and fibronectin matrices ($p \leq 0.003$). The anti-integrin β1 samples and the anti-N-cadherin samples were not significantly different from one another. Within each sample type (media condition), there was no significant difference between the elastic moduli measures on collagen and those on fibronectin.

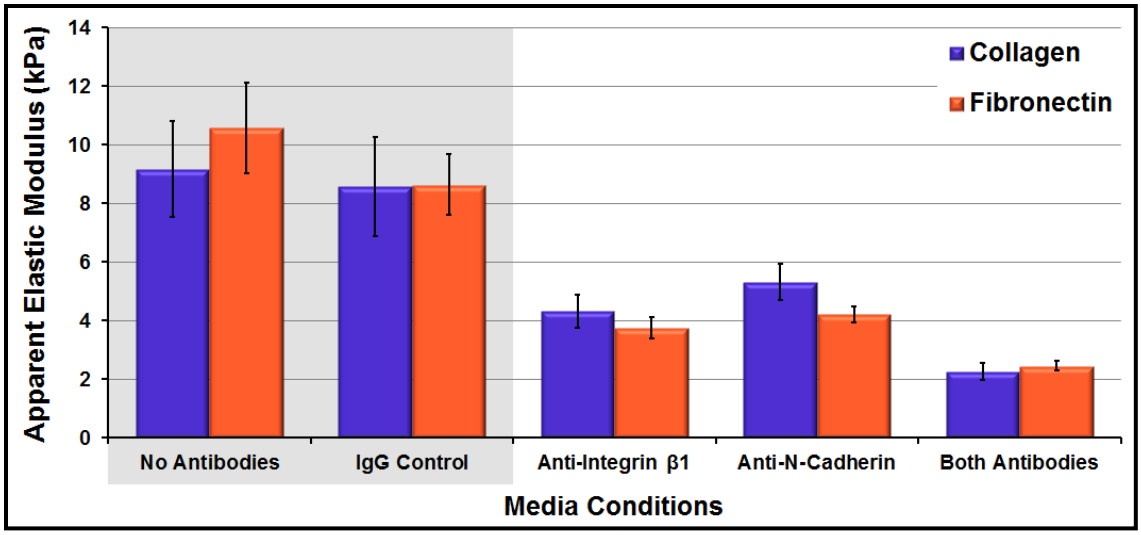

Figure 6.2. Apparent elastic moduli of day 5 VSMCs on unaligned collagen and fibronectin with different media conditions. Data presented as mean ± standard error.

The average cell-to-cell and repeated point elastic modulus COV measures for the cells with the different media conditions can be found in Table 6.1. The average cell-to-cell elastic modulus COV for the control conditions was 71.7%, very close to the average level of variation in VSMC elastic moduli measures in the previous study (70.3%). This measure dropped fairly uniformly from the control samples to the test (antibody) samples to an average of 44.8%. This means that the cells under the test conditions were more homogeneous in their mechanical properties (elastic moduli), than the cells under the control conditions. This was the first significant drop in cellular mechanical heterogeneity within a sample population that was observed in this work and it suggested to us that varying cell-cell and cell-matrix interactions are at least in part to blame for the high level of heterogeneity that is commonly observed in 2D cell culture studies. The repeated point COV measures were much lower than the cell-to-cell COV measures,

indicating that variations in the measurement technique could not account for the cell-to-cell variations that were observed.

Table 6.1. VSMC cell-to-cell and repeated point coefficients of variation (COV) for elastic modulus and percent relaxation measures (average of measures for cells on collagen and fibronectin matrices).

	Sample	Average Cell-to-Cell COV (%)		Average Repeated Point COV (%)
Elastic Modulus	No Antibodies	72.7	Mean = 71.7	17.5
	IgG Control	70.7		7.0
	Anti-Integrin β1	49.7		12.5
	Anti-N-Cadherin	41.6	Mean = 44.8	13.6
	Both Antibodies	43.2		13.4
Percent Relax	No Antibodies	60.9	Mean = 61.9	6.0
	IgG Control	62.8		11.9
	Anti-Integrin β1	31.7		5.3
	Anti-N-Cadherin	21.3	Mean = 27.2	6.8
	Both Antibodies	28.5		8.3

6.3.2 Stress Relaxation

The mean percent relaxation measures for the day 5 VSMCs with the different media conditions on both collagen and fibronectin matrices are shown in Figure 6.3. The cells under control conditions (no antibodies, IgG control) had percent relaxation measures ranging from 31.9 % to 40.3%. For both the collagen and fibronectin samples, there was not a significant difference between these control samples (no antibodies, IgG control) ($p \geq 0.658$). The cells under test conditions (antibodies) had percent relaxation measures ranging from 38.7% to 54.7%. Within the collagen samples, the percent relaxation measure for the N-cadherin sample was significantly higher than the percent

relaxation measures for both control samples ($p \leq 0.029$). Within the fibronectin samples, there were statistically significant differences between the control samples (no antibodies and IgG control) and both the integrin β1 and the "both antibodies" samples ($p \leq 0.026$). Overall, the antibody media conditions promoted cells that relaxed more during the 60 second hold, although this difference wasn't always statistically significant. Within each sample type (media condition), the only significant difference between cells on the different matrices was found between the N-cadherin samples ($p \leq 0.012$).

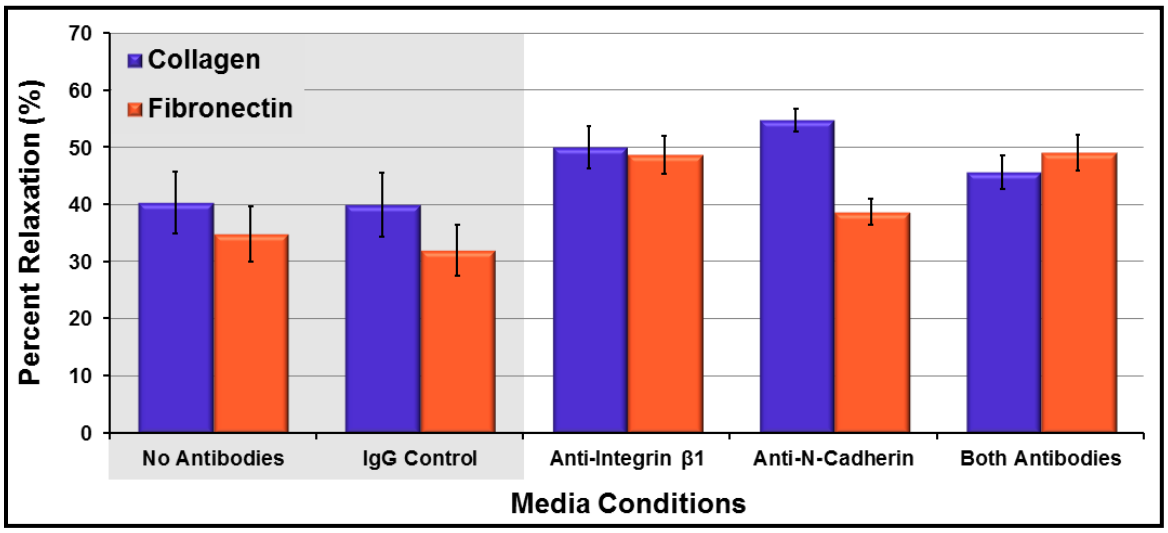

Figure 6.3. Percent relaxation during 60 second hold for day 5 VSMCs on unaligned collagen and fibronectin with different media conditions. Data presented as mean ± standard error.

The average cell-to-cell and repeated point COV for percent relaxation measures for the cells with the different media conditions can be found in Table 6.1. The average cell-to-cell percent relaxation COV for the control conditions was 61.9%, close to the average level of variation in VSMC percent relaxation measures in the previous study

(69.2%). This measure decreased to an average of 27.2% for the samples that had antibodies present in their media, implying that the cells from a sample under the test conditions were more homogeneous in their mechanical properties than cells from a sample under the control conditions. Once again, the repeated point COV measures were low. Combined with the elastic modulus COV results, these measures are compelling evidence that varied cell-cell and cell-matrix interactions contribute to the high level of heterogeneity that is seen within cell populations. Additionally, the QLV model fit the data for all sample types very well with an average R^2 of 0.98 ± 0.03.

6.3.3 Immunofluorescence

The stains for the primary N-cadherin and integrin β1 antibodies that were present in the media are shown in Figure 6.4. Within the N-cadherin sample, we expected the stain to be concentrated at the edges of each cell, where they would normally make connections with neighboring cells. In the samples, however, the cells exhibited staining throughout, with stains most concentrated above the nuclei. We did a positive control on an "anti-N-cadherin media" sample (stained similar to this) but not on a "regular media" sample. It would be interesting to see if the "regular media" sample stained more heavily around the perimeter of the cells, suggesting that blocking the N-cadherin interactions caused these transmembrane proteins to relocate throughout the plasma membrane. In any case, N-cadherin and integrin β1 blocking through media conditions was confirmed.

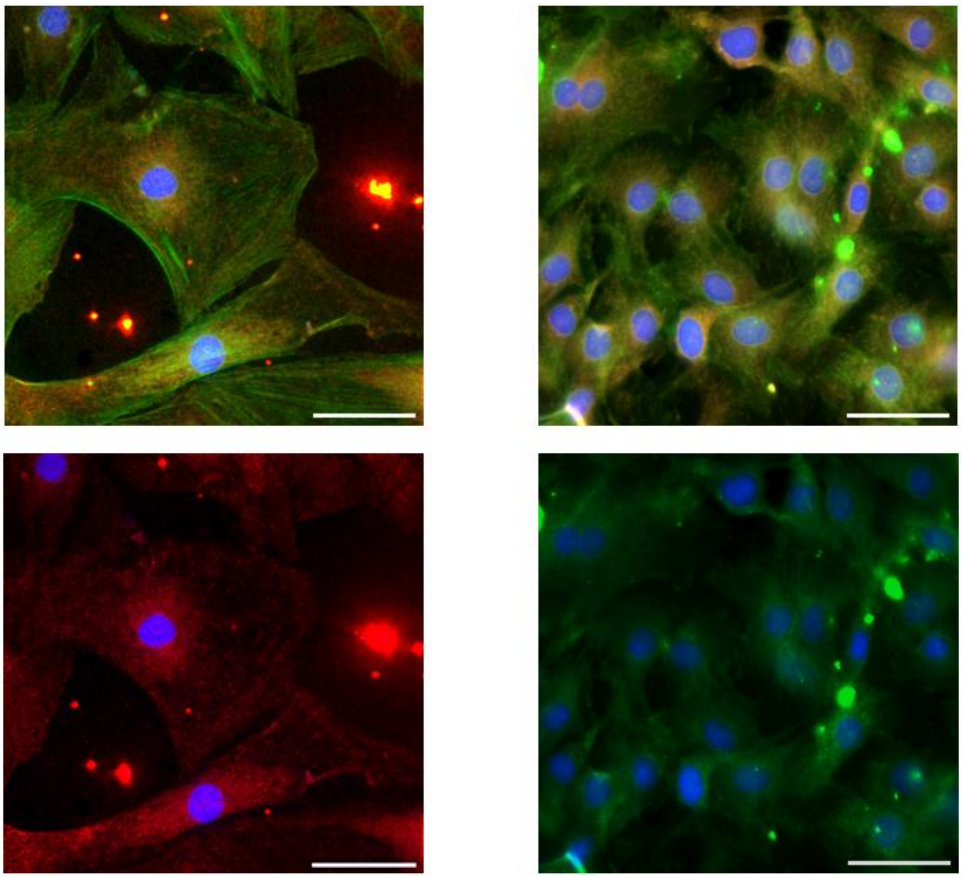

Figure 6.4. Confirmation of antibody blocking in day 5 vascular smooth muscle cells. Cells with anti-N-cadherin media conditions (left) are stained for nuclei (blue), filamentous actin (green), and the N-cadherin primary antibody (red). Cells with anti-integrin β1 media conditions (right) are stained for nuclei (blue), plasma membranes (red), and the integrin β1 primary antibody (green). Top images show all stains and bottom images leave out the actin/plasma membrane stains to highlight the N-cadherin and integrin β1 staining (scale bar = 50 μm).

Stains for nuclei, microtubules, and actin highlighted differences in cell morphology among the samples with different media conditions in this study (Figure 6.5). The VSMCs in the control samples (no antibodies, IgG control) were highly variable in size and generally exhibited more cell extensions and cell-cell connections. A continuum of phenotypes, from contractile to synthetic, were present. VSMCs in the the

anti-integrin β1 samples generally took on a synthetic phenotype while VSMCs in the anti-N-cadherin samples were smaller and more rounded.

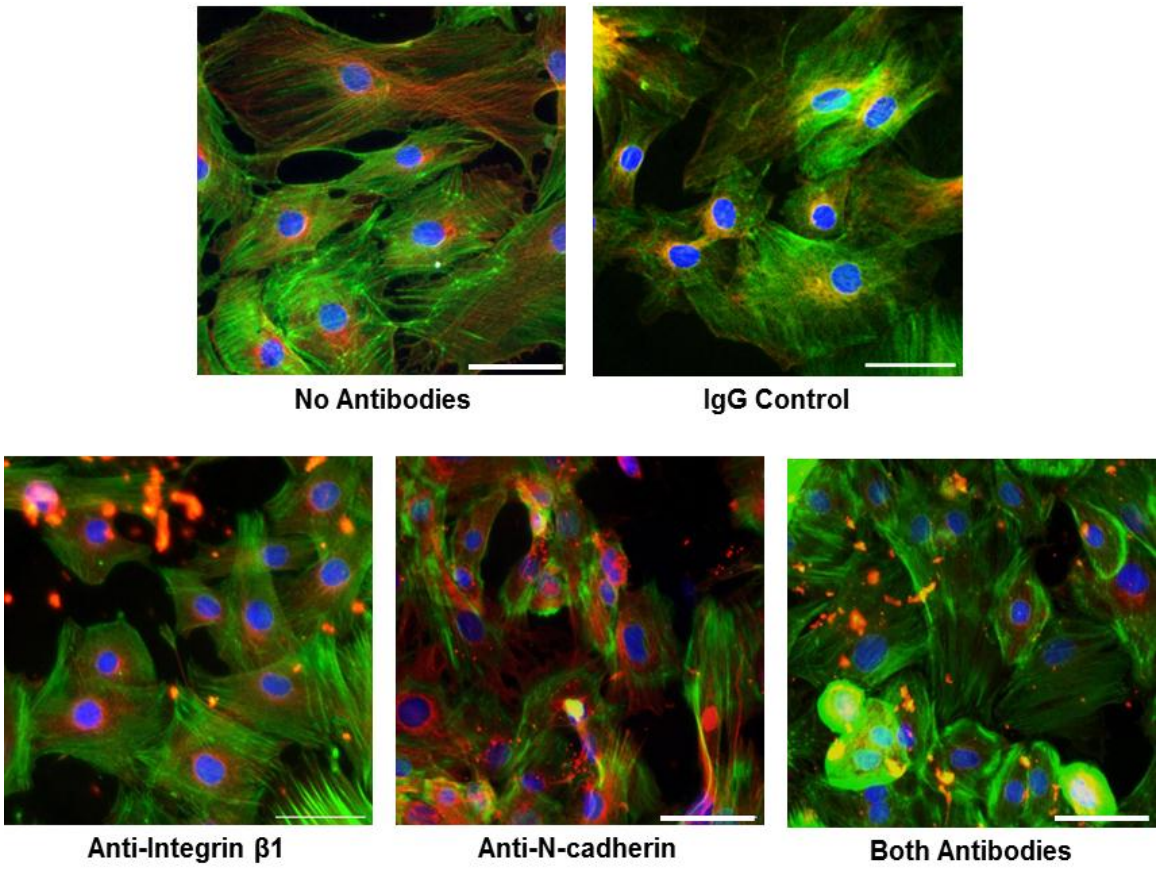

Figure 6.5. Representative immunofluorescence images of day 5 vascular smooth muscle cells with different media conditions (on unaligned collagen, scale bar = 50 μm). Cells are stained for nuclei (blue), filamentous actin (green), and microtubules (red).

6.4 Discussion

In this study, variations in the cellular microenvironment were limited by inhibiting cell-cell and cell-matrix interactions through antibody blocking. Cell-cell and cell-matrix interactions have been inhibited for various purposes in previous research.

Specifically, N-cadherin and integrin β1 interactions have been restricted to study their role in cellular proliferation, migration, differentiation, adhesion, disease progression, and apoptosis [7, 8, 11-16]. This is the first study to investigate the role of N-cadherin and integrin β1-mediatiated interactions in regulating cellular mechanical properties.

Our results showed that both measures of cellular mechanical properties (elastic modulus and percent relaxation) changed under the antibody blocking conditions. On average (for measures on collagen and fibronectin), the elastic modulus decreased from 9.2 kPa with control media to 4.0 kPa with anti-integrin β1 media, to 4.8 kPa with anti-N-cadherin media, and to 2.4 kPa with both antibodies in the media (Figure 6.2). The percent relaxation measures increased from an average of 37% with control media to 49% with anti-integrin β1 media, to 47% with anti-N-cadherin media, and to 47% with both antibodies in the media (Figure 6.3). These values were fairly uniform for antibody conditions, suggesting that integrin β1 and N-cadherin play an equally important role in determining cellular mechanical properties. This finding is similar to findings in another research study, where the resistance to apoptosis provided by cell-cell contacts was found to be of a similar magnitude to that provided by cell-matrix contacts [7].

Immunofluorescence staining provided a measure of cellular phenotype within each of the samples, revealing that the cells on the antibody samples were generally smaller, more rounded, and less contractile in appearance. In combining these findings with our mechanical property measurements, we found supportive evidence for our results. Previous research which has shown that, on day 5, synthetic VSMCs are less stiff than contractile VSMCs [17]. Additionally, decreased cell spreading has been correlated

to reduced cellular stiffness [18]. A less complex actin network (characteristic of synthetic phenotypes) has also been shown to cause increases in relaxation percentage in stress relaxation experiments [19].

The level of cell-to-cell variation (COV) in mechanical properties within each sample decreased from the control conditions to the antibody conditions (Table 6.1). For the elastic moduli measures, the average cell-to-cell COV decreased from 72% to 45%. For the percent relaxation measures, the average cell-to-cell COV decreased from 62% to 27%. These findings were very important. They mean that the antibody samples were more homogeneous in their mechanical properties. This suggests that diversified adhesion binding between neighboring cells and ECM components throughout a cellular population is responsible for a significant amount of the heterogeneity that is observed in 2D cell culture studies.

6.5 Conclusions

The influence of N-cadherin-mediated cell-cell interactions and integrin β1-mediated cell-matrix interactions on cellular mechanics was assessed for the first time in this study. Blocking these interactions individually and in combination resulted in reduced cellular elastic moduli measures (less stiff) and increased cellular percent relaxation measures (more viscous). These results provide researchers with a greater understanding of the role of cellular adhesions in regulating whole cell mechanical properties. Within these measurements, it was found that cells exhibited more homogeneous mechanical properties when their cell-cell and cell-matrix interactions

were limited. This suggests that varying cellular adhesions throughout a sample is responsible, at least in part, for the high level of heterogeneity that is commonly observed in cellular mechanical properties.

6.6 References

1. Jaasma, M.J., W.M. Jackson, and T.M. Keaveny, *The effects of morphology, confluency, and phenotype on whole-cell mechanical behavior.* Annals of Biomedical Engineering, 2006. **34**(5): p. 759-768.

2. Geiger, B., S. YehudaLevenberg, and A.D. Bershadsky, *Molecular interactions in the submembrane plaque of cell-cell and cell-matrix adhesions.* Acta Anatomica, 1995. **154**(1): p. 46-62.

3. Albelda, S.M. and C.A. Buck, *Integrins and other cell-adhesion molecules.* Faseb Journal, 1990. **4**(11): p. 2868-2880.

4. Yoshida, M., et al., *Leukocyte adhesion to vascular endothelium induces E-selectin linkage to the actin cytoskeleton.* Journal of Cell Biology, 1996. **133**(2): p. 445-455.

5. Ingber, D.E., *Tensegrity: the architectural basis of cellular mechanotransduction.* Annual Review of Physiology, 1997. **59**: p. 575-599.

6. Rao, S. and J. Winter, *Adhesion molecule-modified biomaterials for neural tissue engineering.* Frontiers in Neuroengineering, 2009. **2**(6): p. 1-14.

7. Koutsouki, E., et al., *N-cadherin-dependent cell-cell contacts promote human saphenous vein smooth muscle cell survival.* Arteriosclerosis Thrombosis and Vascular Biology, 2005. **25**(5): p. 982-988.

8. McNally, A.K. and J.M. Anderson, *beta 1 and beta 2 integrins mediate adhesion during macrophage fusion and multinucleated foreign body giant cell formation.* American Journal of Pathology, 2002. **160**(2): p. 621-630.

9. Mendrick, D.L. and D.M. Kelly, *Temporal expression of vla-2 and modulation of its ligand specificity by rat glomerular epitheliel-cells in-vitro.* Laboratory Investigation, 1993. **69**(6): p. 690-702.

10. Yiin, J.J., et al., *Slit2 inhibits glioma cell invasion in the brain by suppression of Cdc42 activity.* Neuro-Oncology, 2009. **11**(6): p. 779-789.

11. Hermiston, M.L. and J.I. Gordon, *In-vivo analysis of cadherin function in the mouse intestinal epithelium - essential roles in adhesion, maintenance of differentiation, and regulation of programmed cell death.* Journal of Cell Biology, 1995. **129**(2): p. 489-506.

12. Steinberg, M.S. and P.M. McNutt, *Cadherins and their connections: adhesion junctions have broader functions.* Current Opinion in Cell Biology, 1999. **11**(5): p. 554-560.

13. Uglow, E.B., et al., *Dismantling of cadherin-mediated cell-cell contacts modulates smooth muscle cell proliferation.* Circulation Research, 2003. **92**(12): p. 1314-1321.

14. Li, G., K. Satyamoorthy, and M. Herlyn, *N-cadherin-mediated intercellular interactions promote survival and migration of melanoma cells.* Cancer Research, 2001. **61**(9): p. 3819-3825.

15. Cheng, S.L., et al., *A dominant negative cadherin inhibits osteoblast differentiation.* Journal of Bone and Mineral Research, 2000. **15**(12): p. 2362-2370.

16. Siebers, M.C., et al., *The behavior of osteoblast-like cells on various substrates with functional blocking of integrin-beta 1 and integrin-beta 3.* Journal of Materials Science-Materials in Medicine, 2008. **19**(2): p. 861-868.

17. Hemmer, J.D., et al., *Effects of serum deprivation on the mechanical properties of adherent vascular smooth muscle cells.* Proceedings of the Institution of Mechanical Engineers Part H-Journal of Engineering in Medicine, 2008. **222**(H5): p. 761-772.

18. Domke, J., et al., *Substrate dependent differences in morphology and elasticity of living osteoblasts investigated by atomic force microscopy.* Colloids and Surfaces B-Biointerfaces, 2000. **19**(4): p. 367-379.

19. Hemmer, J.D., et al., *Role of cytoskeletal components in stress-relaxation behavior of adherent vascular smooth muscle cells.* Journal of Biomechanical Engineering-Transactions of the Asme, 2009. **131**(4): p. 9.

CHAPTER SEVEN

EFFECTS OF SUBSTRATE STIFFNESS AND MECHANICAL TENSION ON VASCULAR SMOOTH MUSCLE CELL MECHANICAL PROPERTIES

7.1 Introduction

Within a single population of cells, diversified adhesion binding between neighboring cells and between cells and underlying ECM components has been shown to promote cellular mechanical heterogeneity (Chapter 6). With the overall goal of incorporating realistic levels of cellular mechanical heterogeneity in an *in vivo* model, it is important to consider if diversified adhesions that are present *in vivo* result in similar variability among cellular mechanical properties. This is especially important to consider in cases of disease, where the cellular microenvironment is highly variable and cell-cell and cell-matrix interactions vary extensively. To this end, the antibody blocking study (Chapter 6) was replicated under more *in vivo*-like conditions.

While the matrix-coated coverslips used in the previous studies (and most 2D cell culture experiments) provided a simple substrate with which to test cellular mechanical properties, they are so mechanically stiff that results obtained from their studies cannot be easily related to conditions in the body. Cells have been shown to modify their cytoskeletal architecture, mechanical properties, and traction forces exerted on their substrate based on the substrate stiffness [1]. Healthy VSMCs are embedded in a network of collagen (types I, III, and V), elastin, and proteoglycans within the tunica media of blood vessels. In a study by Oie et al., the elastic modulus was mapped at various points within the tunica media of an artery [2]. The elastic modulus of the

VSMCs and collagen fibrils was found to be 17 ± 9 kPa. The elastin-rich region in the tunica media had an elastic modulus of 51 ± 14 kPa while the elastin-rich region of the internal elastic lamina had an elastic modulus of 69 ± 13 kPa. These measures are orders of magnitude less stiff than glass (GPa). In order to replicate this stiffness in a 2D culture environment, polyacrylamide gels with similar elastic moduli were constructed. These gels were chosen because their elastic moduli can be altered by varying the ratio of acrylamide to bis-acrylamide monomers in solution prior to polymerization [3, 4]. We used gels with elastic moduli of approximately 10 kPa, 25 kPa, and 75 kPa. This stiffness range approximately replicates the range VSMCs would encounter *in vivo* [2].

In the body, VSMCs are oriented circumferentially within the tunica media. They are cyclically deformed with the dilation and retraction of the blood vessel. This cyclic strain is best approximated at 0-4% with a frequency of 1 Hz [5, 6]. Application of this physiologically relevant level of strain has been shown to promote a more contractile phenotype and resulted in an increased expression of several differentiated VSMC markers [7-10]. By simulating these mechanical forces experienced by native VSMCs, we took a step closer to anticipating heterogeneity *in vivo*.

The main objective of this study was to determine if the same trend (reduction in cellular mechanical heterogeneity with decreased variation (inhibition) in cellular adhesions) was observed under more physiologically relevant conditions. For this, we cultured vascular smooth muscle cells on collagen-coated polyacrylamide gels and flexible silicone elastomer membranes for a period of 5 days. Cellular media was supplemented with an antibody to integrin β1, which was hypothesized to reduce the

heterogeneity within the cellular mechanical property measures, based on the results of the previous study. N-cadherin antibody media conditions were not tested because cell-cell interactions were not expected to change (changing substrate properties is more likely to affect cell-matrix interactions). Cellular mechanical properties were measured using AFM techniques and the cells were visualized using immunofluorescence staining.

7.2 Materials and Methods

Many of the methods for this study are similar to the methods outlined in Chapters 5 and 6. Materials and methods that were previously discussed in detail are briefly outlined here, while new concepts are explained in detail.

7.2.1 Samples

Polyacrylamide Gels

Twelve millimeter diameter glass slides (Fisher) were plasma cleaned for 10 minutes, followed by UV sterilization in 70% ethanol for at least 1 hour (same as in previous studies). Polyacrylamide gels were then created and deposited in a thin layer on top of the glass slides, following the protocols outlined by Tse et al. and Wang et al. [4, 11]. The entire protocol, including slight modifications for this work, can be found in Appendix D, but the essential steps are outlined here. First, the slides were activated to allow the polyacrylamide gels to adhere. For this, the slides were first cleaned with in a sodium hydroxide solution for several minutes. They were then allowed to dry, leaving a thin layer of sodium hydroxide on the surface. Next, the same surface of each slide was

coated with 3-aminopropyltrimethoxy silane (APTES) for 5 minutes. The slides were then rinsed with water 3 times, with care taken to ensure the activated side of each slide remained facing upwards. This side of each slide was then coated with 0.5% gluteraldehyde for 30 minutes, before rinsing with water 3 more times. The slides were allowed to dry as the gels were prepared.

Polyacrylamide gels with elastic moduli of approximately 10 kPa, 25 kPa, and 75 kPa were prepared in separate 25 ml glass beakers. The components listed in Table 7.1 were first combined and gently stirred. Then, 30 µl of ammonium persulfate and 20 µl of tetramethylethylenediamine (TEMED) were added and mixed very quickly. Immediately, 6 µl of the solution was pipetted onto each activated slide and another clean slide was placed on top to spread the gel over the slide surface. Once the gels had polymerized (~10 minutes), the samples were flooded with 50 mM HEPES and forceps were used to remove the top slides. This left a thin layer of the polyacrylamide gel securely adhered to the glass slide.

Table 7.1. Ingredients for making polyacrylamide gels with different elastic moduli [4, 12].

Final Acryl / Bis %	40% Acrylamide (µl)	2% Bisacrylamide (µl)	1 M HEPES (µl)	Water (µl)	Elastic Modulus (kPa) (Literature)
8 / 0.8	1,000	2,000	50	1,950	75.1
8 / 0.3	1,000	750	50	3,200	26.0
8 / 0.1	1,000	250	50	3,700	9.8

In order to be consistent with the previous studies, the gels were coated with the same 1 mg/ml collagen solution (BD Biosciences). For this, the crosslinker sulfo-SANPAH was used to covalently bind the collagen proteins to the polyacrylamide gels. Specifically, the gels were coated with 0.2 mg/ml of sulfo-SANPAH and exposed to long wave UV light for 10 minutes. They were then rinsed twice with 50 mM HEPES and 47 µl of the collagen solution was spread over the surface of each gel. The samples were placed in an incubator (37 °C) overnight. The next day, each sample was rinsed in PBS and UV sterilized for 30 minutes before plating the VSMCs on them.

AFM indentation experiments were performed on the gels with and without collagen to confirm their stiffness values. The methods for this work were very similar to the methods used to determine the elastic moduli of cells. The specific experimental protocol and data analysis techniques are outlined in detail in Appendix E. Table 7.2 lists the results of this testing. Our measurements of elastic moduli for each gel were very close to the reported literature values. The measurements with collagen were used to define our gels (elastic moduli of 18 kPa, 28 kPa, and 72 kPa), since this is the stiffness the cells would experience.

Table 7.2. Comparison of measured gel stiffness to previously reported values [4, 12]. Measured values presented as mean (± standard error).

	Literature Value: Plain Gel (kPa)	Measured Value: Plain Gel (kPa)	Measured Value: Gel With Collagen (kPa)
Gel 1	9.8	11.7 ± 0.2	**17.7 ± 1.4**
Gel 2	26.0	32.3 ± 1.5	**28.4 ± 1.4**
Gel 3	75.1	55.3 ± 1.2	**72.3 ± 2.4**

Vascular smooth muscle cells were isolated, passaged, and plated on the collagen-coated gels as outlined in section 5.2.2. Throughout the culture period, 3 different media conditions were used (from section 6.2.1): regular VSMC media, VMSC media with 50 μg/ml integrin β1 antibody, and VSMC media with 50 μg/ml of a non-immune IgG (control). N-cadherin antibodies were not included because cell-cell interactions were not expected to change from the previous study. The 3 media conditions combined with the 3 gel stiffnesses made a total of 9 samples. Figure 7.1 illustrates the cellular microenvironment in this study.

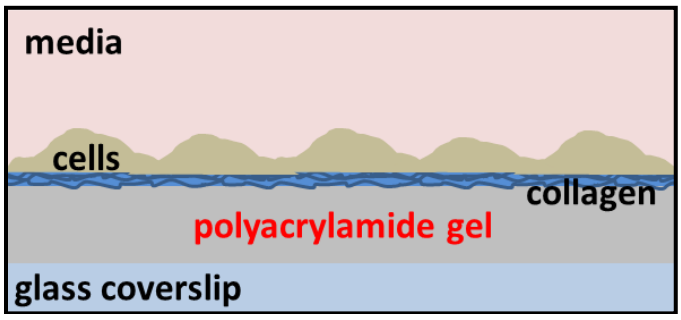

Figure 7.1. Schematic of cellular microenvironment with cells atop a less stiff polyacrylamide gel.

Tension Conditions

Flexible silicone elastomer membranes (0.020 inch thick) with type I collagen covalently bonded to their surface were used as the substrates for the tension work in this study. These membranes are commercially available within the wells of 6-well culture plates (Figure 7.2, BioFlex culture plates, Flexcell International, Hillsborough, North Carolina, USA). These plates are sterile so the VSMCs were able to be plated directly

onto the membranes within each well. The VSMCs were isolated, passaged, and plated as outlined in section 5.2.2. As with the gel samples, there were 3 media conditions used throughout the study (from section 6.2.1): regular VSMC media, VMSC media with 50 μg/ml integrin β1 antibody, and VSMC media with 50 μg/ml of a non-immune IgG (control). There were 2 tension conditions (cyclic tension and no tension), for a total of 6 samples for the tension work.

For the first 48 hours, cells on all samples ("cyclic tension" and "no tension") were cultured under standard conditions to allow for adequate cell adhesion to the substrates. All samples were then loaded into the Flexcell FX-3000 tension system bioreactor (in an incubator), with a plug blocking the vacuum pressure from beneath the "no tension" samples. The tension regime was specified in the Flexcell FX-3000 software, which regulates the vacuum pressure beneath the membranes in the bioreactor. Figure 7.2 outlines the overall setup. The tension group was then subjected to 0-4% cyclic strain first at 0.1 Hz for 30 minutes, then at 0.5 Hz for 30 minutes (preconditioning regimen). For the remaining 3 days in culture, these samples were cyclically strained (0-4%) at 1 Hz, a physiologically relevant level for VSMCs in a healthy blood vessel [6, 13].

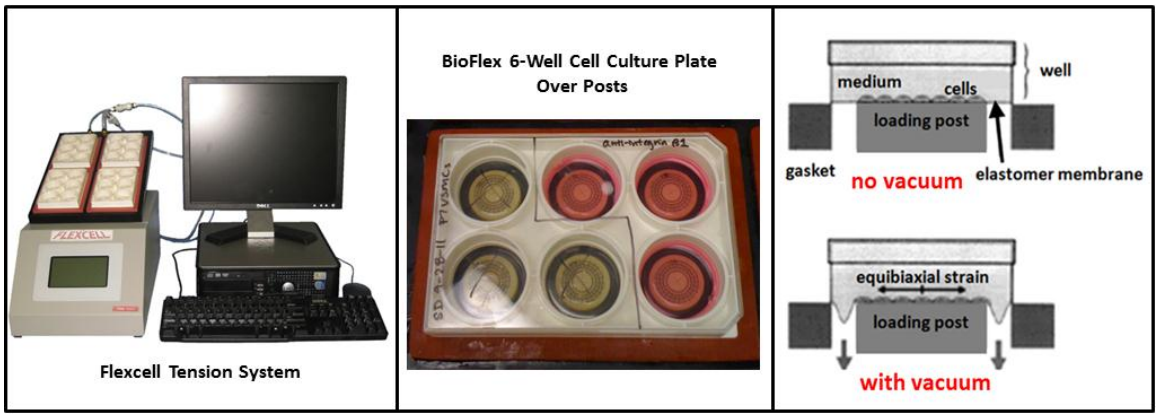

Figure 7.2. Flexcell Tension System. A computer-regulated bioreactor (left) uses vacuum pressure to apply cyclic strain to cells (right) cultured on flexible-bottomed culture plates (center) [14, 15].

7.2.2 AFM Testing and Data Analysis

The tension samples had to be cut out of their wells using a scalpel and placed on a glass slide in order to do AFM testing on these cells. This was necessary because a hard surface is required underneath the sample and the AFM head is too wide to fit down into the wells of the plate. It was important to test cells at equal radial positions on the elastomer membranes, as they had experienced equal levels of strain. This was accomplished by testing cells that were located on each membrane over the very edge of the loading posts. The grease from the loading posts remained on the bottom side of the membranes, so it was possible to find cells just outside this area using the optical microscope within the AFM.

The same AFM cytoindentation experiments and data analysis as outlined in sections 5.2.3 through 5.2.6 were performed on all samples in this study (gel and tension conditions). In short, day 5 VSMCs from each sample were mechanically probed using

AFM indentation-(hold)-retraction techniques. On each sample, 20 cells were repeatedly probed in this manner at a speed of 1 μm/sec, resulting in 5 force curves and 2 stress relaxation curves per cell. The Hertz model was fit to the first 300 nm of indentation in each force curve to estimate the apparent elastic modulus for the cells. The stress relaxation data was normalized and the percent relaxation over the 60 second hold was calculated. The QLV model was also fit to this data and R^2 values for this fit were assessed. Student's t-tests were used to determine any statistically significant differences between elastic moduli and percent relaxation measures for the different samples. Cell-to-cell and repeated point coefficients of variation were calculated to access the variation within each sample.

7.2.3 Immunofluorescence

In order to visualize structural differences between day 5 cells on the different samples, all samples were fixed and stained for nuclei, filamentous actin, and microtubules, as outlined in section 5.2.7. Additionally, the anti-N-cadherin and anti-integrin β1 samples were stained to confirm antibody blocking, as outlined in section 6.2.3. Because these samples were on softer substrates, they were not mounted on microscope slides. Instead they were kept in their well plates, covered in PBS, and stored in the dark after staining and during imaging.

7.3 Results

7.3.1 Polyacrylamide Gels

Elastic Modulus

The mean apparent elastic moduli measurements for day 5 VSMCs on each of the gels are shown in Figure 7.3, along with elastic moduli results for cells on glass slides (from previous study) for reference. On the softest (18 kPa) gel, the VSMCs with anti-integrin β1 media conditions exhibited significantly lower elastic moduli than the VSMCs with the IgG control media conditions ($p = 0.005$). There were no significant differences among samples types for cells on the 28 kPa gel. On the stiffest (72 kPa) gel, the VSMCs with anti-integrin β1 media conditions were significantly less stiff than the cells with the control conditions (no antibodies and IgG control) ($p \leq 0.048$). For all sample types (media conditions), cellular elastic moduli measures increased with increasing substrate stiffness. For the "no antibody" control condition, cellular stiffness increased significantly from the 18 kPa and 28 kPa gel samples to the 72 kPa gel and glass slide samples ($p \leq 0.015$). For the IgG control condition, elastic moduli measures increased significantly from the 18 kPa gel to the 72 kPa gel and to the glass slide, and from the 28 kPa gel to the glass slide ($p \leq 0.012$). Within the anti-integrin β1 sample, significant increases were observed between the 18 kPa gel and all the other samples ($p \leq 0.005$). Overall, the VSMCs on the gels had elastic moduli in the range of 1.8 kPa – 6.9 kPa, while the VSMCs on the stiffer glass substrates had moduli in the range of 4.3 kPa – 9.2 kPa.

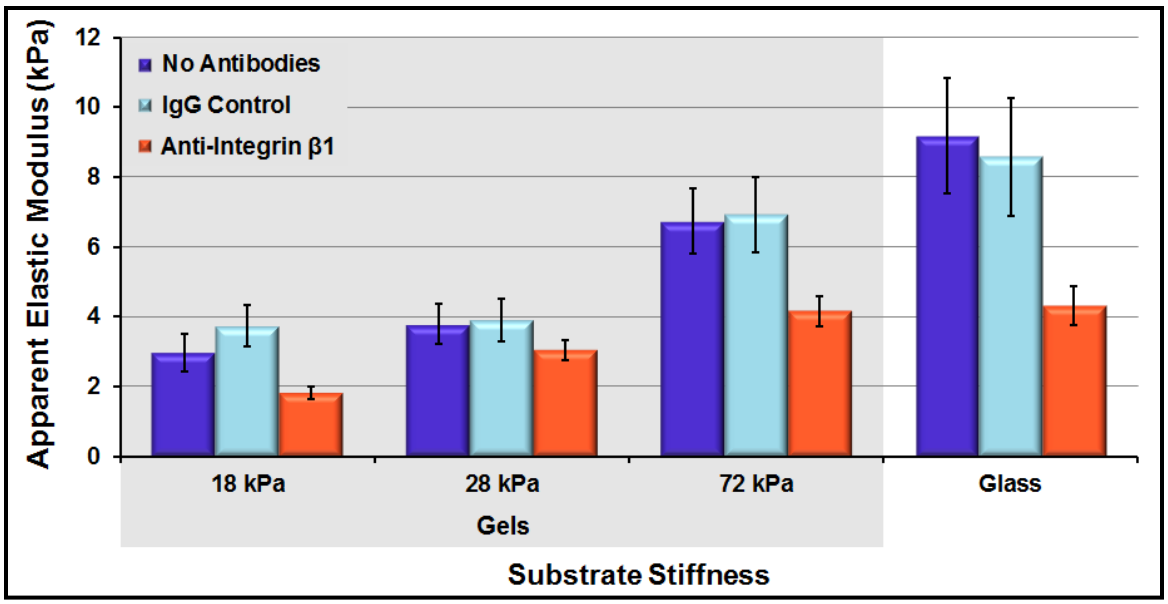

Figure 7.3. Apparent elastic moduli of day 5 VSMCs on substrates of varying stiffness. Data presented as mean ± standard error.

Table 7.3 contains the average cell-to-cell and repeated point COV measures for cellular elastic moduli on the gels with the different media conditions. The level of variation across the gels for a specific sample type (media condition) was consistent so these values were averaged to compare the different media conditions. The average cell-to-cell elastic modulus COV for the control conditions was 70.2%. This amount of variation is almost identical to the variation that was found in elastic moduli measures for control samples in the two previous studies (70.3%, 71.7%). Once again, the level of variation in the anti-integrin β1 samples decreased, this time to 43.4%. This level of variation is similar to the level found in the anti-integrin β1 samples on glass slides (previous study, 49.7%). Therefore, blocking cell-matrix interactions led to a similar decrease in the mechanical heterogeneity within the sample for both stiff and soft

substrates. Once again, the repeated point COV measures for elastic moduli data averaged approximately 13% for all samples.

Table 7.3. Day 5 VSMC cell-to-cell and repeated point coefficients of variation (COV) for elastic modulus and percent relaxation measures (averages for all measures on gels).

	Sample	Average Cell-to-Cell COV (%)		Average Repeated Point COV (%)
Elastic Modulus	No Antibodies	69.9	Mean = 70.2	13.9
	IgG Control	70.4		11.6
	Anti-Integrin β1	43.4		14.9
Percent Relax	No Antibodies	40.7	Mean = 42.0	6.3
	IgG Control	43.3		7.1
	Anti-Integrin β1	17.2		5.7

Stress Relaxation

The mean percent relaxation measurements for day 5 VSMCs on each of the gels are shown in Figure 7.4, along with percent relaxation results for cells on glass slides (from previous study) for reference. On each gel, there were no significant differences among sample types (media conditions). Within the "no antibody" control group, the cells on the 28 kPa and 72 kPa gels exhibited significantly higher percent relaxation measures than the cells on the glass slides ($p \leq 0.037$). Within the IgG control group, the only statistically significant difference was between the cells on the softest (18 kPa) gel and the cells on the glass slide ($p = 0.022$). Finally, within the anti-integrin β1 group, the cells on the 72 kPa gel relaxed more during the hold than cells under the same media conditions on the glass slide ($p = 0.026$). Overall, the VSMCs on the gels tended to relax more during the 60 second hold on the gels than the same cells on the stiffer glass slides

(statistically significant for about half the samples). Looking specifically at the gels (not glass), there were no significant differences in relaxation behavior among the different gel stiffnesses or across the different media conditions.

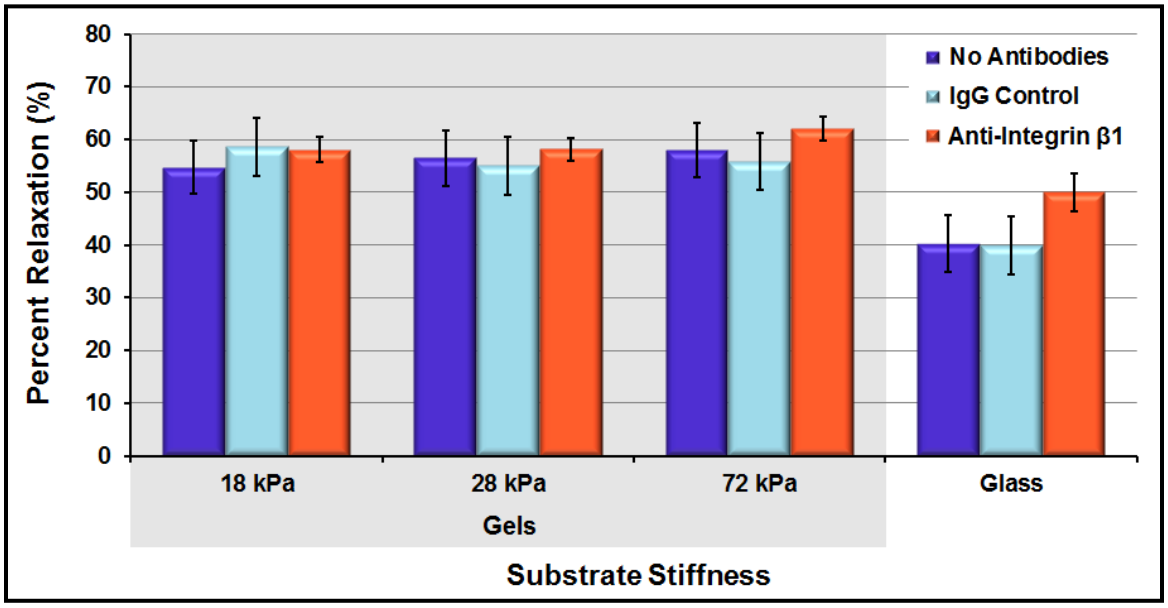

Figure 7.4. Percent relaxation during 60 second hold for day 5 VSMCs on substrates of varying stiffness. Data presented as mean ± standard error.

The average percent relaxation COV measures for the gel samples with the different media conditions can be found in Table 7.3. The level of variation in percent relaxation measures across the gels for a specific sample type (media condition) was consistent so these values were averaged to compare the different media conditions. The average cell-to-cell percent relaxation COV for the control conditions was 42.0%. This amount of variation is lower than the variation that was found in percent relaxation measures for control samples on glass slides (~60% in previous 2 studies). This suggests

that there might be less variation among cellular viscoelastic properties (relaxation measures) on a softer gel substrate (compared to glass). When the anti-integrin β1 media was used, the cells exhibited very uniform percent relaxation measures, with a cell-to-cell COV of only 17.2%. Again, this measure is lower than the same measure on glass slides (from previous chapter, 31.7%). This is the least amount of mechanical heterogeneity in cellular mechanical properties that was observed in all our work. The repeated point percent relaxation COV measures remained very low at approximately 6% for all samples in this study. Additionally, the QLV model fit the data well for all sample types with an average R^2 of 0.98 ± 0.02.

Immunofluorescence

The stains for nuclei, actin, and microtubules, shown in Figure 7.5, were used to compare VSMC structure among samples. No clear differences were observed between the cells on each of the gels. For the control conditions (regular media and IgG control), the cells appeared to be similar, with various sizes and shapes present within each sample. Many cells had long extensions reaching in all directions (more than in previous study on glass substrate). The cells on all gels with anti-integrin β1 conditions were uniformly smaller and did not exhibit extensive cellular extensions, like the control cells did. Occasionally, these several of these cells were found clumped together. Otherwise, they were typically isolated from one another. Higher magnification images to better visualize cytoskeletal structure were not obtained because the resolution was too low when viewing through the gels.

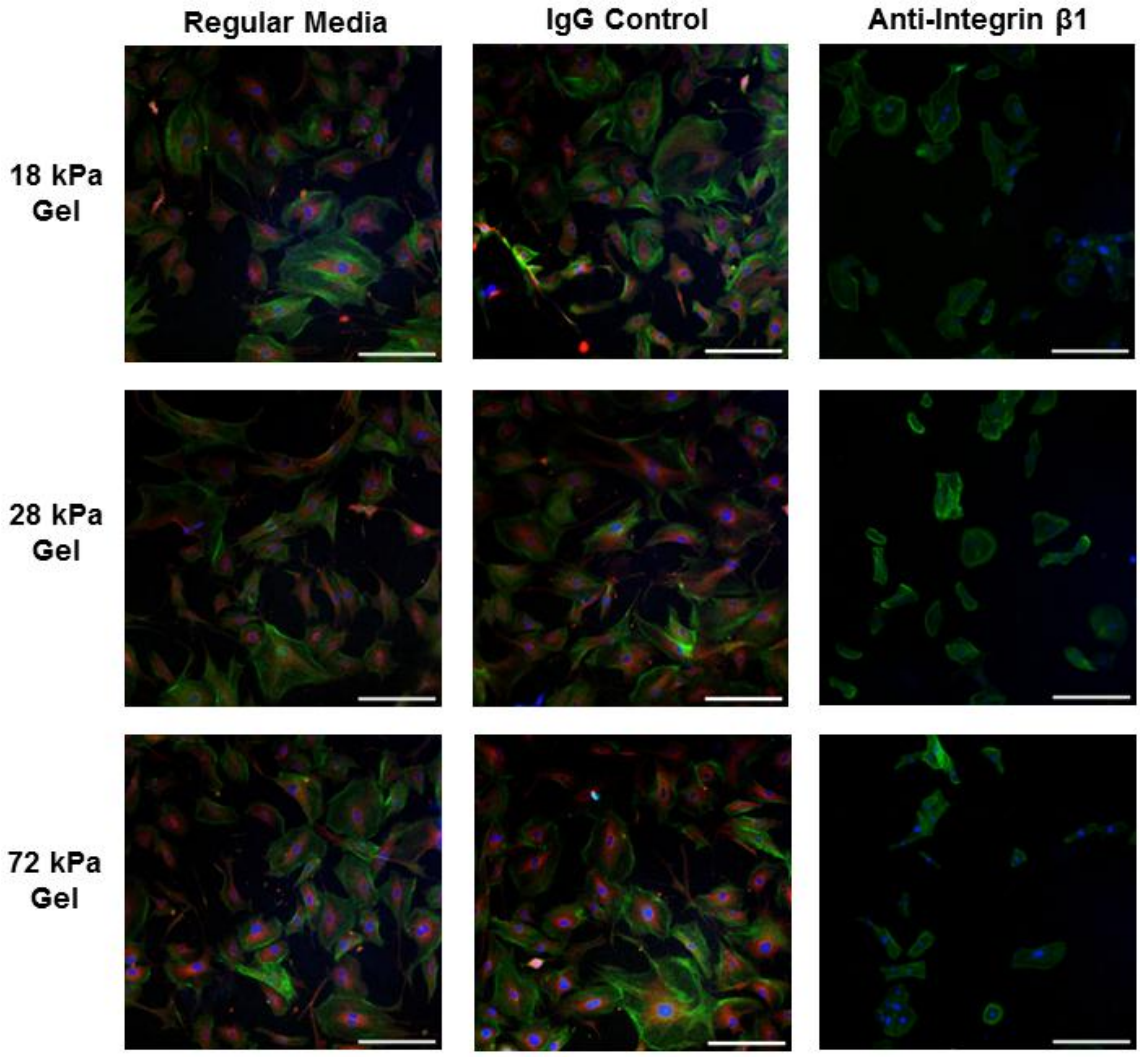

Figure 7.5. Representative immunofluorescence images of day 5 vascular smooth muscle cells on each gel with the different media conditions (scale bar = 200 μm). Cells are stained for nuclei (blue), filamentous actin (green), and microtubules (red). Microtubule stain in anti-integrin β1 samples had a lot of artifacts so not included.

7.3.2 Tension Conditions

Elastic Modulus

The mean apparent elastic moduli measurements for day 5 VSMCs with and without tension conditions are shown in Figure 7.6, along with the elastic moduli results for cells on glass slides (from previous study) for reference. For the cells without tension conditions, the cellular elastic moduli measures ranged from 2.5 kPa for anti-integrin β1 conditions to 3.4 kPa for IgG control media conditions, with no significant differences among sample types. All of these measures were significantly lower than the elastic moduli measures for samples that underwent cyclic tension and for the cells on the glass slides from a previous study ($p \leq 0.007$). These "no tension" measurements were similar to the elastic moduli measurements for cells on the 28 kPa gel (Figure 7.3), suggesting that the silicone elastomer membrane was of similar stiffness to this gel. For the cells with tension conditions, the cellular elastic moduli measures remained low for the anti-integrin β1 sample (3.8 kPa) but increased dramatically (from the no tension conditions) for the control samples (~11 kPa). None of these measurements were considered significantly different from the elastic moduli measures on glass slides.

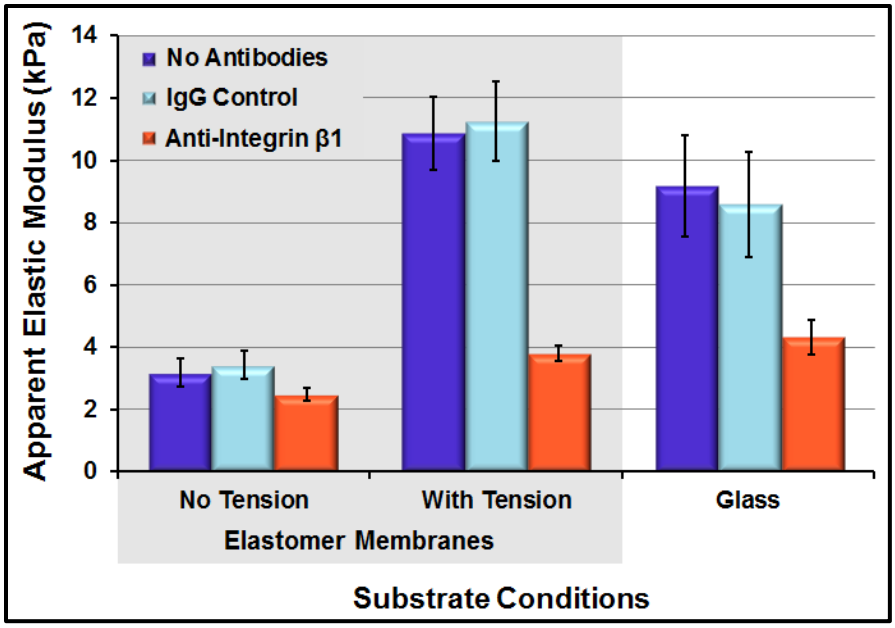

Figure 7.6. Apparent elastic moduli of day 5 VSMCs with and without tension conditions. Data presented as mean ± standard error.

Table 7.4 contains the cell-to-cell and average repeated point COV measures for cellular elastic moduli under different media conditions, with and without tension. The average cell-to-cell COV in the static controls is 61.2%, slightly lower than the variation found in elastic moduli measures for control samples in the previous studies (~70%). The level of variation drops to 38.4% in the anti-integrin β1 sample. This is consistent with cell-to-cell COV measures for anti-integrin β1 samples from previous studies (~45%). Interestingly, under tension conditions, the level of variation decreases among the control samples to 49.5%. This is the lowest cell-to-cell elastic moduli COV measure among all control samples in this work, indicating that the tension conditions promoted more homogeneous mechanical properties for cells throughout the population. Within the tension samples, the cell-to-cell elastic moduli COV measure decreased to 28.8% for

cells with anti-integrin β1 conditions, as expected. The repeated point COV measures were low, confirming that the variations in the elastic moduli measurements was not due to the measurement technique.

Table 7.4. VSMC cell-to-cell and repeated point coefficients of variation (COV) for elastic modulus and percent relaxation measures with and without tension conditions.

		Sample	Cell-to-Cell COV (%)		Average Repeated Point COV (%)
Elastic Modulus	Static	No Antibodies	61.6	Mean = 61.2	5.6
		IgG Control	60.7		5.5
		Anti-Integrin β1	38.4		8.0
	Tension	No Antibodies	48.0	Mean = 49.5	7.9
		IgG Control	50.9		9.8
		Anti-Integrin β1	28.8		8.3
Percent Relax	Static	No Antibodies	42.4	Mean = 45.7	4.4
		IgG Control	49.0		5.6
		Anti-Integrin β1	21.6		7.9
	Tension	No Antibodies	37.5	Mean = 35.5	5.8
		IgG Control	33.4		4.9
		Anti-Integrin β1	7.1		3.9

Stress Relaxation

The mean percent relaxation measurements for day 5 VSMCs with and without tension conditions are shown in Figure 7.7, along with the percent relaxation results for cells on glass slides (from previous study) for reference. The cells without tension conditions exhibited the largest percent relaxation during the 60 second hold, at approximately 60% (no significant differences between media conditions). This measure is close to the relaxation measure for cells on gels, again suggesting that the elastomer membrane is providing a similar "less stiff" substrate that the cells are responding to.

The cells subject to the cyclic tension conditions relaxed less during the 60 second hold, at approximately 50% (no significant differences between media conditions). The control samples (no antibodies and IgG media) had significantly higher relaxation percentages on the elastomer membrane without tension than the cells under the same media conditions on glass slides ($p \leq 0.044$). Otherwise, there were no significant differences across the samples on the different substrates.

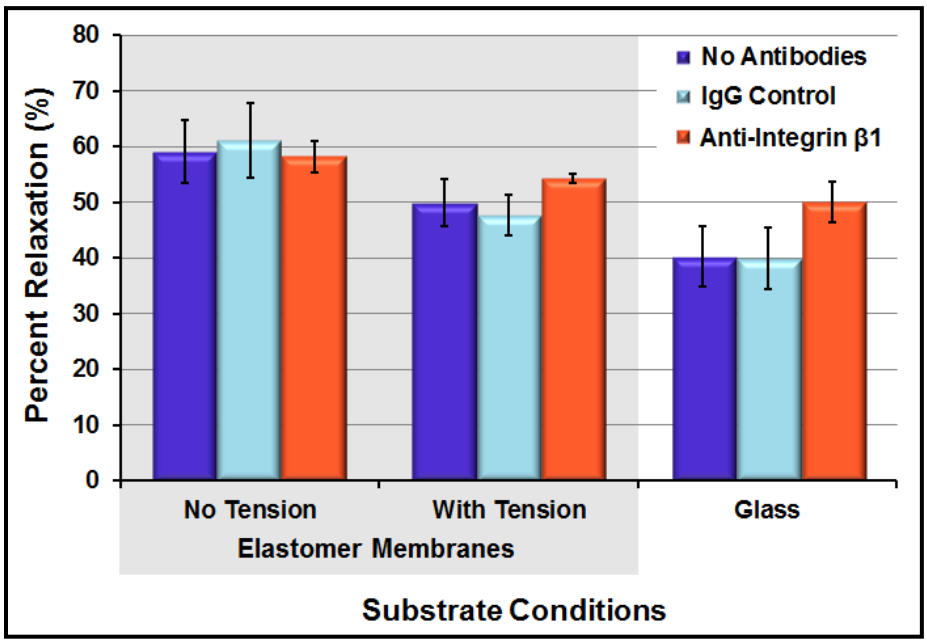

Figure 7.7. Percent relaxation during 60 second hold for day 5 VSMCs with and without tension conditions. Data presented as mean ± standard error.

Table 7.4 contains the cell-to-cell and average repeated point COV measures for cellular percent relaxation measures under different media conditions, with and without tension. The average cell-to-cell COV in the static controls is 45.7%. This is similar to the level of variation found among percent relaxation measures for control samples on

gels (COV = 42%, Table 7.3). Within the "no tension" (static) condition, the percent relaxation COV drops to 21.6% in the anti-integrin β1 sample (similar to COV for same media conditions on gels, COV = 17%). Under tension conditions, the average control COV is 35.5%, ten percent lower than the same measure on static conditions. This drop was also found in the elastic moduli COV measures, suggesting that tension conditions promote more mechanically homogeneous cells. Within the tension condition, the percent relaxation COV drops to only 7.1%, the lowest COV measure in all our work. The repeated point COV measures were low, confirming that the variations in the percent relaxation measurements was not due to the measurement technique. Additionally, the QLV model fit the data well for all sample types with an average R^2 of 0.97 ± 0.04.

Immunofluorescence

The stains for nuclei, actin, and microtubules, shown in Figure 7.8, were used to compare VSMC structure among samples. On the samples without tension, cells on the control samples (regular media and IgG control) appeared to be similar, with mostly synthetic cells that were variable in size. Most cells had cell extensions in several directions. The "no tension" VSMCs with the anti-integrin β1 media conditions were generally smaller, more rounded, and had fewer cell extensions. These results are similar to the observations of the cells on the gel substrates. On the samples with tension, the VSMCs were much smaller. Within the control conditions, cells were elongated and took on a more contractile phenotype. They even appeared to align along the direction of strain. The "with tension" anti-integrin β1 cells were less elongated and did not exhibit a

specific directionality. Higher magnification images were not obtained because the resolution was limited when viewing through the elastomer membrane.

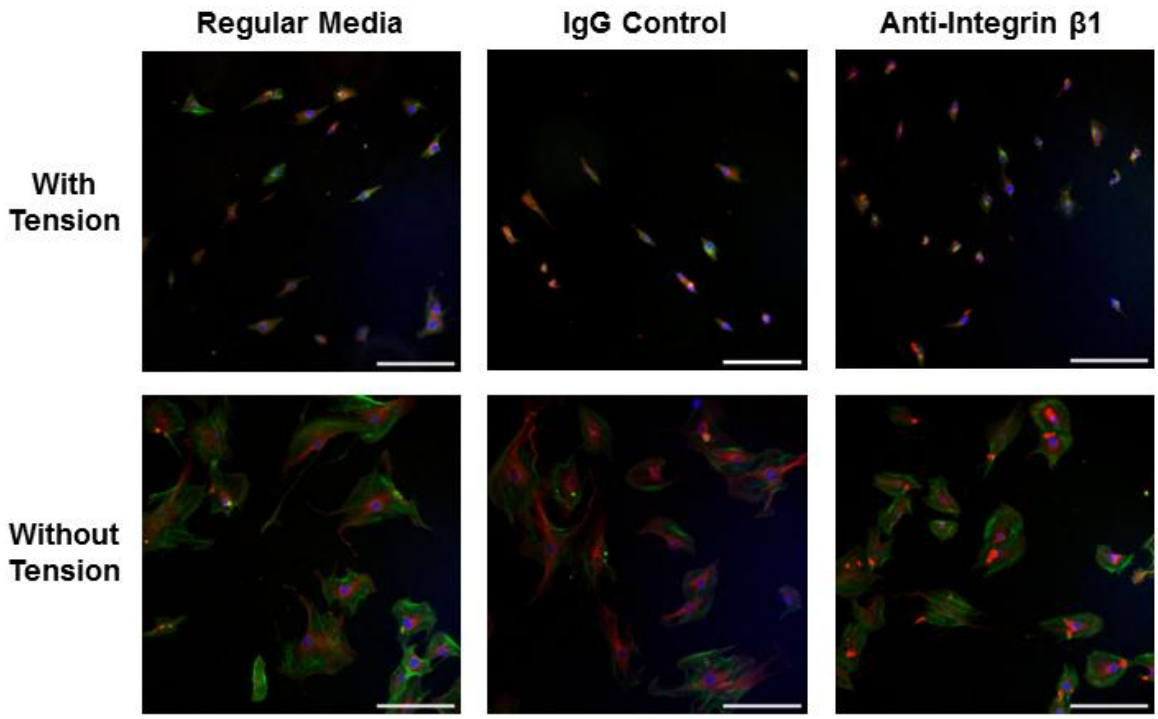

Figure 7.8. Representative immunofluorescence images of day 5 vascular smooth muscle cells with and without tension conditions with the different media conditions (scale bar = 200 μm). Cells are stained for nuclei (blue), filamentous actin (green), and microtubules (red).

7.4 Discussion

In this study, VSMCs were cultured under more *in vivo*-like conditions and their overall appearance and mechanical properties were evaluated. We were particularly interested in finding if the drop in mechanical heterogeneity with antibody media

conditions occurred for VSMCs under these conditions, as it did for VMSCs on glass slides in Chapter 6.

For the gel samples, significant differences were observed in both elastic moduli and percent relaxation measures for the VSMCs cultured on the gels, in comparison to the stiffer glass slides. For all samples (media conditions), cellular elastic moduli increased with increasing gel stiffness. On the substrates: 18 kPa gel, 28 kPa gel, 72 kPa gel, and glass, the average cellular elastic moduli for control samples were 3.4 kPa, 3.8 kPa, 6.8 kPa, and 8.9 kPa respectively (Figure 7.3). Within these samples, blocking integrin β1 resulted in lower elastic moduli measures when compared to control media conditions (consistent with results on glass). In a study on fibroblasts, Solon et al. found that cellular elastic moduli were 4.5 kPa on a 10 kPa gel, 5 kPa on a 20 kPa gel, and 7 kPa on glass [16]. They found that elastic moduli measurements did not increase significantly on gels with stiffnesses between 20 kPa and glass. Although this was a different cell type, our results were very similar in magnitude and trend. Percent relaxation measures generally increased for the cells on the gels, but there was no trend with gel stiffness (Figure 7.4). Within these samples, blocking integrin β1 resulted in small, non-significant increases in percent relaxation measures. Immunofluorescence staining provided a measure of cellular phenotype within each of the samples, revealing similar cellular structure across all control samples and across all anti-integrin β1 samples. The lack of changes across gel samples with different stiffness was observed previously, as Solon et al. did not see any changes in cell morphology/spreading on substrates over 10 kPa [16]. The cellular extensions that we observed are typical of cells

grown on gels before confluency is reached [17]. Again, the cells cultured under integrin β1 media conditions were smaller and more rounded. The cell-to-cell COV measures for the gel samples decreased from control samples to anti-integrin β1 samples for both elastic moduli measures (70% to 43%) and percent relaxation measures (42% to 17%) (Table 7.3). This reduction in mechanical heterogeneity is very similar to the reduction that was observed on glass slides (72% to 45% and 62% to 27%), indicating that blocking cell-matrix interactions resulted in a more mechanically homogeneous cell population for both glass and gel samples.

For the tension samples, elastic moduli measures decreased significantly from the measurements on glass slides from the previous study (controls ~ 8.9 kPa) to the measurements on the static (no tension) samples (controls ~ 3.3 kPa) (Figure 7.6). Although the silicone elastomer membranes were found to be stiffer than the gels (AFM indentation measurement), there was no underlying glass substrate in culture so the membrane must have "felt" less stiff to the cells (similar to gels). The tension conditions resulted in a significant increase in cellular elastic moduli measures in control samples (3.3 kPa to 11.0 kPa). Within the tension sample, the average elastic modulus for anti-integrin β1 remained very low (3.8 kPa), indicating that these cells were limited in their mechanotransduction abilities. Percent relaxation measures revealed that the cells relaxed the most on the static sample, followed by the "with tension" sample, and finally the glass sample (few differences considered statistically significant) (Figure 7.7). Immunofluorescence imaging provided insight to the cellular phenotype within each of the samples. The reduction in size from static to cyclic tension samples was significant

(Figure 7.8). According to a previous study where the same level of cyclic tension was applied for a period of 24 hours, VSMCs from the cyclic tension group exhibited significantly lower cell area compared to controls [5]. In the same study, cells that underwent cyclic tension contained higher levels of SM α-actin, a phenotypic marker for contractile VSMCs. Because our study lasted three times longer, we could expect these findings to be more pronounced. This appeared to be the case with the very small, elongated VSMCs under the tension conditions. Again, the cells cultured under integrin β1 media conditions were smaller and more rounded when compared to their respective controls. The cell-to-cell COV measures decreased from the static controls (61% for elastic modulus, 46% for percent relaxation) to the tension controls (50% for E, 36% for relax), indicating that the cyclic tension conditions promoted a more mechanically homogeneous sample. Within the tension samples, the heterogeneity further decreased under anti-integrin β1 conditions (50% to 29% for E, 46% to 36% for relax), indicating that blocking cell-matrix interactions resulted in a more mechanically homogeneous cell population under tension conditions.

7.5 Conclusions

The influence of integrin β1-mediated cell-matrix interactions on cellular phenotype and mechanics was assessed under *in vivo*-like conditions. Both softer polyacrylamide gel substrates and the application of cyclic tension resulted in changes to cellular phenotype and mechanical properties. Within these samples, however, the level of variation in mechanical properties among cells decreased in a manner similar to that on

glass. These results suggest that VSMCs most likely exhibit heterogeneous mechanical properties *in vivo*, especially in conditions were their cell-cell and cell-matrix interactions are highly variable.

7.6 References

1. Ghosh, K., et al., *Cell adaptation to a physiologically relevant ECM mimic with different viscoelastic properties.* Biomaterials, 2007. **28**(4): p. 671-679.

2. Oie, T., et al., *Local elasticity imaging of vascular tissues using a tactile mapping system.* Journal of Artificial Organs, 2009. **12**(1): p. 40-46.

3. Engler, A.J., et al., *Matrix elasticity directs stem cell lineage specification.* Cell, 2006. **126**(4): p. 677-689.

4. Tse, J. and A. Engler, *Preparation of hydrogel substrates with tunable mechanical properties.* Current Protocols in Cell Biology, 2010. **10**(16).

5. Acampora, K.B., et al., *Development of a novel vascular simulator and injury model to evaluate smooth muscle cell response following balloon angioplasty.* Annals of Vascular Surgery, 2007. **21**(6): p. 734-741.

6. Acampora, K.B., *Effect of clinically relevant mechanical forces on smooth muscle cell response in model of balloon angioplasty*, in *Bioengineering*2008, Clemson University: Clemson, SC.

7. Williams, B., *Mechanical influences on vascular smooth muscle cell function.* Journal of Hypertension, 1998. **16**(12): p. 1921-1929.

8. Stegemann, J.P., H. Hong, and R.M. Nerem, *Mechanical, biochemical, and extracellular matrix effects on vascular smooth muscle cell phenotype.* Journal of Applied Physiology, 2005. **98**(6): p. 2321-2327.

9. Tock, J., et al., *Induction of SM-alpha-actin expression by mechanical strain in adult vascular smooth muscle cells is mediated through activation of JNK and p38 MAP kinase.* Biochemical and Biophysical Research Communications, 2003. **301**(4): p. 1116-1121.

10. Birukov, K.G., et al., *Stretch affects phenotype and proliferation of vascular smooth muscle cells.* Molecular and Cellular Biochemistry, 1995. **144**(2): p. 131-139.

11. Wang, Y.L. and R.J. Pelham, *Preparation of a flexible, porous polyacrylamide substrate for mechanical studies of cultured cells*, in *Molecular Motors and the Cytoskeleton, Pt B*1998. p. 489-496.

12. Datko, L., *M.S. Thesis: Effects of microenvironment on growth and differentiation of human dental pulp cells*, 2011, Clemson University.

13. Giddens, D.P., C.K. Zarins, and S. Glagov, *The role of fluid-mechanics in the localization and detection of atherosclerosis.* Journal of Biomechanical Engineering-Transactions of the Asme, 1993. **115**(4): p. 588-594.

14. *Flexcell Internation Corporation: Products*. 2010 [cited 2010; http://www.flexcellint.com/gallery.htm].

15. Triantafillopoulos, I.K., et al., *Nandrolone decanoate and load increase remodeling and strength in human supraspinatus biloartificial tendons.* American Journal of Sports Medicine, 2004. **32**(4): p. 934-943.

16. Solon, J., et al., *Fibroblast adaptation and stiffness matching to soft elastic substrates.* Biophysical Journal, 2007. **93**(12): p. 4453-4461.

17. Yeung, T., et al., *Effects of substrate stiffness on cell morphology, cytoskeletal structure, and adhesion.* Cell Motility and the Cytoskeleton, 2005. **60**(1): p. 24-34.

CHAPTER EIGHT

CONCLUSIONS AND RECOMMENDATIONS

8.1 Conclusions

This research was motivated by the observation that cells exhibit a very high level of variation in their mechanical properties within a single population. If this level of variation is present in cells in the body, it should be incorporated into mechanical models as it will likely affect the mechanical behavior of the overall tissue. The cellular cytoskeleton is the primary structural component of a cell and is physically coupled to neighboring cells and to underlying matrix scaffolds. As such, we hypothesized that variations in the cellular microenvironment (number of cell-cell and cell-matrix interactions) lead to differences in the internal cytoskeletal structure of the cells, which result in the highly variable mechanical properties that have been observed from cell to cell. We set out to limit the variability in the microenvironment in an attempt to determine the exact source of this heterogeneity. In addition to characterizing cellular mechanical heterogeneity, this work resulted in several important findings from a basic science perspective.

In the first study, a novel inkjet printer-based method for created aligned ECM proteins was outlined. Collagen and fibronectin solutions were printed onto glass substrates in a line pattern without significant heat denaturation. Within the printed lines, the ECM fibers showed alignment, particularly at the edges of the printed lines. This alignment technique combined the best aspects of the methods currently in use –

accuracy, simplicity, and low cost, and may be useful in many broader tissue engineering and biomaterial applications in the future. For our purposes, it was used to create a more uniform ECM for cell culture in our next study.

Cardiomyocytes and vascular smooth muscle cells were then cultured on the printed collagen and fibronectin matrices, with the hypothesis that, on the more uniform aligned matrices, the cells would have more uniform cell-cell and cell-matrix interactions, and therefore more homogeneous mechanical properties. The results of this study suggest that cells actively respond to their culture environment over time as cardiomyocyte mechanical properties changed (elastic modulus increased, percent relaxation decreased) over the first five days in culture before reaching a plateau. For both cardiomyocytes and vascular smooth muscle cells, aligned matrices were shown to promote cells with higher elastic moduli and lower percent relaxation measures. In a similar fashion, fibronectin matrices were shown to promote the same trends in comparison to collagen matrices. The cells on the aligned substrates also took on a much thinner, more elongated morphology. Within each sample, however, the level of variation in cellular mechanical properties did not decrease for cells on aligned matrices in comparison to cells on unaligned matrices. Therefore, it was concluded that the microenvironment differences between aligned and unaligned matrices must not be large enough to cause a difference in mechanical heterogeneity, so more drastic changes were investigated.

In the next study, N-cadherin-mediated cell-cell and integrin β1-mediated cell-matrix interactions were blocked with antibodies. We theorized that any drop in cellular

mechanical heterogeneity in these samples could be attributed to diversified cell-cell and cell-matrix interactions throughout the sample. Blocking N-cadherin and integrin β1 interactions individually and in combination resulted in greatly reduced cellular (VSMC) elastic moduli measures (less stiff) and increased cellular percent relaxation measures (more viscous). These significant changes in mechanical properties suggest that each individual cell-cell and cell-matrix interaction (within adherens junctions and focal adhesion complexes) has a very large influence on the overall mechanical behavior of the cell. Within the mechanical measurements, it was found that cells exhibited more homogeneous mechanical properties when their cell-cell and cell-matrix interactions were limited. This suggests that varying cellular adhesions throughout a sample are responsible, at least in part, for the high level of heterogeneity that is commonly observed in cellular mechanical properties.

Finally, these antibody blocking experiments were replicated under more *in vivo*-like conditions to get an estimate of the level of cellular mechanical heterogeneity that may exist in the body. Both softer polyacrylamide gel substrates and the application of cyclic tension resulted in changes to cellular phenotype and mechanical properties. The VSMCs cultured on gels behaved very similar to the VSMCs cultured on glass, but their elastic moduli measures decreased with decreasing gel stiffness. The VSMCs that were subjected to tension conditions were much stiffer, and smaller and more elongated than VSMCs without tension. Within both the gel and tension samples, the level of variation in mechanical properties among cells decreased in a manner similar to that on glass. These results suggest that VSMCs most likely exhibit heterogeneous mechanical

properties *in vivo*, especially in conditions were their cell-cell and cell-matrix interactions are highly variable (Figure 8.1).

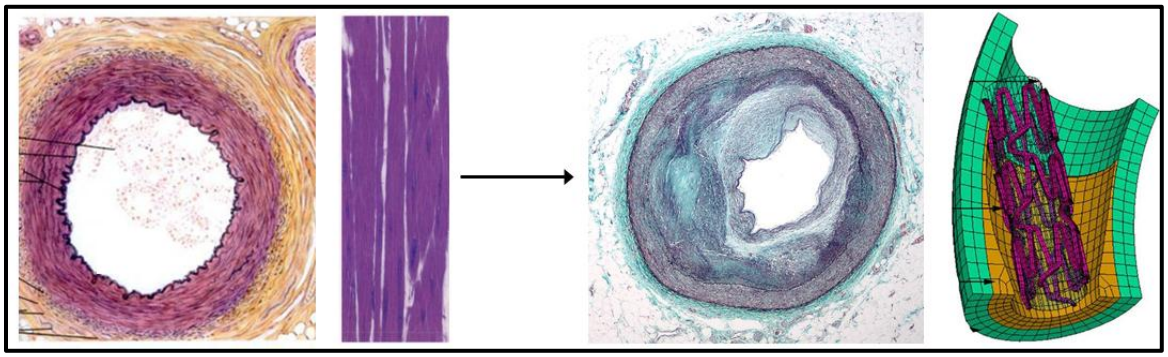

Figure 8.1. Comparison of VSMC microenvironment in healthy and diseased arteries. In a healthy artery, the VSMC microenvironment is fairly uniform (left). In contrast, the VSMC microenvironment is highly variable in case of atherosclerosis (right). Mechanical models should take this mechanical heterogeneity into account in order to better predict tissue behavior [1, 2].

8.2 Recommendations

8.2.1 Create two-layer model for cellular mechanical behavior on gels

In this work we calculated the mechanical properties of VSMCs on soft gels using the same mechanical models that we used for cells on glass substrates. When a cell is probed on a stiff glass slide, the slide itself does not deform, but rather all deformation can be attributed to the cell. On the gels, however, the applied force may have been transmitted to the underlying gels. We do not believe that this was a significant issue as the cellular elastic moduli measures were significantly less stiff than the stiffness of the gels they were cultured on. However, we suggest that a simple two-layer finite element model be created (gel layer and cell layer) to remove the gel as a possible source of

deformation. Re-analyzing our data with this model and comparing it to our current measurements will reveal if the mechanical properties that we reported here are in fact measures drawn entirely from the cells.

8.2.2 Replicate experiments with other cell types

The overall goal for our work is to provide an approximation for cellular mechanical heterogeneity based on known *in vivo* microenvironment conditions for any cell type. To do this, we must first determine if our results our applicable to other cell types. Specifically, do other cells respond to blocking cell-cell and cell-matrix interactions in the same manner (reduced heterogeneity)? In our first aim, we found differences in overall cellular heterogeneity levels from cardiomyocyte samples (elastic modulus COV = 57%) to VSMC samples (elastic modulus COV = 70%). We hypothesize that despite these differences in the initial level of heterogeneity, the blocking experiments will result in a similar level of reduced variability and our results will be useful for all cell types. In order to prove this, the experiments should be replicated with several cell types.

8.2.3 Obtain better whole-sample measurements

In this work, we mechanically probed twenty cells from throughout each sample and took representative immunofluorescence images of cells on each sample. In order to get a better measure of the mechanical properties and phenotype for the cells within a

given sample, cell location could be tracked during mechanical testing and Western Blot analysis performed for smooth muscle α-actin.

In our theory of cellular mechanical heterogeneity, variations in ECM concentration and orientation give rise to stronger cell-matrix interactions in some locations than other locations on the same sample. As such, neighboring cells would have similar cell-ECM interactions. Neighboring cells would also likely have similar numbers of cell-cell contacts. Therefore, we would expect neighboring cells to be more mechanically homogeneous. In our studies, we tested 20 cells from throughout each sample area without taking note of cell location. It would be interesting to keep track of cell location during AFM testing to determine if cells that are closer together are more mechanically homogeneous. Specifically, you could investigate "clusters" of cells or aligned cells on printed matrices. For the aligned cells you could measure each cell in line and investigate if mechanical properties change as you move further down the line. If neighboring cells are found to be more mechanically homogeneous, our theory would gain support and this concept would be useful in creating a better *in vivo* model (assign neighboring cells more similar properties). By keeping track of cellular locations, cells with similar microenvironment conditions could be compared across sample types and variations due to inconsistencies in cell selection would be eliminated.

In this work, we primarily associated thin, elongated cells with a contractile phenotype and cells that were more spread with a synthetic phenotype (morphology differences). While VSMCs in culture typically take on a continuum of phenotypes between the two extremes, there are several differences between the two phenotypes (not

just morphology). One such difference is cellular smooth muscle α-actin content. In future studies, we recommend using Western blot analysis to detect levels of this contractile phenotype marker. Increased levels of smooth muscle α-actin expression indicate a more contractile VSMC phenotype. This analysis will give a quantitative measure for phenotypic differences for cells on one sample versus cells on another sample. These results can be correlated with the mechanical property data and allow for a more thorough comparison among the test groups.

8.2.4 Make more controlled culture conditions

In this work, cell-cell and cell-matrix interactions were inhibited to create more uniform cellular microenvironments. For example, adding N-cadherin antibody to the VSMC media removed variations in N-cadherin mediated cell-cell interactions (all cells had zero N-cadherin interactions). This, in effect, lowered the overall microenvironment variability from one cell to another within the sample. Rather than limiting the cellular microenvironment by inhibiting interactions in this manner, it is possible to create more uniform microenvironment conditions to begin with. Using technology such as laser patterning, researchers can position cells in culture with great precision. This technology could be used to study the impact of one cell-cell interaction vs. two cell-cell interactions vs. three cell-cell interactions, etc. Cells could also be positioned atop a specific concentration of ECM proteins to better investigate the importance of cell-matrix interactions. In a simpler technique, cells could be seeded at different densities to study different levels of cell-cell interactions. At a lower density, cells would have fewer cell-

cell interactions than cells at a higher density (near confluent). These strategies could provide further, more detailed insights into the importance of cell-cell and cell-matrix interactions in determining cellular mechanical properties.

8.2.5 Create tissue-level mechanical models that incorporate realistic levels of cellular heterogeneity

This work provided some insights into the level of cellular mechanical heterogeneity that is present within tissues in the body. At this point, it is important to take the next step and construct a finite element model of a tissue that incorporates realistic levels of cellular mechanical heterogeneity. From here, researchers can determine what level of mechanical heterogeneity at the cellular level has an effect on the overall tissue behavior. Perhaps the level of variability we found in our work does not make a significant impact at the tissue level. In that case, these models should be used to determine what level of heterogeneity does have a significant impact. There are most likely certain tissue types and disease conditions where incorporating heterogeneity will be more valuable in determining overall tissue behavior than others. If the level of heterogeneity that was discovered in this study is found to not have a significant impact at the tissue level, researchers will have evidence to justify their assumption of homogeneous cellular mechanical properties in their tissue-level mechanical models. Additionally, this work will still have been worthwhile as the impact of the cellular microenvironment on cell structural and mechanical behavior has been highlighted through several interesting findings.

8.3 References

1. Eroschenko, V., *Atlas of Histology with Functional Correlations*. 11th ed2008: Lippincott Williams & Wilkins. 177.

2. Junqueira, L.C. and J. Carneiro, *Basic Histology: Text and Atlas*. 11th ed2005: McGraw-Hill.

APPENDICES

Appendix A

Vascular Smooth Muscle Cell Isolation

Aortic VSMCs were isolated from week 12 Sprague-Dawley rats via the following protocol [1]. The rats were first euthanized by carbon dioxide asphyxiation. The abdomen was split longitudinally from the pelvis to the clavicle. The internal organs were dissected away to expose the aorta along the posterior abdominal wall. The aorta was then clipped at the pelvic bifurcation and dissected away from the dorsal abdominal wall to the aortic arch. Approximately 3 ml of cold transport medium (Dulbecco's Modified Eagle's Medium (DMEM, Fisher Scientific, Pittsburgh, PA, USA) + 100 µg/ml penicillin/streptomycin (Sigma-Aldrich, St. Louis, MO, USA) + 2 µg/ml fungizone (Sigma-Aldrich)) was used to flush the aorta via hypodermic injection through the wall of the left ventricle. The aorta was then clipped at the aortic arch and placed in cold transport medium for transport from the animal facility to the lab. Next, excess fat and the adventitial layer of the artery were peeled away, in the presence of PBS to prevent drying and to maintain cell viability. Arterioles were then trimmed away and the aortic segments split lengthwise and laid open with the intima facing up. A sterile scalpel was used to scrape away the endothelial layer of the vessel. The aortic segments were then rinsed in PBS to remove any loose cells on the surface. Sterile scissors were used, under magnification, to finely mince the segments into approximately 0.5 mm pieces. The minced artery segments were placed in 15 ml tubes, each containing 10 ml of a DMEM/protease digestion solution (10 ml DMEM + 10 mg collagenase type II

(Worthington Biochemical, Lakewood, NJ, USA) + 2.5 mg elastase (Worthington Biochemical) + 1.5 mg soybean trypsin inhibitor (Worthington Biochemical)). The 15 ml tubes were placed in an incubator for 20-25 minutes at 37ºC and 5% carbon dioxide with mixing (gently inverting tubes 2-3 times) every 5 minutes. The aortic segments settled at the bottom of the tubes and the digestion solution was then aspirated. Next, the segments were resuspended in 10 ml of vascular smooth muscle cell (VSMC) media (DMEM + 10% FBS (Sigma-Aldrich) + 1% antibiotic/antimycotic solution (Sigma-Aldrich)) to dilute and deactivate the digestion solution. A sterile scalpel blade was then used to lightly scratch a small asterisk shaped pattern on the bottom of each well in a six well plate to aid in the adhesion of the tissue segments. Four arterial segments were placed in each well directly atop the scratched pattern, with a single drop of VSMC media to keep them moist and viable without allowing them to move from the scratched surface. The plates were incubated for 24 hours to allow for adhesion and then supplemented with 1.5 ml additional media, being careful not to dislodge the attached tissue. The plates were incubated for the next 7 to 10 days (until cells could be seen growing away from the tissue segments in several patches), with media changes every 48 hours. When the patches of adherent cells reached confluence, the tissue segments were carefully removed and the cells passaged and cultured with 12 ml media in T75 flasks.

Appendix B

MATLAB Elastic Modulus Scripts

Example of what to call in command window:

```
e = massexcompile('Day 5 VSMC')        (folder containing exported data)
```

Scripts:

massexcompile.m

- Loads raw AFM force-indentation data

```
function [elasticity Curves] = massexcompile(folderin)
% folderin should be the folder your data is in. something like
"C:\Documents and Setting\My Documents\MyData"
mainfolder = cd
format long
fnames = dir(folderin);
numfids = length(fnames);
cd(folderin);
%filtering out irrelevent "files" such as '.' and '..'
cellnames = {};
for s = 1:numfids;
    if 'c' == fnames(s).name(1) % 'c' represents the letter that the
relevent file names begin with
        cellnames{end+1} = fnames(s).name;
    end
end
%combine every 3 files and write
counter = 1;
numcell = length(cellnames);
numfile = 1;
elasticity = [];

% OMIT THIS WHILE LOOP IF YOU WANT TO LOAD CELLS INDIVIDUALLY
Curves(numcell, 1) = struct('extension', [], 'retraction', []);
CurrentCell =1;
while counter <= numcell
    a = load(cellnames{counter});
```

```
    c = load(cellnames{counter+2});

    cd(mainfolder);
    [elasticity(end+1,1) xe ye xr yr] =
elast_analysis(c,a,mainfolder,counter);
    Curves(CurrentCell).extension = [xe ye];
    Curves(CurrentCell).retraction = [xr yr];
    %figure('Name',sprintf('Cell %d', ((counter-
1)/3)+1),'NumberTitle','off')  %comment out in order to turn plotting
off
    %plot(c,a)                  %comment out in order to turn plotting
off

    counter = counter+3;
    CurrentCell = CurrentCell+1;
    cd(folderin);
    %numfile = numfile+1
end
cd(mainfolder)
```

elast_analysis.m

- Fits Hertz model to force-indentation data and outputs apparent elastic modulus measures in Pascals for each indentation file in input folder
- Calls AFM_butter.m and xycorrect.m scripts

```
function [e xe ye xr yr] = elast_analysis(c,a,mainfolder,counter)
cd(mainfolder)
format long
k = 0.12; %spring constant value N/m
v = 0.5; %poisson's ratio
R = 2.5*10^-6;  % tip radius in meters
L = 30*10^-9 ;     %lower bound for elasticity (in m from contact
point)
U = 300*10^-9 ;   %upper bound for elasticity (in m from contact point)


%adjust deflection
ak = a;
%filter deflection values
d = AFM_butter(ak);
%Separation of extension and retraction
l = floor(length(c)/2);
xe = c(200:l);% add 200 in order to omit first several data points
(irratic behavior due to filtering
ye = d(200:l);
if rem(length(c),2)==0;
    xr = c(end-200:-1:l+1); % subtract 200 in order to omit first
several data points
    yr = d(end-200:-1:l+1);
    else
    xr = c(end-200:-1:l+2);
    yr = d(end-200:-1:l+2);
end


%correct x,y offsets
[xe,ye] = xycorrect(xe,ye);
[xr,yr] = xycorrect(xr,yr);

ye = k * ye;
yr = k * yr;

format long;
erange = [];
for i = [1:1:length(xe)];
    if xe(i)>=L && xe(i)<=U;
        erange(end+1) = i;
```

```
    end;
end;
rrange = [];
for i = [1:1:length(xr)];
    if xr(i)>=L && xr(i)<=U;
        rrange(end+1) = i;
    end;
end;


emodulus = mean((3.*ye(erange).*(1-
v^2))./(4.*xe(erange).^(3/2).*R.^(1/2)));
%rmodulus = mean((3.*yr(rrange).*(1-
v^2))./(4.*xr(rrange).^(3/2).*R.^(1/2)));
figure('Name',sprintf('Sample %d', ((counter-
1)/3)+1),'NumberTitle','off')
plot(xe,ye)
hold on
plot(xe(erange),ye(erange),'r')

e = [emodulus];
```

AFM_butter.m

- Applies Butterworth filter to data

```
function [i] = AFM_butter(x) %applies butterworth filter to data
format long
[b,a]=butter(3,.025);
i=filter(b,a,x);
```

xycorrect.m

- Corrects x and y offsets in data to set contact point to (0,0)

```
function [xc,yc] = xycorrect(x,y)
s = 0.008; %slope sensitivity


%correction for y
format long
region = [1:length(x)/4];
slope = polyfit(x(region),y(region),1);
yci = y-(polyval(slope, x));

%correction for x
numslope = diff(yci)./diff(x);
index = 1;
condition = 0;
contactx = 0
while condition == 0 && index ~= length(numslope)
    if numslope(index) > s && mean(numslope(index:5:index+200)) > s;
        condition = 1;
        contactx = index;
    end
    index = index+1;
end

xc = x-x(contactx)-yci;

% correct again for y
yc = yci-yci(contactx);
```

Appendix C

MATLAB Stress Relaxation Scripts

Example of what to call in command window:

```
[StressRelax]=hdrload('cell 1.000.txt');
[data_final change_strain] = stressrelax(StressRelax, 1);
plot(data_final(:,2),data_final(:,1))
G60 = data_final(60)
[r2 fit1 coef1] = SLSfit(data_final);
[r2 fit1 coef1] = QLVFit(data_final);
```

Scripts:

hdrload.m

- Loads raw AFM stress relaxation data
- Adapted from MathWorks (Natick, MA, USA) script [2]

```
function [data] = hdrload(file)


% HDRLOAD Load data from an ASCII file containing a text header.
%     [header, data] = HDRLOAD('filename.ext') reads a data file
%     called 'filename.ext', which contains a text header.  There
%     is no default extension; any extensions must be explicitly
%     supplied.
%
%     The first output, HEADER, is the header information,
%     returned as a text array.
%     The second output, DATA, is the data matrix.  This data
%     matrix has the same dimensions as the data in the file, one
%     row per line of ASCII data in the file.  If the data is not
%     regularly spaced (i.e., each line of ASCII data does not
%     contain the same number of points), the data is returned as
%     a column vector.
%
%     Limitations:  No line of the text header can begin with
%     a number.  Only one header and data set will be read,
```

```
%     and the header must come before the data.
%
%     See also LOAD, SAVE, SPCONVERT, FSCANF, FPRINTF, STR2MAT.
%     See also the IOFUN directory.


% check number and type of arguments
if nargin < 1
  error('Function requires one input argument');
elseif ~isstr(file)
  error('Input must be a string representing a filename');
end


% Open the file.  If this returns a -1, we did not open the file
% successfully.
fid = fopen(file);
if fid==-1
  error('File not found or permission denied');
  end


% Initialize loop variables
% We store the number of lines in the header, and the maximum
% length of any one line in the header.  These are used later
% in assigning the 'header' output variable.
no_lines = 0;
max_line = 0;


% We also store the number of columns in the data we read.  This
% way we can compute the size of the output based on the number
% of columns and the total number of data points.
ncols = 0;


% Finally, we initialize the data to [].
data = [];


% Start processing.
line = fgetl(fid);
if ~isstr(line)
  disp('Warning: file contains no header and no data')
  end;
[data, ncols, errmsg, nxtindex] = sscanf(line, '%f');


% One slight problem, pointed out by Peter vanderWal: If the
% first character of the line is 'e', then this will scan as
% 0.00e+00. We can trap this case specifically by using the
```

```
% 'next index' output: in the case of a stripped 'e' the next
% index is one, indicating zero characters read.  See the help
% entry for 'sscanf' for more information on this output
% parameter. We loop through the file one line at a time until
% we find some data.  After that point we stop checking for
% header information. This part of the program takes most of the
% processing time, because fgetl is relatively slow (compared to
% fscanf, which we will use later).
while isempty(data)|(nxtindex==1)
  no_lines = no_lines+1;
  max_line = max([max_line, length(line)]);
  % Create unique variable to hold this line of text information.
  % Store the last-read line in this variable.
  eval(['line', num2str(no_lines), '=line;']);
  line = fgetl(fid);
  if ~isstr(line)
    disp('Warning: file contains no data')
    break
    end;
  [data, ncols, errmsg, nxtindex] = sscanf(line, '%f')
  end % while


% Now that we have read in the first line of data, we can skip
% the processing that stores header information, and just read
% in the rest of the data.
data = [data; fscanf(fid, '%f %f')];
fclose(fid);


% Create header output from line information. The number of lines
% and the maximum line length are stored explicitly, and each
% line is stored in a unique variable using the 'eval' statement
% within the loop. Note that, if we knew a priori that the
% headers were 10 lines or less, we could use the STR2MAT
% function and save some work. First, initialize the header to an
% array of spaces.
header = setstr(' '*ones(no_lines, max_line));
for i = 1:no_lines
  varname = ['line' num2str(i)];
  % Note that we only assign this line variable to a subset of
  % this row of the header array.  We thus ensure that the matrix
  % sizes in the assignment are equal. We also consider blank
  % header lines using the following IF statement.
  if eval(['length(' varname ')~=0'])
    eval(['header(i, 1:length(' varname ')) = ' varname ';']);
    end
  end % for


% Resize output data, based on the number of columns (as returned
% from the sscanf of the first line of data) and the total number
```

```
% of data elements. Since the data was read in row-wise, and
% MATLAB stores data in columnwise format, we have to reverse the
% size arguments and then transpose the data.  If we read in
% irregularly spaced data, then the division we are about to do
% will not work. Therefore, we will trap the error with an EVAL
% call; if the reshape fails, we will just return the data as is.
eval('data = reshape(data, ncols, length(data)/ncols)'';', '');
%data(:,2) = [];
```

stressrelax.m

- Normalizes and truncates stress relaxation data
- Note: Sampling frequency occasionally varies for data from Asylum AFM (e.g., 0.0005 second intervals for baseline data and 0.1 second intervals for relaxation data) – manually adjusted raw data to normalize frequency and adjusted interval time in this script accordingly (set at 0.01 seconds here (sampling interval for Veeco AFM data))

```
% function [data_final, depth, delta_strain] = stressrelax(data,
defsens, ramp)
function [data_final change_strain] = stressrelax(data, defsens)


%lintime = linspace(0.01,120,12000)';
HoldTime = 60;
HoldSamples = HoldTime/0.01;
lintime = data(:,1);
data= data(:,2);
baseline_shift = mean(data(1:100));
data_shift = (data-baseline_shift);
data_small = data_shift(1:1000);
[y n] = max(data_small);
data_norm = (data_shift(n+1)).\(data_shift(n+1:n+HoldSamples));
sum(data_norm);
for i = 1:length(data_norm),
    if data_norm(i) < 0
        data_norm(i) = 0.01;
    end
end
data_final = [data_norm(1:HoldSamples) lintime(1:HoldSamples)];
% lintime2 = linspace(0,120,12000)';
% depth = [data_norm lintime2];
% delta_strain = (((defsens*y)-(defsens*data_norm(12000)))/depth)*100;
change_strain = (((data_shift(n)-
data_shift(HoldSamples))*defsens)/1000)*100
% G120=data_final(100)
maxforce = data_shift(n)*60*0.12
minforce = data_shift(HoldSamples)*60*0.12
% delta_strain = (((maxforce-minforce)/0.12)/1000)*100
% data_shift(n)



end
```

TheGFunction.m

- Used in conjunction with QLVFIT.m to fit Quasilinear Viscoelastic reduced relaxation function to normalized relaxation data

```
function G = TheGFunction(a, t)
G = 0*t;
C = a(1);
tau1 = a(2);
tau2 = a(3);
dtau = (tau2-tau1)/800;
taus = linspace(tau1, tau2,800)';
for i = 1:length(t),
%     fun1 = @(tau) (exp(t(i)/tau)/tau);
%     fun2 = @(tau) (1/tau);
%     int1 = quad(fun1, tau1, tau2);
%     int2 = quad(fun2, tau1, tau2);
    int1 = sum(exp(-t(i)./taus)./taus)*dtau;
    int2 = sum(1./taus)*dtau;
    G(i) = (1 + C.*int1)./(1+ C.*int2);
end
```

QLVFit.m

- Used in conjunction with TheGFunction.m to fit Quasilinear Viscoelastic reduced relaxation function to normalized relaxation data
- Outputs R^2 value for QLV fit

```
function [R2, fit, coefEsts] = QLVFit(data);

% QLVfun2 = @ (a,t) [1+a(1).*quad((exp(-t./a(2))./a(2)),a(3),a(4))] ./
[1+a(1).*quad((1./a(2)),a(3),a(4))];

%
lintime = linspace(0.01,120,12000)';
logtime = log10(lintime);


% t=logspace(-2,2.079,100)';
StartingVals = [1 0.5 100];
coefEsts = nlinfit(data(:,2), data(:,1), @TheGFunction, StartingVals)
%xgrid = logspace(-2,2.079,100);
xgrid = data(:,2);
plot(xgrid, data(:,1), '.')
plot(xgrid, TheGFunction(coefEsts, xgrid), 'r');
hold on
fit = TheGFunction(coefEsts, xgrid);
R = corr2(fit, data(:,1));

R2 = R^2
```

SLSFit.m

- Fits Standard Linear Solid reduced relaxation function to normalized relaxation data
- Outputs R^2 value for SLS fit

```
function [R2 fit coefEsts] = SLSfit(data);

t= logspace(-2,2.079,100)';
t = data(:,2);
% a(1)=ER, a(2)=taustress, a(3)=taustrain
SLSfun = @(a,t) a(1).*(1-(1-a(2)./a(3)).*exp(-t./a(3)));
StartingVals = [1 1 1];
coefEsts = nlinfit(t, data(:,1), SLSfun, StartingVals)
xgrid = logspace(-2,2.079,100);
xgrid = t;
line(xgrid, SLSfun(coefEsts, xgrid), 'Color','m');
fit = SLSfun(coefEsts, xgrid);
R = corr2(fit, data(:,1));
R2 = R^2
```

Appendix D

Polyacrylamide Gel Protocol

Note: To combat cellular contamination problems, we filtered the solutions highlighted in red before using them in this protocol. All work was conducted in a biohazard laminar flow hood, except for the long wave UV step.

Materials:

- Glass Slides (12 mm diameter)
- Distilled water (sterile Millipore water)
- NaOH pellets (NaOH solution)
- 3-aminopropyltrimethoxy silane (APTES)
- 0.5% gluteraldehyde in PBS
- 1 M HEPES
- 50 mM HEPES (500 uL of 1 M HEPES per 10 mL of PBS)
- 40% Acrylamide and 2% Bis
- Ammonium Persulfate (10 mg in 100 µl of PBS – prepare immediately before use)
- tetramethylethylenediamine (TEMED)
- Collagen (1 mg/mL in H_2O)

Slide activation:

1. Put several (~5) NaOH pellets in a weigh boat and add distilled water. When they dissolve, add slides for a few minutes, then remove and let dry on a kimwipe. (Neutrilize HaOH solution before disposal)
2. Coat one side of the slides (in a new weigh boat) with STERILE 3-aminopropyltrimthoxy silane (APTES) (Waste goes in biohazard waste container)
3. Incubate at room temperature for 5 minutes
4. Rinse with distilled water and shake for 5 minutes
5. Repeat #4 two more times **make sure to get all the APTES off or the slides will have a reddish tint when you add gluteraldehyde**
6. Coat the same side of the slides with 0.5% gluteraldehyde for 30 minutes at room temperature (Gluteraldehyde waste must go in specific waste container)
7. Repeat the rinsing process (steps 4 and 5)

Acrylamide preparation:

1. Make acrylamide solution in a 25 mL glass breaker according to Table D.1
2. Add 30 µl ammonium persulfate and 20 µl TEMED to the acrylamide solution and mix gently
3. IMMEDIATELY pipet 6 µl onto activated slide and quickly place another slide on top
4. Leave remaining acrylamide in beaker (Once this has polymerized, gel on slide has also polymerized)
5. Flood the bottom of the dish with ~2 mL of 50 mM HEPES
6. Remove the top slide (with scalpel or forceps). Substrates can now be stored in PBS for up to 2 weeks at 4 °C

Table D.1. Ingredients for making polyacrylamide gels with different elastic moduli [3, 4].

Final Acryl / Bis %	40% Acrylamide (µl)	2% Bisacrylamide (µl)	1 M HEPES (µl)	Water (µl)	Elastic Modulus (kPa) (Literature)
8 / 0.8	1,000	2,000	50	1,950	75.1
8 / 0.3	1,000	750	50	3,200	26.0
8 / 0.1	1,000	250	50	3,700	9.8

Preparing substrate for cells:

1. Coat gels with 0.2 mg/mL sulfo-SANPAH in H_2O for 10 minutes under long wave UV
2. Rinse 2x with 50 mM HEPES (All sulfo-SANPAH waste into designated container)
3. UV sterilized samples for 20 minutes to combat possible contamination from taking out of hood for long wave UV
4. Add 47 µl collagen solution to substrate and store overnight at 37°C (incubator)
5. Rinse and store in PBS at 4°C for up to one week
6. Before plating, UV sterilize substrates for 15-30 minutes

Appendix E

Elastic Moduli of Polyacrylamide Gels

Atomic force microscopy (AFM) indentation experiments were performed on the polyacrylamide gels with and without collagen. The gels were tested 1 day after they were made, having been stored in PBS at 4 °C overnight (same conditions as when cells would be plated on the gels). An Asylum Research MFP-3D AFM (Asylum Research, Santa Barbara, CA, USA) was operated in contact mode with a fluid cell. The gels were maintained in PBS throughout the study. A 5 μm diameter borosilicate spherical-tipped AFM probe on a silicon-nitride cantilever with a spring constant of 0.425 N/m (Novascan, Ames, IA, USA) was used to mechanically probe the gels. Before each experiment, the deflection sensitivity (nm/V) was determined by indenting onto a clean glass slide with PBS present. Ten locations from throughout each sample were tested, with 5 indentation-retraction experiments (force curves) per location. For each force curve, the sample was indented to approximately 3 μm depth at 1 μm/sec.

The force curves were exported from the AFM software and a custom MATLAB script (MathWorks, Natick, MA, USA) was used to normalize and shift the curves to a common zero point. The contact point was determined as the point where the slope of the curve changes by fitting the curve to a 2-region model [5]. To obtain a measure of gel stiffness at each location, the apparent elastic modulus was calculated by fitting the Hertz model to the data. This model was fit to the first 1 μm of indentation. The Hertz model for a spherical indenter is defined by the following equation:

$$F = \frac{4}{3}\frac{E}{(1-\upsilon^2)}R^{\frac{1}{2}}\delta^{\frac{3}{2}}$$

In this equation, F is the measured force (N), E is the apparent elastic modulus (Pa), υ is Poisson's ration (0.45), R is the radius of the spherical indenter (2.5 μm), and $\boldsymbol{\delta}$ is the indentation depth (m). Poisson's ratio was assigned a value of 0.45, based on measurements of gels with similar acrylamide/bisacrylamide concentrations [6-8]. All MATLAB scripts that were used to calculate the apparent elastic modulus can be found in Appendix B.

Figure E.1 outlines the results of this study, compared to previously reported elastic moduli values for the same gels [3, 4]. Our measurements are generally very close to the literature values. For work using these gels (Chapter 7), the measured values for the gels with collagen were used as the assumed elastic moduli, as this is the stiffness the cells cultured upon the gels would "feel."

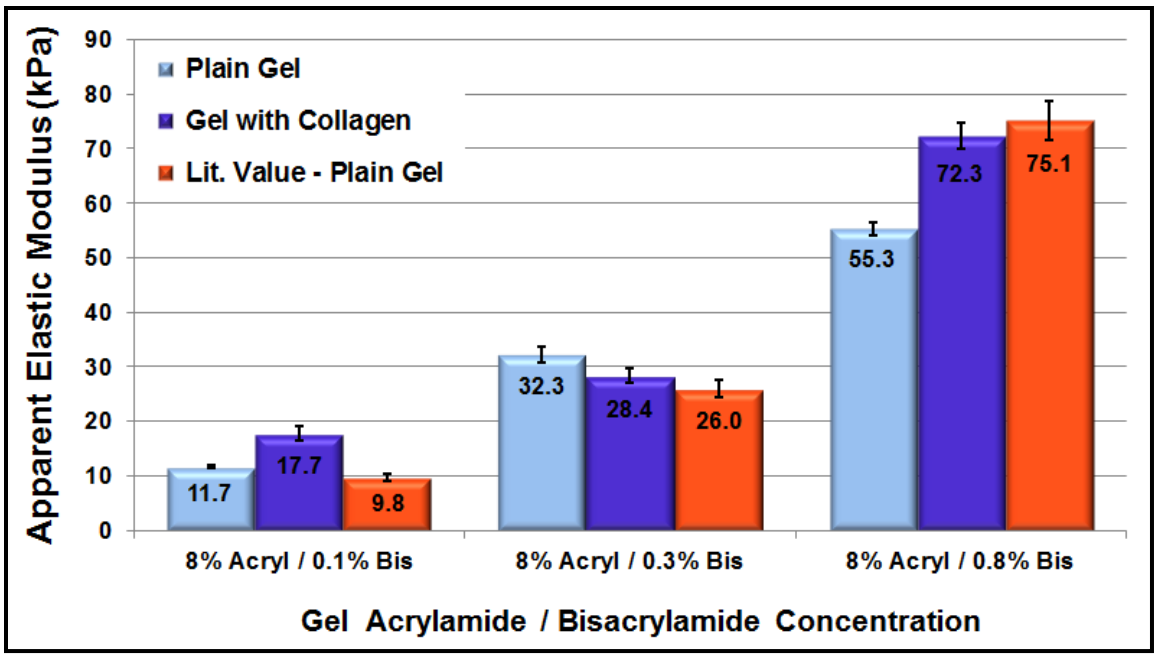

Figure E.1. Apparent elastic moduli of polyacrylamide gels with different acrylamide / bisacrylamide concentrations. Comparison of our measurements (light and dark blue) to literature values (orange) [3, 4]. Data presented as mean ± standard error.

References for Appendices

1. Winn, B., et al., *Rat aortic smooth muscle cell primary isolation protocol*, 2009. p. 1-2.

2. MathWorks. *Reading data files with text headers with MATLAB.* 2011; Available from: http://www.mathworks.com/support/tech-notes/1400/1402.html.

3. Tse, J. and A. Engler, *Preparation of hydrogel substrates with tunable mechanical properties.* Current Protocols in Cell Biology, 2010. **10**(16).

4. Datko, L., *M.S. Thesis: Effects of microenvironment on growth and differentiation of human dental pulp cells*, 2011, Clemson University.

5. Jaasma, M.J., W.M. Jackson, and T.M. Keaveny, *Measurement and characterization of whole-cell mechanical behavior.* Annals of Biomedical Engineering, 2006. **34**(5): p. 748-758.

6. Boudou, T., et al., *An extended relationship for the characterization of Young's modulus and Poisson's ratio of tunable polyacrylamide gels.* Biorheology, 2007. **44**(2): p. 139-139.

7. Geissler, E. and A.M. Hecht, *The Poisson ratio in polymer gels.* Macromolecules, 1980. **13**(5): p. 1276-1280.

8. Takigawa, T., et al., *Poisson's ratio of polyacrylamide (PAAm) gels.* Polymer Gels and Networks, 1996. **4**(1): p. 1-5.